Master of Science Thesis

Investigation on the influence of scaling effects in propeller testing through the use of theoretical prediction codes

Thomas De Leeuw

... 2013

Delft University of Technology
Dept. of Aerospace Engineering
Delft, the Netherlands

Delft University of Technology

Contents

Abstract

Although extensive research has been done on the performance and behavior of propellers, little is known about the effects they might have on other devices. More specifically there is an increasing demand of knowledge on how the slipstream influences the wings and empennage. Because these effects are hard to map with only theoretical methods, the use of wind tunnel is often required. An important issue that rises here is the one of scaling when comparing the full scale and wind tunnel data as it contributes a great part to the eventually made error. The goal in this project is to concentrate on scaling effects. Many studies were executed to determine the influence of scaling effects on important parameters like lift and drag. A good understanding of the uninstalled (performance, slipstream) and installed propeller (interference effects) is therefore mandatory. Many of these aspects are refreshed in this project. We start by choosing a representable propeller program for the investigation. This is done by validating the performance characteristics, taken from reference, into the program. In a next step, we determine the propeller characteristics by using test data from wind tunnel and full scale. Thereafter, a further research is done to see how the differences in performance between WT and FS are translated into the slipstream of the propeller. We will focus on the induced flow speed components of the propeller since they are relevant for the propeller-wing interaction. In a last stage, a propeller interaction program is used to see how the difference in induced components will influence the wing and more specific how the loading distribution over the wingspan is changed.

By doing this research on the uninstalled and installed propeller, an overall impression is obtained on how scaling effects, characterizing a deviation in data between the wind tunnel and the full scale case, will result in a possible deviation of the slipstream and even on parts further downstream. It is apparent that an error in propeller performance due to scaling will proceed in an error in the slipstream. Despite the fact that we expect errors due to scaling, it is not straightforward since a lot of different variables play a role in the behavior of a propeller i.e. rate of turbulence, inclination, etc. This will be explained throughout the report.

Nomenclature

α	Angle of attack (°)
α_i	Induced angle of attack (°)
β	Blade angle (°)
η	Efficiency of the propeller
ν	Kinematic viscosity (m^2/s)
ω	Propeller rotational speed (rad/s)
ρ	Air density (kg/m^3)
φ	Local inflow angle (°)
κ_w	Local wake advance ratio
λ	Taper
a	Axial inflow factor
a'	Radial inflow factor
b	Wing span (m)
c	Chord length (m)
c_p	Local propeller blade chord (m)
c_w	Wing chord (m)
dQ	Differential torque (Nm)
dr	Annulus width of blade element (m)
dT	Differential thrust (N)
l	Reference length (m)
n	Number of rotations (Hz)

r	Sectional propeller radius (m)
V_∞,V	Freestream velocity (m/s)
V_a	Axial velocity component at blade element (m/s)
V_e	Resultant velocity at blade element (m/s)
V_s	Velocity in the far wake (m/s)
V_t	Tangential velocity component at blade element (m/s)
V_{eff}	Effective velocity at propeller blade (m/s)
C_d	Drag coefficient, 2D
C_l	Lift coefficient, 2D
C_P	Power coefficient
C_Q	Torque coefficient
C_T	Thrust coefficient
$C_{l_{max}}$	Maximum lift coefficient, 2D
$C_{l_{min}}$	Minimum lift coefficient, 2D
Re	Reynolds number
Re_c	Chord Reynolds number
Γ	Strength of bound vorticity on propellor blade (m^2/s)
A	Propeller disk area (m^2)
B	Number of blades
D	Propeller diameter (m)
F	Modified Prandtl's factor
J	Advance ratio
M,M_∞	freestream Mach number
M_t	Tip Mach number
P	Power (W)

R	Propeller radius (m)
T	Thrust (N)

ABBREVIATIONS

FS	Full scale
RPM	Revolutions per minute
WT	Wind tunnel

1. Introduction

1.1. The propeller

In the last decades a lot of renewed attention has been given to the use of advanced propellers in transport aviation [33]. This re-appreciation is mainly due to the beneficial aspects such as fuel efficiency and T/O thrust although these are limited to a certain region of Mach number when comparing them to other forms of propulsion, i.e. turbofans or prop-fans as shown in Figure 1.1.

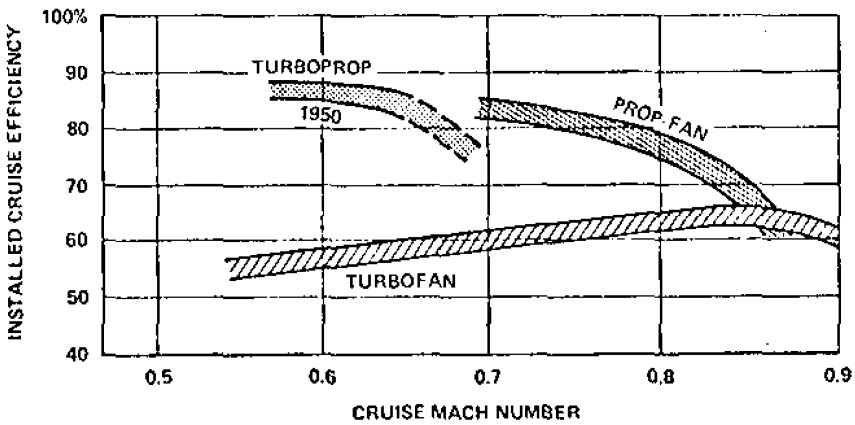

Figure 1.1.: Installed cruise efficiency versus cruise Mach number for different types of propulsion.[43]

In the low speed region (M<0.3) propeller-driven aircraft have the ability to quickly accelerate a large volume of air, which translates into a shorter take-off length and climbing time. These features are especially attractive for use in military aircraft [32]. Due to the mutual interaction between propeller and other aircraft parts, a propeller driven aircraft in tractor configuration produces a complicated flow field. In investigating the performance and interference of the propeller, one of the difficult challenges is to receive a reliable simulation of full flight conditions through wind tunnel models. As it is also quite expensive to execute wind tunnel tests in the preliminary stages of the propeller design, we will make a comparison between WT results that are obtained with scaled propeller models and those found in full scale. Our goal is then to map the general differences between them.

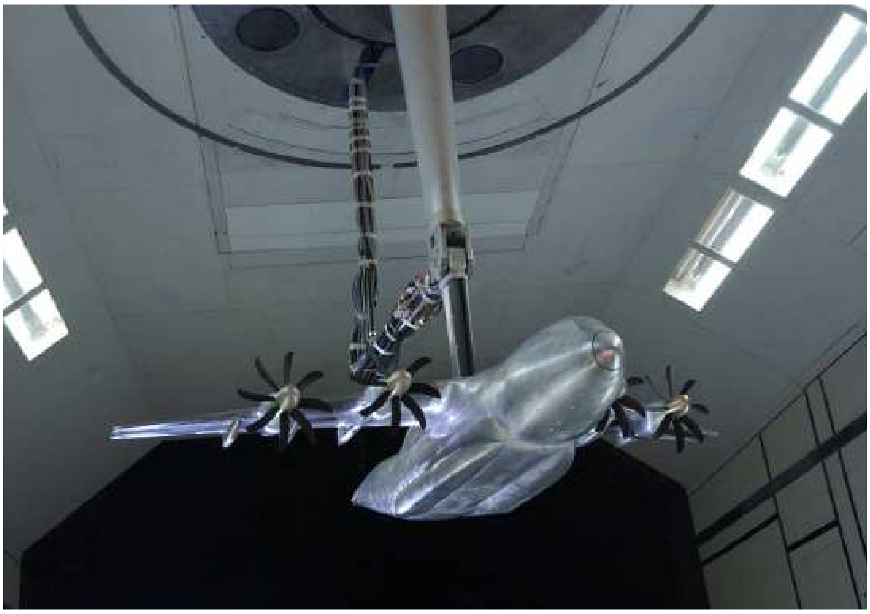

Figure 1.2.: A400M model in a wind tunnel with dorsal strut configuration. [58]

1.2. Propeller testing

When performing research on propeller driven aircraft, extensive wind tunnel investigations are absolutely necessary. One of the reasons is that the flow over the wings and empennage becomes more complex is due to the interaction with the propeller slipstream. A further explanation is made in chapter 2. Another reason is that the forces generated by the installed propeller are different to those produced by the propeller in free flow. These effects and interactions play an essential role in the stability, handling qualities and investigation of the propeller characteristics (i.e. performance). As they are very hard to predict through the use of only numerical and theoretical methods, it becomes evident that the need for wind tunnel tests is required. In Figure 1.2 a specific example is shown where a wind tunnel test is done on a model of the A400M. One of the main objectives of the test was to obtain handling quality data for the aircraft. The simulation in a wind tunnel often sets high requirements. In this particular case the engine system required hydraulic engines, an engine control unit, a main balance system, rotary shaft balances and a data acquisition system [58]. The information that is of interest to the engineer comes primarily from two sources, i.e. the main balance and the four rotary shaft balances. These balances measure the forces and moments on the complete model and on each one of the four hubs respectively.

When performing WT tests, we try to simulate the full scale operational conditions as good as possible. So when the data from a model is applied to a flight problem, the condition that should be satisfied is that the flows for the two cases should be similar. The Reynolds number, indicating the ratio of the mass forces to the viscous forces in aerodynamics, is commonly used as the criterion of similarity. The need for similarity between the flow around a model and the flow around the full scale object in flight becomes apparent from the fact that the aerodynamic coefficients, per definition, vary with changes in Reynolds number [9]. This will be explained in the next section and is referred to as a scale effect. Because the conditions in a wind tunnel are never entirely the same as for the FS case, errors will be made when performing investigations on important issues like the performance characteristics. It is general knowledge that these errors made during testing are largely caused by scaling effects and only a minor part is caused by the interference of the propeller [42]. These scaling effects arise as it is almost impossible to represent the full scale in its entire form. In the handling of propeller dimensional problems, the Reynolds number and the Mach number have become two important parameters. In a wind tunnel it is not possible to simulate the high values of Reynolds number that are normally seen in the real operating environment. To give the reader an idea of the commonly used values in the different cases, the next section is attributed to *Re* and *M* regimes.

1.3. Re and M regimes

When a comparison is made between the experiment and the full scale case, we encounter Reynolds numbers in quite a large range. What follows is a general outline of the order of magnitude that is normally used, based on data and experiments that were executed in the past. Caution should be paid when information is found on the effect of Reynolds number, as we need to make a distinction between the Reynolds number for propeller blades and wing airfoils. By looking at the next two formula, it becomes clear that we are working with different values of *Re*.

$$(Re_c)_p = \frac{V_{eff} c_p}{\nu} \tag{1.1}$$

Where V_{eff} is the effective velocity at the propeller blade section, c_p is the local blade chord at the 0.75 radius station of the propeller and ν is the viscosity.

$$(Re_c)_w = \frac{V_{eff} c_w}{\nu} \tag{1.2}$$

Where V_{eff} is the effective velocity at the wing section, c_w is the blade chord of the wing and ν is the viscosity.

In order to avoid confusion, it will be mentioned if the paper is concerned with a general airfoil Reynolds number (wing) or with a blade Reynolds number. The preferred modeling technique is the one where the model scale is large enough in order to minimize or eliminate the need for Reynolds number correction. Published data has shown that corrections for propeller models having Re_c in excess of $7{\times}10^5$ are small compared to full scale [44]. As in many atmospheric wind tunnels, lower Reynolds numbers will have to be used because of several limitations such as the available drive motor horsepower or blockage by the wind tunnel.

Several lower limits for the use of Re_c in wind tunnel tests have been put forward in the past. For these cases, performance adjustments could be useful in the form of data correlations of different propellers as seen in Figure 1.3. Values of $5{\times}10^5$–$6{\times}10^5$ were brought up, depending on the investigated conditions [45]. Through several tests a rule of thumb was derived stating that above $3{\times}10^5$ rather good results could be attained based on the stabilization of circulation around the airfoil section and the overall disappearance of the typical negatives flow effects at (extreme) low Reynolds numbers [46]. This will be discussed later on in this section.

One of the disadvantages when dealing with lower values would be the lack of validated propeller characteristics concerning the range of Re_c, i.e. $1{\times}10^5 - 6{\times}10^5$.

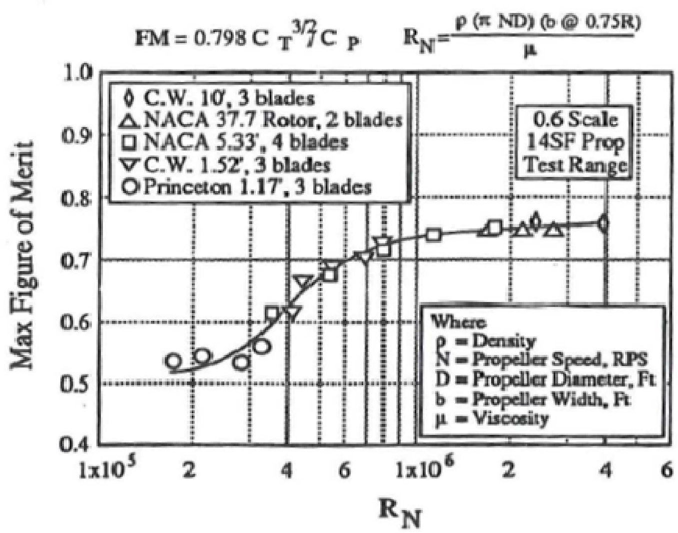

Figure 1.3.: Data correlations over a range of Reynolds numbers. [44]

As for tip Mach numbers, typical values for full scale are found in the range of 0.5–0.8 as based on selected aircraft data [47],[48]. Other investigations were done for the critical tip Mach number, i.e. the tip Mach number that can be reached before serious losses in maximum efficiency are encountered. It was shown that these values are found in the order of 0.88 to 0.91 [49]. Applying this to the wind tunnel scale, more in particular the low speed case where we encounter low free stream Mach numbers, we have to deal with lower values of tip Mach numbers, i.e. 0.2−0.5. Especially when focusing on the larger transport aircraft. The use of a certain tip Mach number in the wind tunnel is of course highly influenced by the forward speed, so the regime was therefore based on the low speeds (<90m/s) [49].

A simple calculation will be made in Appendix A for both the A400M [58] and the F-50 [31] to verify the typical tip Mach numbers and blade Reynolds numbers that are encountered. The results are listed in Table 1.1.

Tip Mach number	WT	FS
A400M	0.61	0.78
F-50	0.45	0.68

Re_c	WT	FS
A400M	4.8×10^5	5×10^6
F-50	4.8×10^5	3.5×10^6

Table 1.1.: Calculated values of the tip Mach number and Reynolds number for two aircraft.

For the A400M, one of the remarkable adjustments or maybe a random mistake is the following. In order to represent the full scale case in the wind tunnel, we need similarity. This requires that the three parameters of the propeller (C_T, J, C_P) are similar. Because of scaling effects, it is not possible to reproduce these three at the same time [58]. For this reason, only C_T and J are taken similar in the paper. We can see in Appendix A that it requires a RPM value of 4500 for the model. However in the tests, a sequence of 12000 RPM is used. A possible explanation could be found in the scaling effects. When these effects become too large, the similarity between FS and WT can be lost. In the case of 4500 RPM, we end up with a Re_c of 1.9 $\times 10^5$. Further in this section, it becomes clear that scaling effects have a major influence in the region of $Re_c \leq 2{\times}10^5$. A higher RPM is probably chosen to avoid this influence.

Looking at the freestream Mach number, we see a wide range of values as it highly depends on the type of wind tunnel that is used. Focusing on propellers, values of 0.2-0.7 are used in [49], whereas lower maximum values of 0.6 are possible for others due to restrictions on the wind tunnel. For M, the compressibility effects may lead to a loss in accuracy. This means that the lift and drag coefficients could be influenced by a change in M. It was stated in [49] that the thrust and power coefficients for constant J is expected to vary with the M as the lift coefficient varies with the Mach number. Theoretically, for an airfoil, this variation in lift coefficient is proportional to $\frac{1}{\sqrt{1-M^2}}$. However, it should be noted that the focus in the remainder of the report will merely be put on the issue of Reynolds scaling. The reason is that we use data for WT and FS, where a match is found for M in order to avoid the issue of Mach scaling.

1.3.1. Implications of limited Re numbers

It becomes clear that because of the large differences between Reynolds number of full scale and model tests, the WT results are subjected to some error. Before going into the effect of Re scaling on the induced velocities of the propeller and i.e. its effect on the wing, it can be useful to take a look at the influence of these differences in Re number on performance and other characteristics.

1.3.1.1. Influence on lift

As from different data in the past, several standard numbers for propellers like $3{\times}10^5$ have been put forward as extreme minimum value of Re_c that would be assumed to give representable results for the full scale case [46]. Below this range for general airfoil sections, issues appear like non-linearity and hysteresis of the lift curves and a dominant influence from the presence of the laminar separation bubble [18],[19]. These phenomena can make the predictions with propeller models rather inaccurate. One of the goals of this research is to find the limit under which their influence becomes too profound. In the lower regime the boundary layer effects are mainly dominated by the laminar separation bubble which is only marginally stable and bursting can be easily triggered when increasing the angle of attack. When reducing the angle of attack, the hysteresis effect in the lift curve can occur when the bubble does not immediately "unburst" [18]. In the range of $10^5 - 2{\times}10^5$, several papers on airfoils describe the linkage of non-linearity and hysteresis of the lift curves to the laminar separation bubble and argue that for values above $2{\times}10^5$, these effects can be avoided since it is possible to make the transition occur upstream of the adverse pressure gradient [18],[50]. Going to higher values ($<6{\times}10^5$), which is still governed by the problem of the laminar separation bubble, it is well argued that some sort of minimum Reynolds number can be defined based on results where the additional drag due to the bubble becomes negligible [20]. It can be argued that going to higher values in this range, the errors for similarity with full scale become less and even marginal [18], [19]. The performance however is still lower than for the corresponding higher Reynolds number but it becomes apparent that a further improvement is seen as the resistance to separation of the turbulent boundary layer will increase with increasing Re. This improvement occurs more slowly when reaching high values i.e. $>1{\times}10^6$ [18].

For the maximum lift coefficient, we find large variations with Re. Reaching C_{lmax}, separation will occur, leading to a reduction of lift. As already mentioned, the development of separation is dependent on the resistance to separation of the boundary layer. In the case of Reynolds numbers below $5{\times}10^5$, separation most likely occurs in the laminar boundary layer. In the presence of the bubble, the transition point will move forward when the Re is decreased. Here, separation occurs at a lower value of lift coefficient than the C_{lmax} of the full scale Re. This means that the lift curve will have a lower C_{lmax} when decreasing the Re. It can also be seen in [9] that for this lower range of Re ($<5\times10^5$), C_{lmax} changes little with Re. These general trends are illustrated in Figure 1.4, where some cambered airfoil sections have been investigated, together with the polars. An explanation is given in the next section.

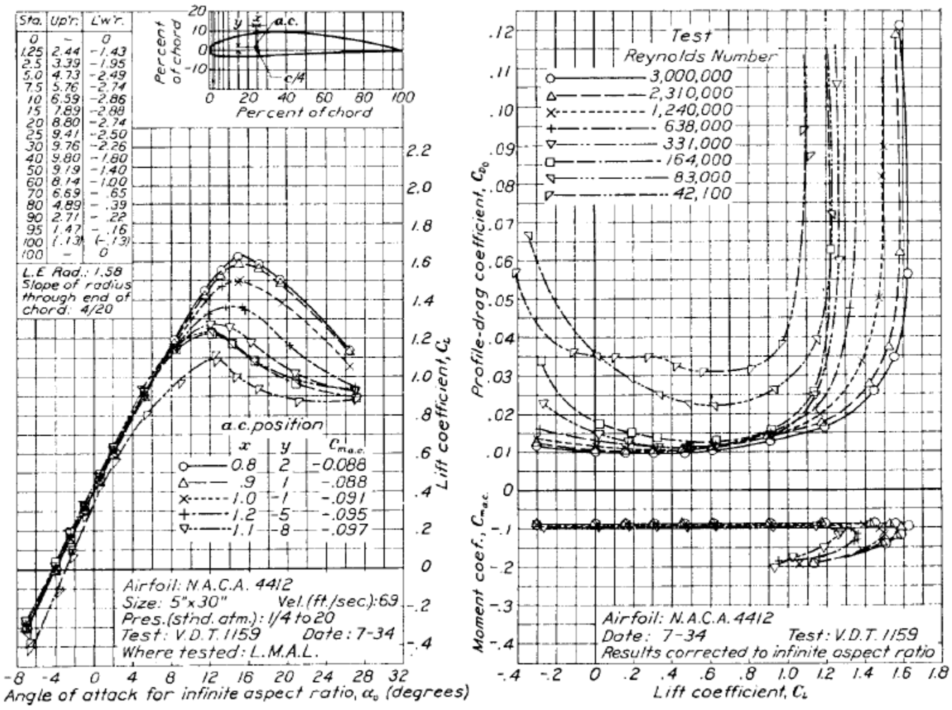

Figure 1.4.: Drag polars and lift curves affected by Reynolds number for a typical propeller airfoil section. [9]

1.3.1.2. Influence on drag

In case of the laminar separation bubble, we know that the separation will cause a much higher drag since the transition occurs behind the separation point [20]. So the undesirable effect at low Re for airfoil sections is the higher drag and the sometimes irregular shapes that are seen in the drag polars [20],[19]. An illustration can be found inFigure 1.4 and Figure 1.5.

Although attention must be paid to the accuracy and correctness of the data at low Re, general thoughts can be drawn. We see that for propellers a higher drag coefficient occurs for a lower value of the lift coefficient without much altering of the minimal value of the drag coefficient (a narrow drag bucket). This can also be seen in Figure 1.4. This happens until a certain value of Re, in the order of 5×10^5, as mentioned in the previous section. Below this value the opposite occurs through a great increase in C_{dmin}. This general irregularity (steep increase) was argued to lay well below the value of 4×10^5 by Sherman [9].

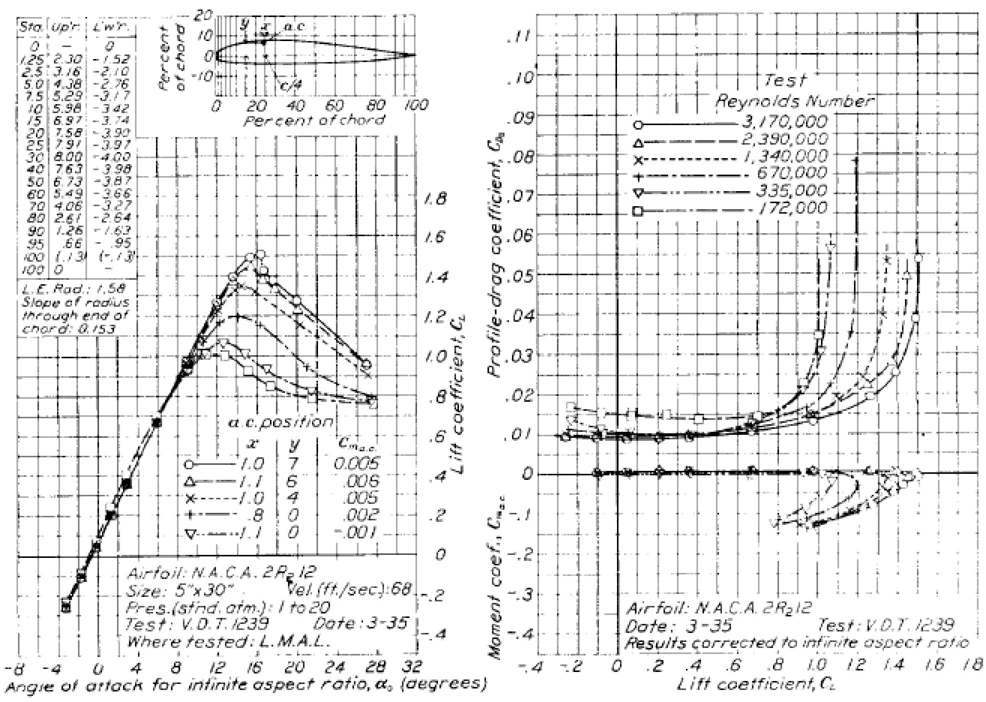

Figure 1.5.: Drag polars and lift curves affected by Reynolds number for a typical propeller airfoil section. [9]

1.4. Implementation of lift and drag polars for (un)installed propeller

As we now have an overall idea what scaling does to the aerodynamic characteristics of airfoils, it should also be pointed out how this translates to the propeller performance and the possible effect on wings.

1.4.1. Propeller performance testing

Beginning with some general thoughts, the report of Lesley [12] pointed out that the scaling effect is the reason for the difference between thrust and power of propellers for the full scale and model. The increase in lift for the full scale propeller sections is such as to increase the power and thrust as noted in Figure 1.6. The corresponding specifications can be seen in Figure 1.7.

In recent years several studies were made on the influence that low Reynolds numbers ($<3\times10^5$) have on the (propeller)performance of UAV, which could give a good indication on the models used for real aircraft. Although geometrical characteristics play a role, general conclusions for propellers can be made on their use and limitations concerning the topic of scaling. An investigation on propellers designed for

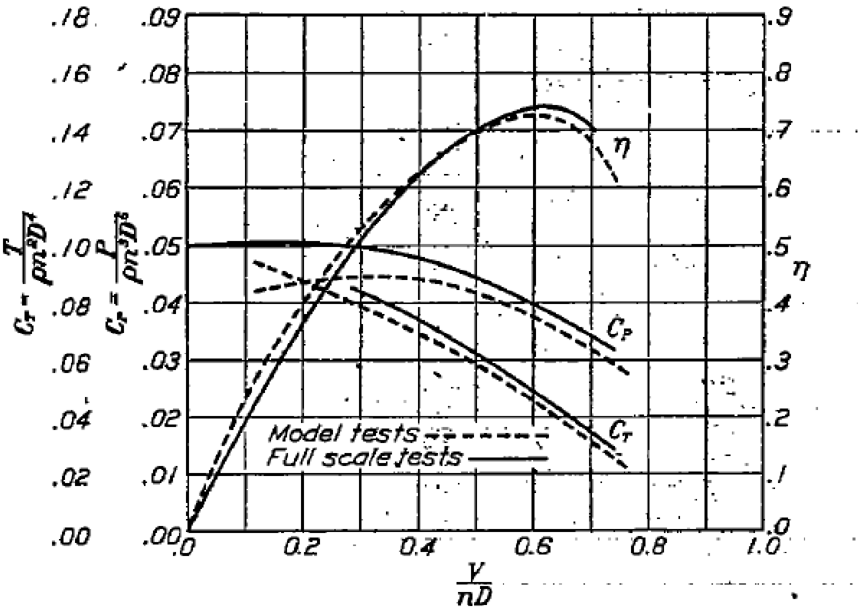

Figure 1.6.: Typical thrust and power characteristics for 2 different propellers. [12]

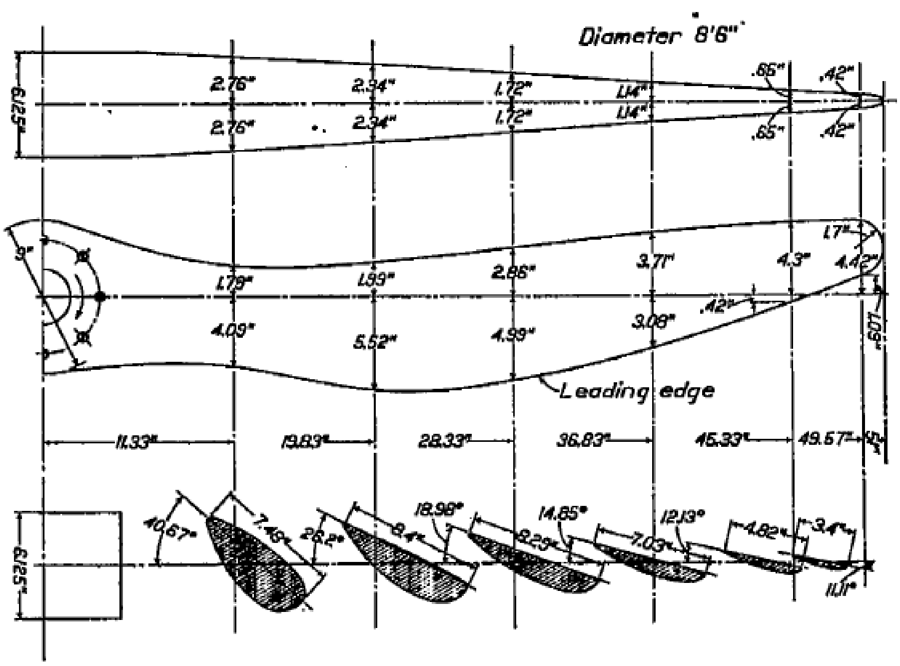

Figure 1.7.: Geometry of propeller B, taken from [12].

Re_c >10^6 [51], confirmed the fact that characteristics became worse with decreasing Re_c and even unworthy of using them for the lowest regime of Re_c(<10^5). Here, the option of redesigning propellers for low Re_c to give better resemblance with flight test, is not a useful solution. In [52] the question was raised if performance tests of models could give accurate representation of the full scale. As a change in tip speed would alter the rotational speed and centrifugal forces on the blades, the question of Re is much more complicated for a propeller than for a wing since now the Re will vary along the blade. This variation, that is more profound at lower speeds when the rotational component dominates the relative velocity, is unimportant at full scale. For the models however, it is likely that the influence of the Re should be divided into the "root effects" and the well-known airfoil effects. At the hub, Himmelskamp [53] showed that better airfoil performance was found due to the delay of separation to larger angles of incidence which meant that a lower Re_c was possible. He noticed that the blade rotation would affect the lift polar in such a way as to delay stall and achieve higher maximum lift values. This effect was more pronounced towards the root due to the lower rotational velocities. The reason is that significant radial flow can only develop in regions of retarded flow such as separated regions. The flow that develops in radial direction, due to the centrifugal forces in the boundary layer of a rotating blade, will result in a Coriolis force that acts as a favorable pressure gradient. This leads to a delay of the boundary layer separation and i.e. to higher lift coefficients [11]. Figure 1.8 shows the increased lift coefficients that are obtained near the hub.

One could conclude that the incorporation of the Himmelskamp effect is justified for every propeller. Further on in the report, it is seen that this is not the case. An explanation for this observation is made in chapter 4.

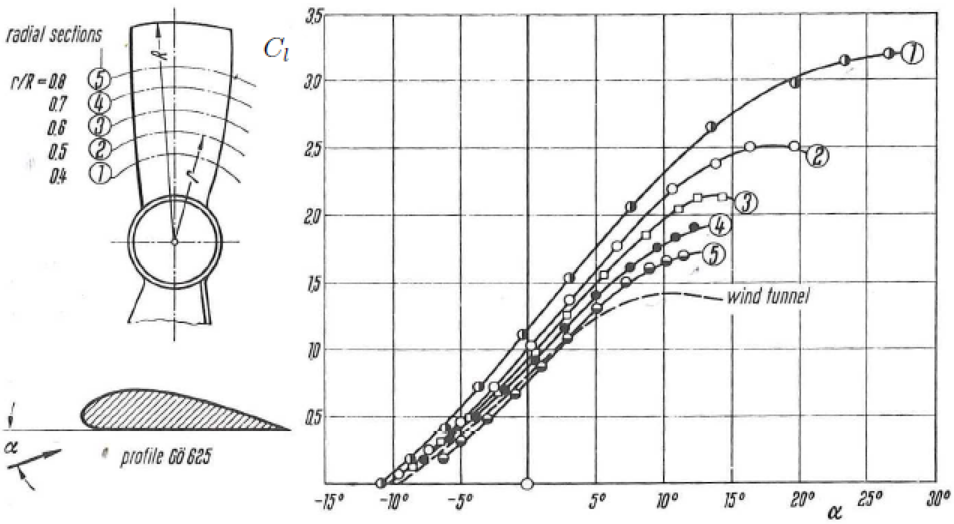

Figure 1.8.: Local lift coefficient at various radial sections on a rotating propeller. [53]

Tests were conducted to investigate the effect of scaling on the behavior of propeller models [52]. It was concluded that models used for performance simulation of the full scale, should not be run well below $5{\times}10^5$ as the efficiency fell dramatically under $3{\times}10^5$. A very important and interesting way of analyzing the *Re* of propeller models was given by Lerbs [46] in relating the lift coefficient of the profile to the thrust coefficient and the measured efficiency to the drag coefficient. He made a general analysis where he defined the *Re* based on the fact that above its value the frictional coefficient of the profile can be deduced from the one of a turbulent flat plate according to a predetermined relation and that at the same time the angle of zero lift of the propeller profile still coincides with the one of the isolated profile, calculated from potential theory. Drag reduction is one of the effects of Reynolds number increase and this drag is mostly accounted for by the skin friction This makes the use of theoretical skin friction drag in Lerbs analysis fairly acceptable [54].

A less clear image is observed w.r.t. the lift coefficient because of the difference in zero lift angle at low Reynolds numbers. Using the hypothesis that the vibration of the rotating propeller provides turbulence, it was shown [45] that a rapidly rotating small propeller approaches the full scale condition more accurately than a slowly rotating large propeller. Still however, the difference in the zero lift angle gives a deviation of the effective pitch angle of a few degrees between the model and full scale [45]. Using this, Lerbs found good agreement between FS and WT tests at $Re_c \sim 0.77{\times}10^6$. More important he observed that tests with Re_c below $3{\times}10^5$ are expected to give results considerably different than the ones for the full scale condition.

1.4.2. Propeller integration effects

In the current interest for the use of propellers not only the direct effects on the propeller performance are important but even more are the effects of the already mentioned scaling issues on parts laying in the wake of the propeller. Therefore, an investigation is needed on how the slipstream is altered by these scaling effects and how this in turn may change the different characteristics of parts behind the propeller, more specifically on the wing.

Focusing on the immersed part of the wing in the slipstream, we see that through a variation in slipstream, the characteristics of the wing will change. Considering now a rectangular, symmetric, untapered and untwisted wing, it is known from theory that the lift distribution at an angle of attack has an quasi-elliptic shape. When the propeller slipstream is introduced, a change in the lift distribution is observed. Inside the slipstream the axial velocity increases, leading to an increase in dynamic pressure. This implies that the local angle of attack will change and therefore the forces on the wing. An illustration of these changes in wing characteristics is shown in Figure 1.9 and Figure 1.10.

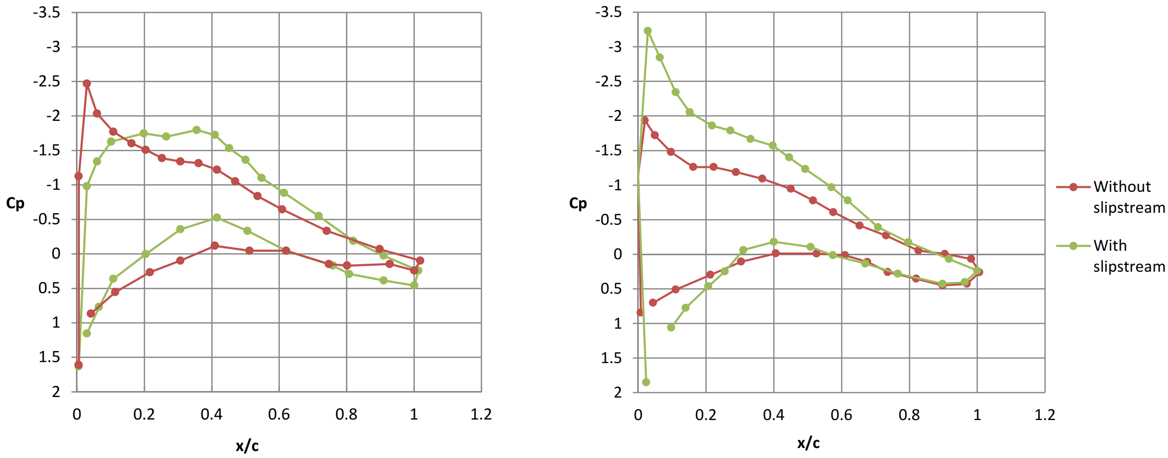

Figure 1.9.: Measured pressure distribution of a wing section behind the propeller (inboard up) on the inboard (right) and the outboard side (left). Data from[31].

According to Veldhuis [23] and Witkowski [24] the axial velocity distribution is more or less symmetrical w.r.t. the propeller thrust and the effect on the wing loading is equal for both the inboard and the outboard side of the nacelle. The effect of the swirl velocity is different because its contribution will be anti-symmetrical. The induced upwash of the upgoing blade will lead to an increase in local wing angle of attack while the downgoing blade will lead to a decreased local wing angle of attack. It is because of this anti-symmetrical behavior that the final shape of the spanwise loading distribution will be dominated by the rotational direction of the propeller. The effect of the induced velocities as explained above is demonstrated in Figure 1.10.

If the effects of the velocities are combined and if we account for the changes that occur outside the slipstream domain, a more complicated loading distribution will be found. It is clearly seen in Figure 1.11 that the effect of the propeller is not limited to the part of the wing that is immersed in the slipstream. The loading of the wing outside the immersed part will change as well, since the wing inflow conditions and the resulting trailing vorticity strength generated by the propeller are also changed.

Earlier observations came up with general concepts as a lift increase due to slipstream [36] or an increase of lift coefficient with increasing *Re* (increasing rotational speed) [30]. In [37], a general consensus stated that the slipstream reduces the laminar flow by forcing the transition to occur earlier. From several investigations it was concluded that the slipstream caused the point of transition to cycle between a forward position near the leading edge and the point of transition without incorporation of the slipstream , although no consistent conclusions resulted from these early observations [37]. Because of adequate research on the propeller wing interaction, it is well known that for the tractor configuration the performance improvement is mainly manifested in a wing drag reduction [24]. Before looking into the interaction

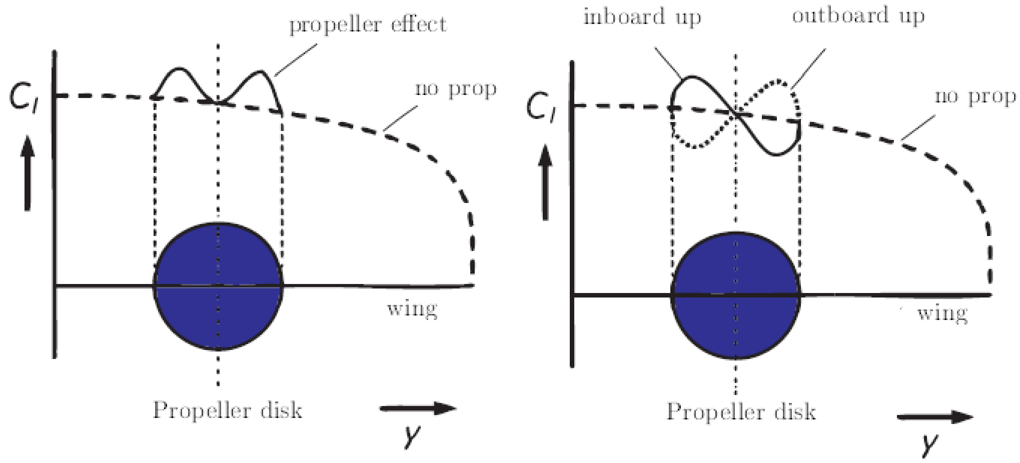

Figure 1.10.: Change in the local lift coefficient due to the axial(left) and swirl(right) velocity in the slipstream for an untapered wing. The effect outside the slipstream is left out [23].

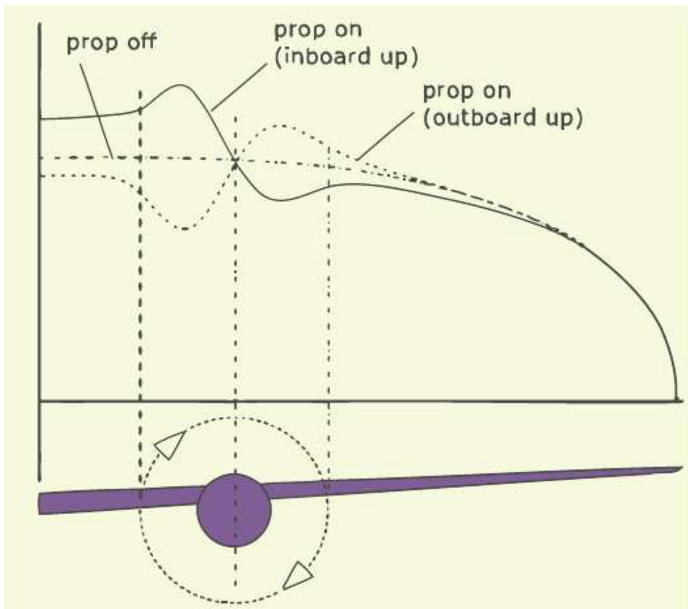

Figure 1.11.: Lift distribution as affected by the combined effect of the axial and tangential velocity [23].

with respect to scale effects, it is important to keep the well know effect of low Reynolds numbers on isolated wings in mind. Studies, as mentioned in the previous section, showed the dominant problem of a laminar separation bubble and other typical phenomena at lower Reynolds numbers. A recent and useful investigation concerned the effect of the propeller slipstream on both the separation bubble and transition process at low chord Reynolds number [55]. An important aspect is the mechanism by which the slipstream is introduced into the boundary layer of the wing. In this work the periodic turbulence, introduced by the propeller, is seen as uniformly distributed along the whole cycle in order to investigate the global effect of slipstream on transition on the wing. This behavior resulted in regions of turbulent packets between which the boundary layer seemed to remain laminar. One of the conclusions was that the transition mechanism associated with laminar separation bubble was changed to a classical transition process associated with increased Reynolds number and that transition moved towards the leading edge. As noted in [55], the lack of the incorporation of this cyclic behavior into earlier studies could make previous conclusions about the flow over the wing in the slipstream incorrect. This was incorporated in [37] since the laminar boundary layer within the slipstream was seen as a boundary layer with a cyclic variation of external flow turbulence. This external flow turbulence is the viscous wake from the propeller blade. Seen from the disturbance model in Figure 1.12, the turbulence near the surface will remain some time after the passage of the external turbulence. In this work [55] and others, like for example Howard R.M. [56], the time-dependent cycle of transitional behavior in the wing boundary layer was studied. He observed that its characteristics were similar to relaminarized flow and laminar flow with external turbulence. More in particular the drag values at low *Re* showed that the propeller slipstream enhances the stability of the boundary layer and reduces the drag coefficient in the laminar portion of the slipstream cycle below its undisturbed value[56],[37].

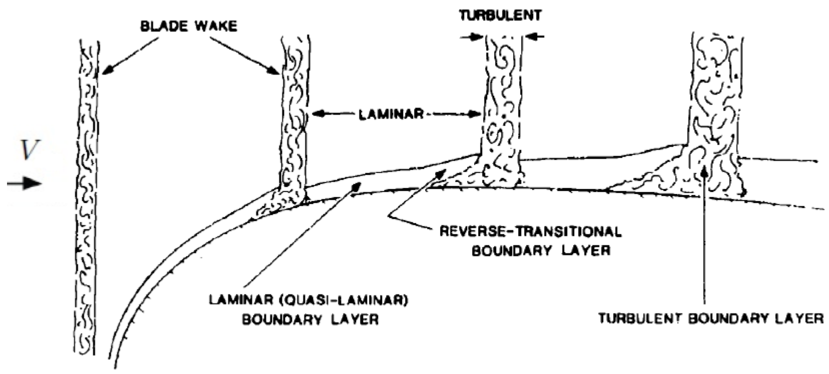

Figure 1.12.: The effect of a passing slipstream on the boundary layer flow over an airfoil. [37]

1.5. Opportunity for further research

It is clear from previous sections that a lot of work has been done on both uninstalled and installed propellers. The issue of scaling on the other hand is a very important topic that needs further investigation. In order to understand the logic in the different steps of this report, listed in the next section, a statement will be made to explain how this topic of research (scaling effects) will be investigated. This statement will be formulated in a main objective and some fundamental questions.

Research questions

- What is the effect of scaling on propellers in wind tunnel tests (i.e. performance and slipstream)?
- What is the influence of scaling on propeller wing interaction due to changes in the propeller slipstream?

Different sub-questions emerge when a thorough investigation is done on these research questions.

- Are the general known limits of values under which resemblance between data is lost actually correct? This merely focuses on the lower limit of the Reynolds number that is generally used in order to be sure that resemblance between full scale and experiment is still present.
- What role do parameters like Mach and Reynolds number have on important aerodynamic parameters, i.e. on lift and drag?

The fundamental work for understanding the background of these problems, i.e. the sub-questions, was shown in the previous sections. The objective can now be stated as follows.

Thesis objective

- Investigate, through the use of theoretical prediction codes, how scaling effects will alter the propeller performance and the slipstream and i.e. how the flow over the wing is changed as a consequence of this alteration.

1.6. Set up of the report

This report will be build up in the following way. First of all a subdivision is made into the four upcoming chapters.

- Chapter 2: Background
- Chapter 3: Preliminary survey
- Chapter 4: Analysis of uninstalled propeller
- Chapter 5: Interference effects of installed propeller

- Chapter 6: Conclusions and recommendations

In Chapter 2 the background theory concerning propellers is stated together with the useful terminology in order to have an idea about the basics needed for a good understanding of the following work.

Chapter 3 handles the description and verification of different theoretical prediction codes that are available for propellers. A short description of the selected prediction program is given after which we will try to investigate how well reference data can be represented in the programs. This is done by taking data from open literature where investigations on propellers were performed and comparing them with data found in the program on similar propellers.

Chapter 4 will take a deeper look into the representation and effect of the Reynolds number in the selected program. In a second stage, this program will be used to validate data from papers and investigate how this data is translated in to parameters like for example the induced velocities of the propeller.

In Chapter 5, an investigation is performed with a propeller interaction program to see how the results from Chapter 4 will affect the wing. In other words, an attempt will be made to provide the reader with consistent information on how the different data of the propeller in full scale and wind tunnel will influence the trailing wing. At the end, an analysis is made to see other effects on the lift distribution, like for example the position of the propeller.

Finally, Chapter 6 contains the conclusions that were drawn and the recommendations for future work.

2. Background

2.1. Propeller theory

In order to have a clear view on every (sub)topic that will be tackled, a short recap of theory and terminology needs to be established. Throughout this work, some information will be added to clarify specific questions like transition, interference effects and more.

2.1.1. Propeller concept

Propeller blades can merely be seen as wing sections producing an aerodynamic force but because of their different application a rotational velocity is added to the forward velocity of the blade flight path resulting in a helical flight path. Since the aerodynamic forces are presented as torque and thrust, a good understanding of the relation between them and the forces on the wing, i.e. lift and drag, is needed. Although the forward velocity over the blade is assumed constant, the rotational velocity will depend on the blade section and α will vary accordingly.

Propellers operate most efficiently if the α is constant over the larger part of the blade (giving the best C_l/C_d ratio for propeller efficiency). For this reason twist is used throughout the blade length.

2.1.2. Propeller aerodynamics

In order to analyze the aerodynamic performance of a propeller by means of a model, different theories can be applied. As a propeller produces thrust by forcing air behind the aircraft, it will produce a slipstream. It can then be crudely considered as a cylindrical tube of spiraling air propagating towards the rear over the wings. In analyzing a propeller model, different approaches can be used in a compatible way; using the blade element theory to predict the propeller forces and the momentum theory to relate the flow momentum at the propeller to the one of the far wake. The reason that these two theories are combined is as follows. In dealing with propeller performance, momentum theory based on the hypothesis of a stream tube enclosing the complete propeller disk, is a simple and classical used method. Because this theory does not provide enough accurate information to find meaningful relationships between the different blade parameters, blade element theory is often used instead. Combining the results of these two analyzes, relations are found for the differential propeller thrust and torque. For this analysis a clarification of the models is needed.

Momentum theory

This work, introduced by Froude and continued by Rankine, is based on the following assumptions:

- The flow is inviscid
- The flow is incompressible
- There is no rotational motion of the flow in the slipstream
- Both the velocity and the static pressure are uniform per unit disk area

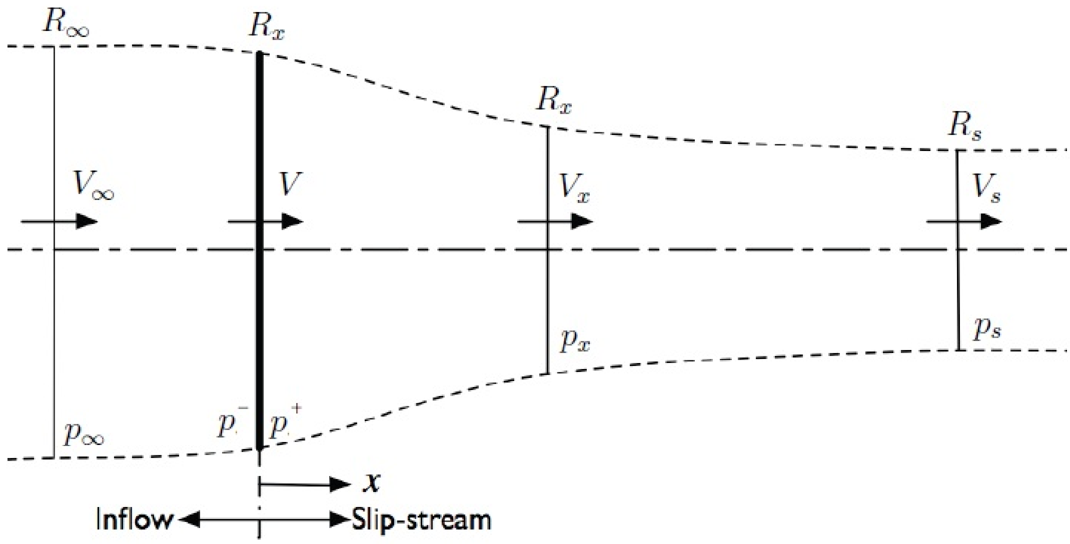

Figure 2.1.: Propeller stream tube indicating the freestream velocities and radius at different axial positions. [35]

This means for the axial direction that the change in flow momentum along a stream-tube starting upstream, passing through the propeller, and then moving forward into the slipstream must equal the thrust produced by this propeller [35].

$$T = \rho \pi R_s^2 V_s (V_s - V_\infty) \tag{2.1}$$

The second implication is that for each cross section the pressure jump over the disc should be equal to the thrust [41].

$$T = (p^{+} - p^{-})A \tag{2.2}$$

Application of Bernoulli's equation both up- and downstream of the disk leads to the following:

$$p^{+} - p^{-} = \frac{1}{2}\rho(V_s^2 - V_\infty^2) \tag{2.3}$$

Combining these equations with the continuity condition results in the proof that the velocity through the disk is equal to the average of both the up- and downstream velocities.

$$V = \frac{V_\infty + V_s}{2} \tag{2.4}$$

Blade element theory (BEM)

In the above theory of momentum there are not enough equations given to come up with the expression for the differential propeller thrust and torque of a given span location. The additional equations that can be used are dependent upon the state of the flow. This flow state is dependent on the characteristics of the propeller blades. These geometrical properties are used in blade element theory in order to determine the forces that the propeller exerts on the flow field. As we are dealing with finite elements, the blade is split into a number of distinct section of width dr. For each element the blade geometry and flow field properties are then related to a differential propeller thrust dT and torque dQ. This is done by making two supplementary assumptions [35]:

- In the analysis, no interaction is present between the blade elements
- The forces exerted on each blade element by the flow are purely determined by the two-dimensional lift and drag characteristics of the blade element

In determining the aerodynamics forces that result on the blade elements, it is helpful to look at the velocity diagram as given in Figure 2.2. The inflow angle based upon the two components of the local velocity vector is found to be:

$$tan\varphi = tan(\varphi' + \alpha_i) = \frac{V_\infty + V_a}{\omega_p r_p - V_t} \tag{2.5}$$

By looking then at Figure 2.2 the following relation is apparent:

$$V_e = \frac{V_\infty + V_a}{sin\varphi_1} \tag{2.6}$$

The induced velocities are function of the forces on the blades and the combination of both theories is used to calculate them.

Finally with the aid of this figure the thrust around an annulus of width dr is equivalent to:

$$dT = \frac{1}{2}\beta\rho V_e^2 \left(C_l cos\varphi - C_d sin\varphi\right) cdr \tag{2.7}$$

and the torque for each annular section is given by:

$$dQ = \frac{1}{2}\beta\rho V_e^2 \left(C_l sin\varphi - C_d cos\varphi\right) crdr \tag{2.8}$$

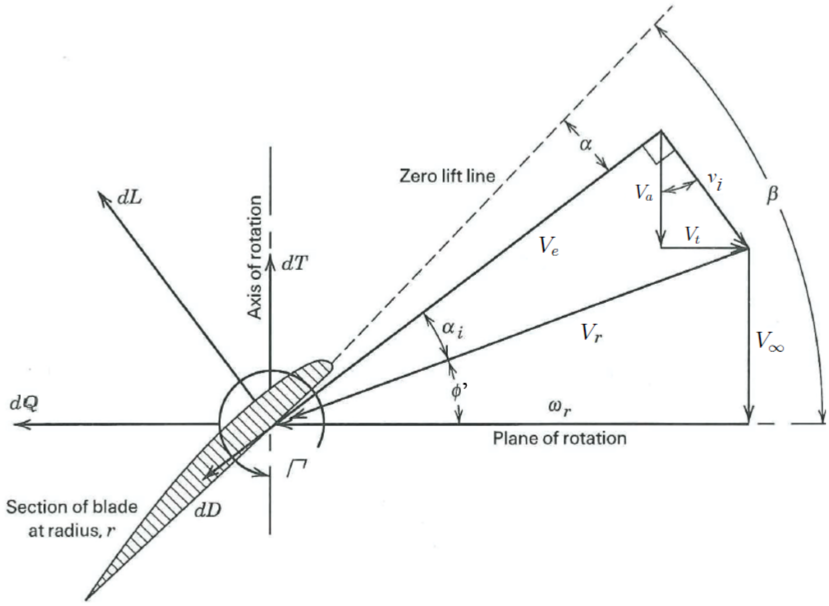

Figure 2.2.: Velocity diagram of a blade element. [28]

From Equation 2.7 and Equation 2.8 we see that for this model the *Re* number directly influences the thrust and torque through the blade airfoil lift and drag coefficient. Therefore the *Re* number dependency of the lift and drag polar form a crucial part of the investigation.

2.2. Interference effects

The flow field of an isolated propeller and an installed propeller differ significantly for reasons that will be explained in this section. It is important to note that we are working with a propeller in tractor configuration. This means that the propeller is situated upstream with respect to the wing. It is evident that the understanding of this topic is very important as the propeller slipstream influences both the performance and aerodynamic behavior of the wing. On the other hand the upwash induced by the wing influences the flow field of the propeller blades. It changes the local angle of attack of the propeller blades similar to an uninstalled propeller subjected to an angle of attack as can be seen in Figure 2.3. The effective velocity experienced by the downward rotating blade is increased by the wing's upwash, which leads to a local angle of attack increase. This results in an increase in elemental lift and blade loading, which augments the thrust and torque on the blade. The upward rotating blade on the other hand experiences a decrease in the local angle of attack leading to a decreased elemental lift and blade loading. Thus the upward rotating blade experiences a decrease in thrust and torque.

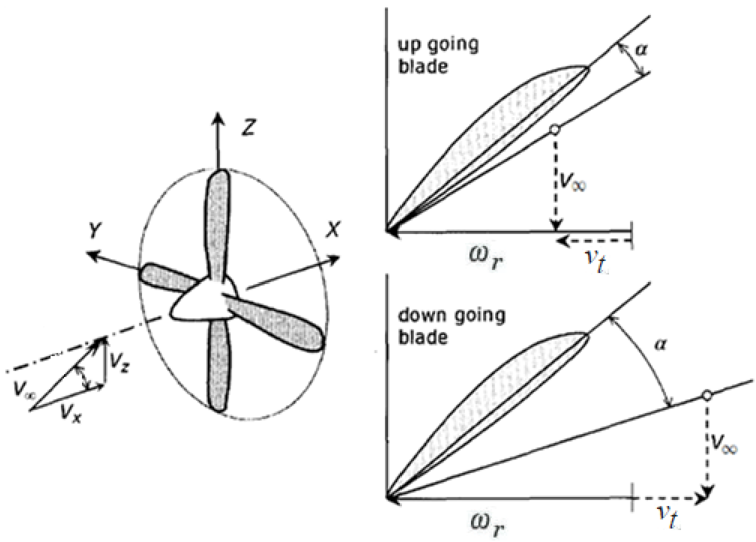

Figure 2.3.: Effect of wing's upwash on the propeller blades. [32]

In the case of the tractor configuration, the wing experiences swirl velocities that initiate from the propeller and result in a deformation of the lift distribution [29].

By using numerical and experimental methods, it was found that the propeller-wing interaction effects for certain tractor propeller configurations resulted in significant wing drag reduction [32]. The interaction between the wing and the propeller is provided by the velocity field induced by the lifting line within the propeller's stream tube and by the velocity field induced by the propeller slipstream on the lifting line. The former will affect the power characteristics of the propeller and the latter will yield the change in wing induced drag [17]. Just as wings can be modeled by vortex line theory, propellers can be modeled by a series of helicoidal vortex sheets. As we are only interested in the overall performance and the effects induced on the wing, this model can be simplified to a vorticity tube model [17]. Through the use of this model, the induced velocities i.e. the axial and swirl component can be calculated and are represented below in Figure 2.4.

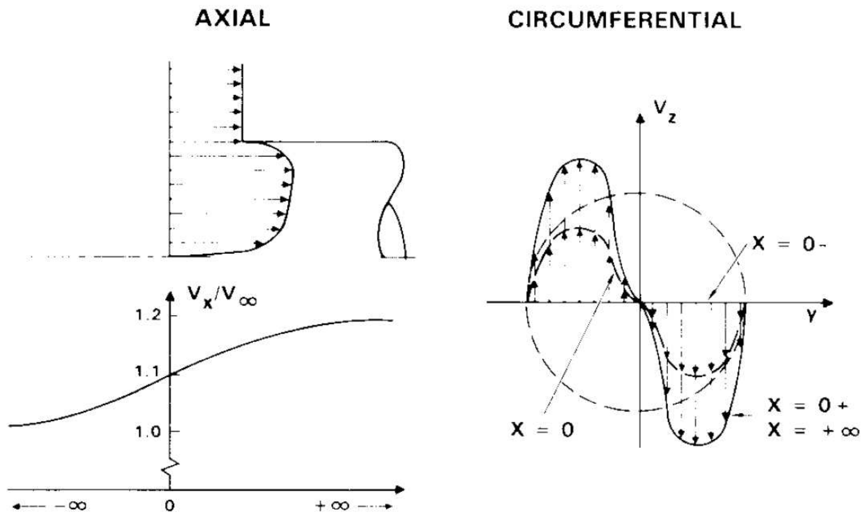

Figure 2.4.: Induced velocities by propeller vorticity tube. [17]

Although there is also a third velocity component in practice, the radial component, the incorporation of it is often left aside as it is small compared to the other induced velocities. As mentioned before, the induced velocities will alter the behavior and performance of the wing. Several studies like the one on the F-50 [31] investigated the effect of the slipstream on the wing by changing the thrust coefficient. The result was a change in the dynamic pressure and swirl angle, i.e. the local angle of attack. The scaling effect on these parameters is an important topic to keep track of. Another aspect that plays an important role in altering the performance is the inclination and position of the power plant with respect to the wing. In [30] it was found that a vertical movement of the propeller towards the wing would produce higher lift than a change in longitudinal direction. Pitching down the propeller/nacelle enhanced the lift performance even more than a vertical or horizontal variation and showed the powered wing to be more sustainable to higher angles of attack near maximum lift.

Although it is wise to keep this aspect in mind, it does not belong to the core of our problem as we best focus on scaling effects in a certain configuration (conventional without inclination).

2.3. Terminology

In this work different definitions will be used to characterize the propeller aerodynamics. As previously mentioned, the torque and thrust force can be found by decomposing the lift and drag forces onto the axis of rotation and the plane of rotation respectively. Another way of expressing them is by using the non-dimensional coefficient, as is done in our case:

- Thrust coefficient

$$C_T = \frac{T}{\rho n^2 D^4} \tag{2.9}$$

- Torque coefficient

$$C_Q = \frac{Q}{\rho n^2 D^5} \tag{2.10}$$

- Power coefficient

$$C_P = \frac{P}{\rho n^3 D^5} \tag{2.11}$$

- propeller efficiency

$$\eta = \frac{T V_\infty}{P} \tag{2.12}$$

These coefficients can also be expressed by using the non-dimensional advance ratio J. This parameter gives the ratio of the distance $\frac{V_\infty}{n}$ that the aircraft moves per revolution to the propeller's diameter D.

$$J = \frac{V_\infty}{nD} \tag{2.13}$$

3. Preliminary survey

3.1. Available propeller programs

Before starting the investigation on scaling effects in propeller testing, a verification of different propeller programs is needed in order to see if there is an acceptable program available that can give good resemblance between data from wind tunnel testing. Different reports will be used as reference and their results (i.e. C_T versus J) will be compared with the ones we get from the specific propeller prediction program. At the end a preference should then be made about which calculation approach and program serve best for the purpose of representing scaling effects on propellers. An important aspect is how accurate the effect of Re_c on propeller performance can be represented. As for all investigations where we want to analyze a certain effect, only one parameter may vary in time. In our case the change in thrust coefficient C_T for a constant advance ratio J will be used for the visualization of this effect. Since it is needed to implement the effect that Reynolds number has on the propeller, we limit ourselves to the application of Blade Element Methods (BEM).

3.2. Programs

3.2.1. PropCalc

PropCalc is a program, based on the blade element theory, that only needs a large amount of parameters to specify the design. BEM, as already mentioned, is a method where the blade is divided into small sections, which are handled independently from each other. Each segment has a chord and a blade angle and associated airfoil characteristics. The theory makes no provision for three dimensional effects, like sweep angle or cross flow. But it is able to find the additional axial and circumferential velocity added to the incoming flow by each blade segment. It offers a large edibility when specifying the data, which makes this program very useful. The lift and drag polars for example, are represented by specifying each data point separately. Further information can be found in [2]. One of the drawbacks is the limitation in Re: values above $1{\times}10^6$ can't be applied as the program only works with values up to 5 digits. This problem can actually be avoided by filling in lower values for higher polars. In this way, the effect of Re can still be visualized. A comparative study will be made with several reports, from which the most important features can be found in table 3.1. The reference data from the reports and the data from the program i.e. C_T versus J can be found in Appendix A. Our main goal is to look how well the reference data is attained with the use of the program. The results can be found in the next section, in order to make the comparison with the last program that will be discussed.

	Report 640[3]	Report 378[4]	TN 1111[5]	Report 712[6]
Diameter⌀[m]	3.05	2.89	3.72	1.22
Number of blades	3	2	2	2
β at 0.75R [deg.]	35	19	29.2	32
Airfoil section	Clark Y	Clark Y	Clark Y	NACA 4412

Table 3.1.: Specific features of propellers used in different reports.

3.2.2. Qprop

In Qprop, the analysis of the propeller is based upon an extension of the blade element theory and the incorporation of vorticity. In vortex theory, circulation is present around each blade. This circulation vanishes towards the tip and root. The blade may be replaced by a bound vortex system which, for simplicity, can be approximated by a bound vortex line. It was stated that if the distribution of the strength of the vortex along the blade, equal to Γ, is such that the energy lost per unit time is a minimum for a given thrust, then the flow far behind the screw is the same as if the screw surface formed by the trailing vortices is rigid and moved backwards with a constant velocity. In this case the circulation round any blade section is equal to the discontinuity in velocity potential at the corresponding point of the screw surface. With this statement, a calculation can be made for the circulation distribution by solving the potential problem of the screw surface. The complete elaboration can be found in [57]. It only uses a simple linear C_l-line with minimum and maximum values. For the drag characteristic a limited amount of values is used, which are fitted to form a quadratic function. An explanation of these techniques will be given in section 3.4. One would assume that because of these approximations, the result would be less accurate than with PropCalc, but the opposite is true as can be seen later on. More background information is given in [7]. Data obtained from Qprop can also be found in appendix A, together with the other data. Care has been taken that geometry, sections and blade angle distribution are the same for both programs with respect to the different reports. The results can be seen in Figure 3.1 through Figure 3.4.

3.3. Validation of the programs

With the aid of the information in table 3.1 and the polars that characterize the specific airfoils, the performance characteristics can be drawn by using the different programs. These polars can be found in the relevant papers or in airfoil databases [3, 4, 5, 6]. Several known experimental data sets are used to see what kind of general results can be expected.

We see that there is a good representation of the experiment in both Qprop and PropCalc for higher J, but the curve starts to break down on the left side. However, it can be seen that the results from Qprop give a better fit with the experiment than the ones from PropCalc. In the thesis of Momchil Dimchev [8], the focus for comparison was put on the later linear part of the curve. He concluded that Qprop gave a close match with experimental results while at lower J the results start to diverge considerably. A possible explanation is that this region is characterized by the onset of flow separation and cannot be handled accurately by BEM. It is one of the reason that we will focus on higher J for our further research. Another reason is that the literature, like the one from Dimchev, also focuses on these higher J. As an illustration, the results from Dimchev's thesis can be seen in Figure 3.5.

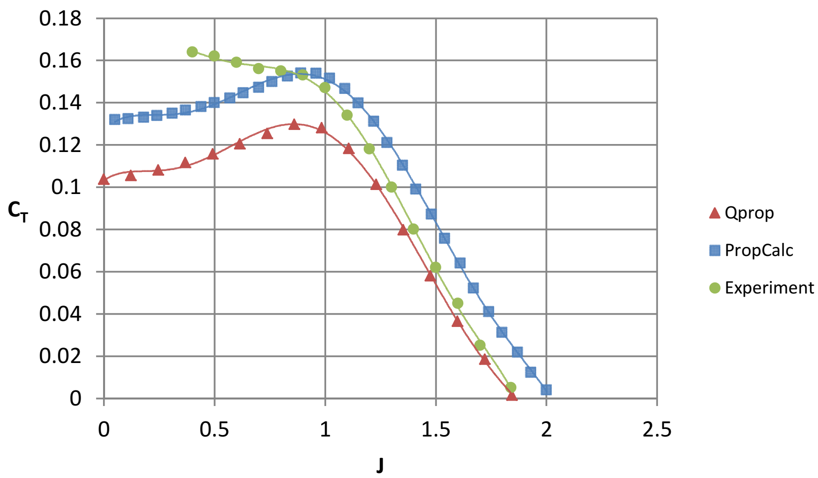

Figure 3.1.: Comparison of thrust coefficient C_T versus advance ratio J with experimental values attained from [3].

As a result, the exact same conclusion can be drawn in our case: Qprop gives a very good match with the experimental results, which is better than the results obtained from PropCalc.

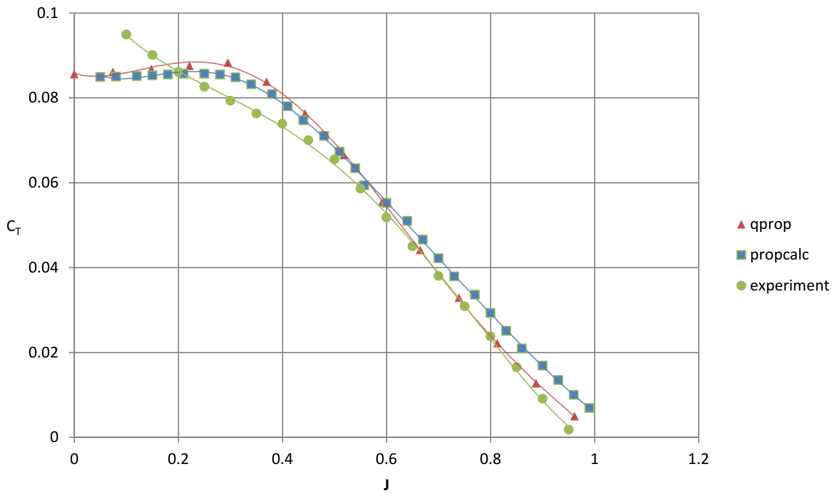

Figure 3.2.: Comparison of thrust coefficient C_T versus advance ratio J with experimental values attained from [4].

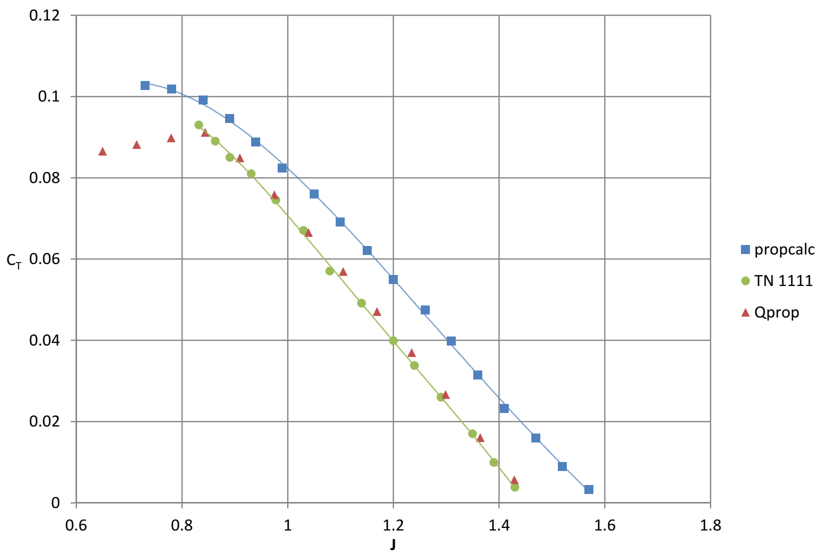

Figure 3.3.: Comparison of thrust coefficient C_T versus advance ratio J with experimental values attained from [5].

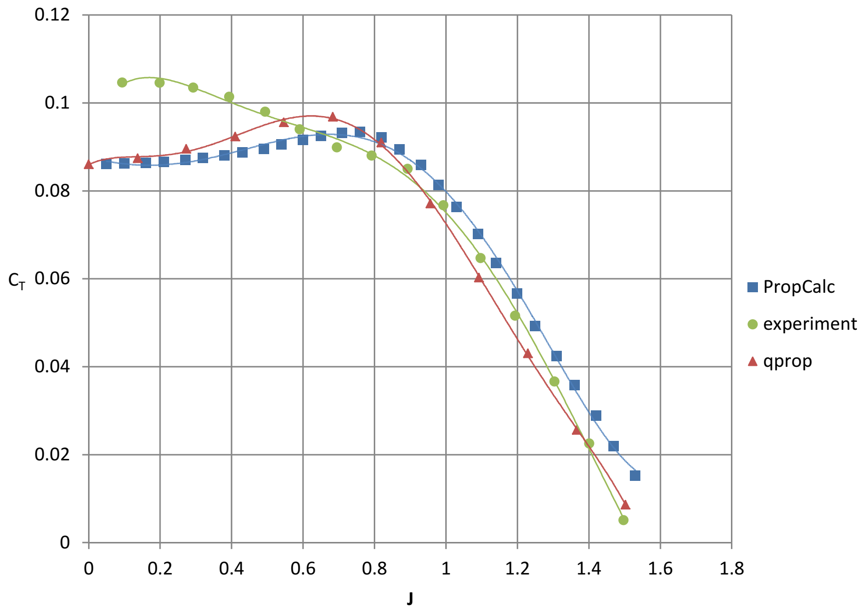

Figure 3.4.: Comparison of thrust coefficient C_T versus advance ratio J with experimental values attained from [6].

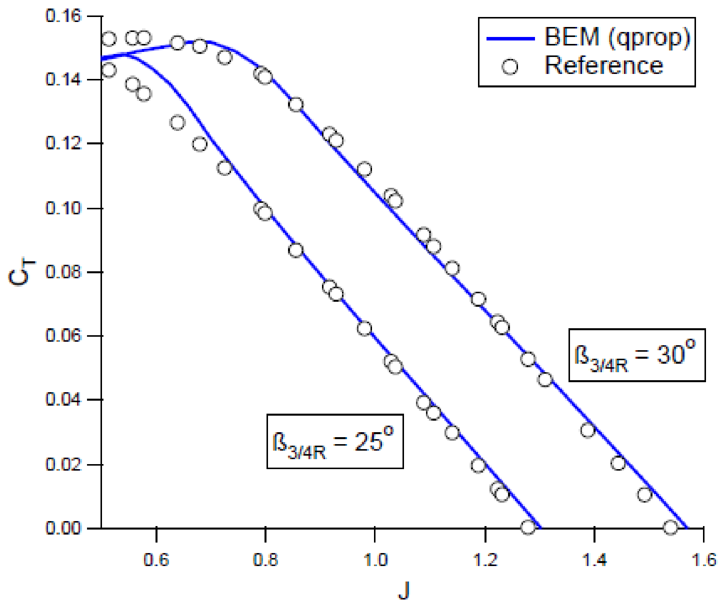

Figure 3.5.: Thrust coefficient versus advance ratio for two propeller blade angles. Figure from Dimchev[8]

3.4. Set up of selected prediction program

Based on the results of the comparison between experiment and the different propeller programs, Qprop was chosen as a prediction program for our further research, since a better match is found with the experiments.

3.4.1. Theory of Qprop

Flow velocities

In a first instance, the axial and tangential components (V_a, V_t) of the resultant velocity V_e are decomposed with the aid of Figure 2.2. Then a relation is made between the total circulation over all the blades $(B\Gamma)$ and the local swirl velocity. The total derivation of the velocities is given in [62]. The formula for V_t is given as follows:

$$V_t = \frac{B\Gamma}{4\pi r} \frac{1}{F\sqrt{1 + (4\kappa_w R/\pi B r)^2}} \tag{3.1}$$

And assuming that v_i is perpendicular to V_e, we can write V_a as follows:

$$V_a = V_t \frac{(\omega r - V_t)}{(V_\infty + V_a)} \tag{3.2}$$

Blade geometry and analysis solution

The local lift and drag coefficients are calculated together with the local blade circulation. The blade circulation for a local lift coefficient and local chord length is defined as follows:

$$\Gamma = \frac{1}{2} V_e c c_l \tag{3.3}$$

The input file contains the blade geometry (c, β), blade airfoil properties (c_l, c_d) for each radius, and operating variables V_∞ and rotational rate. With this information, the radial circulation distribution $\Gamma(r)$ can be calculated for each radius independently. This is performed by solving the preceding nonlinear governing equations via the Newton method. In this method, the solution is approximated by iterating over a certain function with a predetermined value of the solution. Rather than iterating on Γ directly, it is beneficial to instead iterate on a the dummy variable. This dummy variable parametrizes all the other variables.

Thrust and Torque relations

After applying the Newton method for each radial station, the overall circulation distribution is known. This then allows the calculation of the overall thrust and torque of the rotor. The total thrust and torque are obtained by integrating the local thrust dT and local torque dQ as defined in the previous chapter.

Analysis

The analysis problem contains the determination of the loading on a rotor of given geometry and airfoil properties, with some suitable imposed operating conditions. We still have 4 unknowns $(\Gamma, V_\infty, RPM, \beta)$. The constraints on $\Gamma(r)$ are the Newton residuals defined as:

$$\Re(\Gamma(r)) = \Gamma - \frac{1}{2} V_e c c_l \tag{3.4}$$

The other unknowns are specified at the start of the analysis. The three residuals that constrain these unknowns are then simultaneously driven to zero in the Newton iteration method.

In Figure 3.6, a flow diagram is given for clarification. It contains the different steps of the theory as explained in this section. The input for Qprop consists out of two parts. One includes the specifications for the blade geometry, number of blades, diameter and the lift-drag polars. In the other part, the three remaining unknowns are specified.

3.4.2. Data input

3.4.2.1. Definition and measurement techniques

By requiring a rather detailed description of the propeller input file, Qprop is able to accurately capture the propeller's performance. In this file the geometry can be specified for up to ten radial positions together with the number of blades and diameter. For the drag and lift polar, a specific technique is used to prescribe the aerodynamic characteristics. In Figure 3.7, it is seen that for the drag polar a parabolic fit is used and a linear fit for the lift polar. After implementation of the fitting technique, the different parameters needed for the input file can be derived.

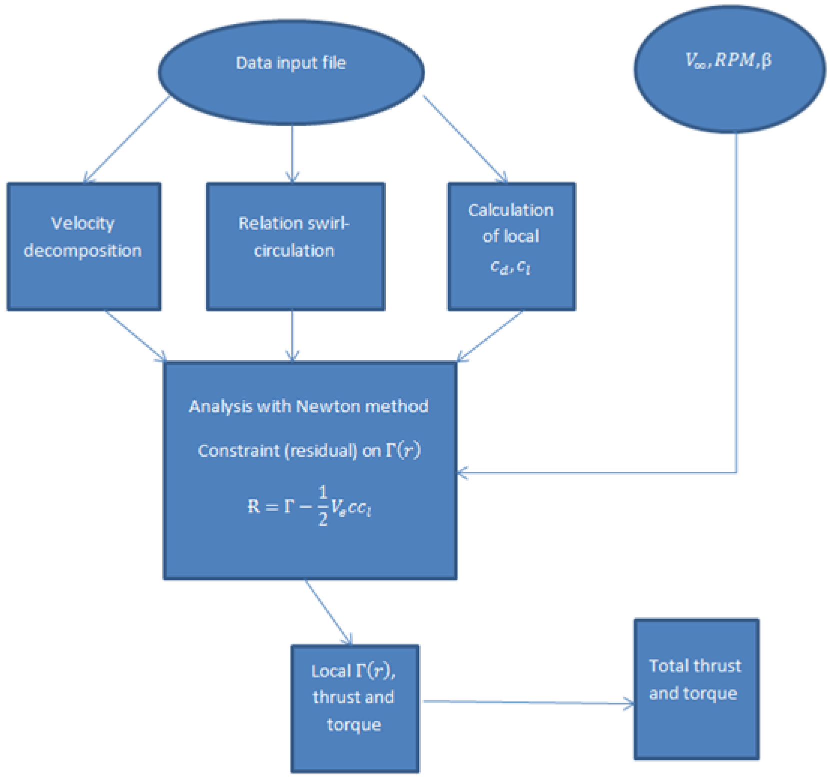

Figure 3.6.: Flow diagram for the analysis part of Qprop.

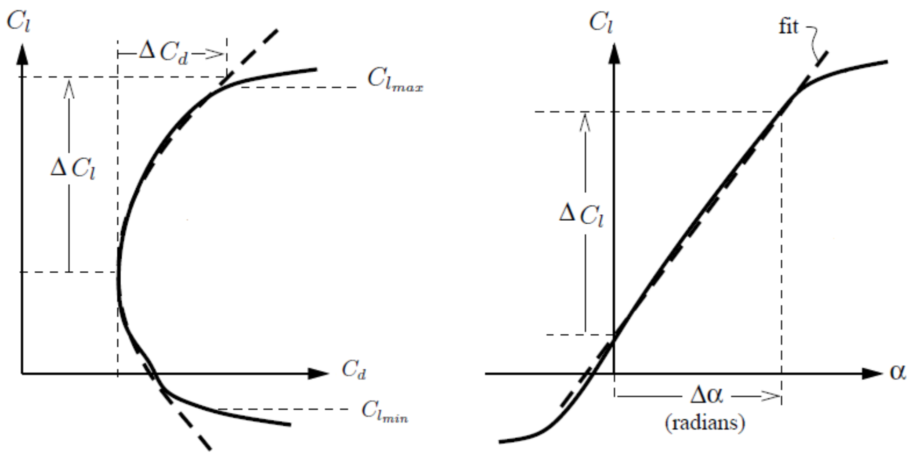

Figure 3.7.: Parabolic and linear fitting of the drag and lift polar respectively, in order to represent the aerodynamic characteristics of the blade section airfoils [34].

3.4.2.2. Reynolds influence

Qprop uses a parabolic fit for the drag polars, which could imply that the effect of a drag bucket with irregular shape becomes harder to represent in the program. This possibility is of less importance due to the fact that the irregular shapes are mostly characterized by extreme low Re as seen in Figure 1.4. The general influence of an increased Reynolds number on the drag polar, as mentioned in section 1.3, is mainly seen in a wider drag bucket and less in a reduction of the minimal value of the drag coefficient (i.e. a lower drag bucket) when comparing the WT to the FS case. In the next chapter this conclusion can be confirmed when a representation is made of the Reynolds variation.

The influence of the Reynolds number on the linear fit of the lift polar is much more pronounced: increasing Re results in a higher maximum lift coefficient, slope and zero angle of attack. These are three direct inputs in the input file. In will be seen once more in the next chapter that the Re influence of the lift polar has more effect on the performance calculations than the one of the drag polar.

4. Analysis of uninstalled propeller

4.1. Reynolds variation and limitations

First and foremost, we want to know how well typical wind tunnel tests can simulate the propeller performance data of the full scale. It is therefore important to validate how these characteristics are influenced by Re variation. It was stated in section 2.1 that when different propeller theories are combined, a clear relationship exists between thrust and torque and some fundamental coefficients. It also explains how coefficients like the lift and drag polar are influenced by the scale effect. This is the reason that in the following investigation different polars will be used and compared in the program. In this chapter a validation is made on the influence of the Reynolds effect in the propeller program. What follows is the incorporation of possible improvements to the chosen program. By doing so, we will be able to have a better understanding of the errors between full scale and wind tunnel tests as affected by differences in Reynolds number. In a next stage, an investigation is done on what this means for other areas of interest, i.e. the slipstream and the wing.

4.1.1. Re influence on propeller characteristics

In the previous chapter the choice was made to take Qprop as a standard reference propeller program since it turned out to have the best resemblance with known WT test data. Another aspect that we would like to investigate is how well the Reynolds variation is translated in the characteristics of propellers. In order to do this, the polars will be altered in Qprop as if they were affected by the Reynolds number. The results show that the errors in similarity between experiment and full scale become marginal when we increase the Re_c ($> 5-7\times10^5$) [18],[44]. This value, as mentioned before, is taken at $r = 0.75$. Unfortunately a difference remains w.r.t. the corresponding full scale Reynolds number as the lift characteristic of these high values ($> 1\times10^6$) is not reached yet. The reason being that the resistance to separation of the turbulent boundary layer increases due to a reduction of the skin friction with increasing Re_c. Note however that this improvement will occur more slowly when reaching higher values, i.e.$> 1\times10^6$ [18]. In representing the Re influence, we need to bare in mind that in general the lift decreases both in slope and maximum value with decreasing Re_c. On the other hand, the drag coefficient increases, mostly on the 'sides' of the drag bucket. This can be seen with the aid of

Figure 1.4 and [9]. In [9], different polars are given for specific Reynolds numbers and the influence on the performance characteristic can be seen in Figure 4.1, with the aid of Qprop. The geometry of the propeller is given in Table 4.1[1]. The polars from [9] are used and can be seen in Figure 1.4.

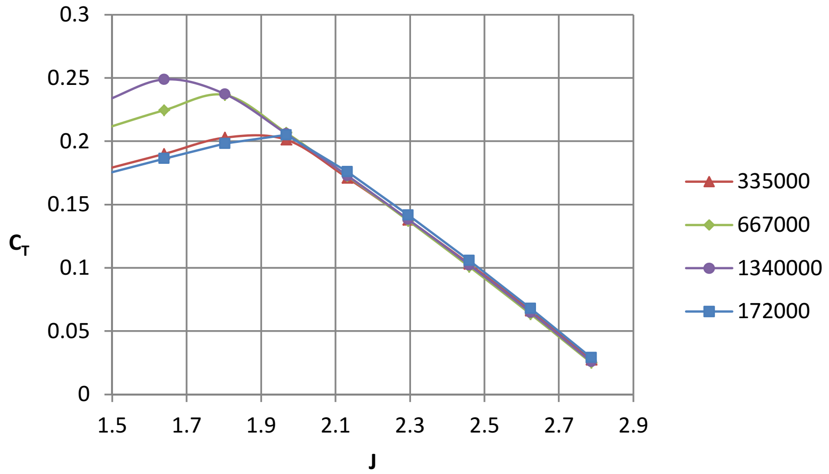

Figure 4.1.: Propeller performance characteristics affected by different Re_c numbers.

$\frac{r}{R}$	0.2	0.3	0.4	0.5	0.6	0.7	0.8	0.9	1.0		
chord [mm]	25	51	77	91	99	100	92	72	3	Diameter$\varnothing$[m]	2.2
β [deg.]	79	73	67	62	57	52	48	45	42	Number of blades	6

Table 4.1.: Geometry of propeller used for the representation of Re_c effect.

In this particular case, the influence of Reynolds number remains small since the differences between the polars are also rather limited. In Figure 4.3, we take the case where the Re_c is equal to 1.72×10^5 and make visible adaptions to the polar in order to see the influences on the performance characteristic. These adaptations are based on data, found in [9]. Here, different polars are given that are characterized by different values of Re for typical (propeller) sections. It then becomes easier to see the influences of the polars on the performance characteristic. These adaptations are illustrated in Figure 4.2.

From Figure 4.3, it becomes clear that the main differences are caused by a change in the maximum lift coefficient and lift slope. We can then assume that the lift adaptations have the most influence in Qprop, although a change in drag polar can still cause some changes.

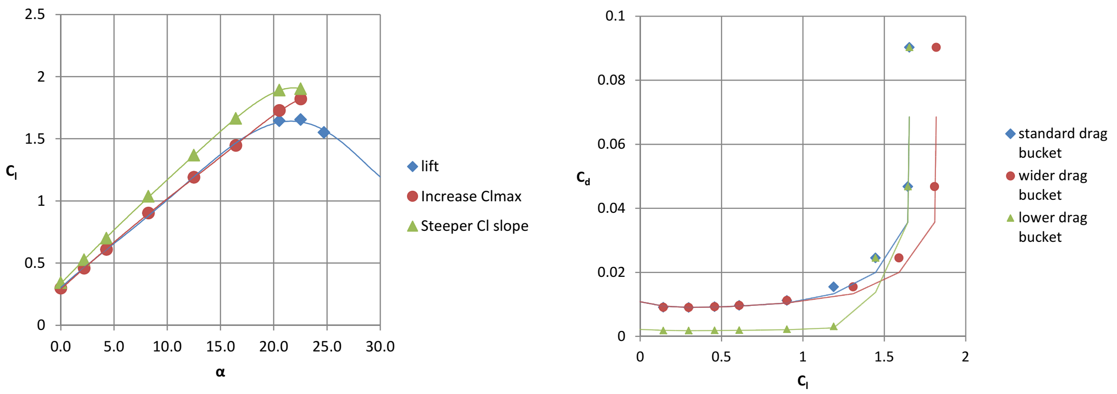

Figure 4.2.: Different type of adaptations in the lift and drag polars.

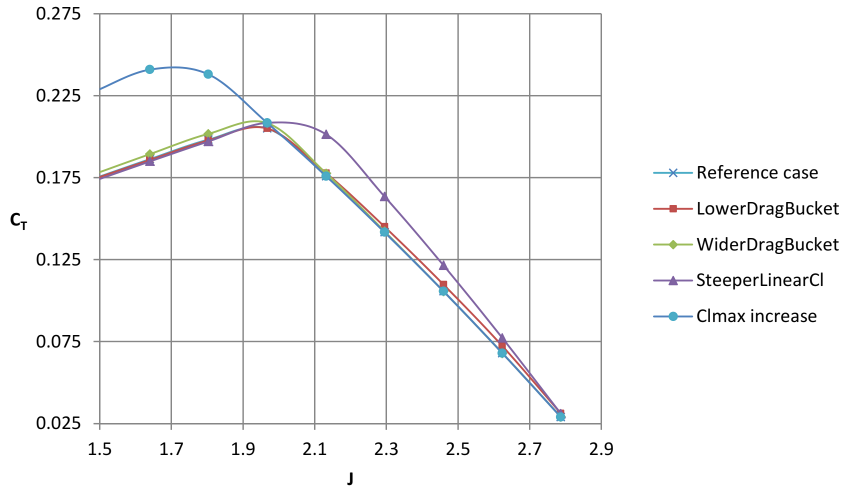

Figure 4.3.: Influence of polar adaptations on the propeller performance characteristic with reference case, Re_c equal to 1.72 $\times 10^5$.

4.1.2. Improvements

In chapter 3, Qprop was chosen because of its good representation of experimental data. For low advance ratios however, it was explained that the difference with test data was significant and not even representable. Different flow phenomena that characterize propellers are not included in the program since we only use a basic model. One can anticipate that building the effect of these phenomena into the program will possibly lead to an improvement for the higher advance ratios.

4.1.2.1. Stall delay

One of the phenomena that was first observed by Himmelskamp [10] was a rotational effect called stall delay. An explanation of this phenomena, characterized by an increase in lift curve, was given in the introduction. Several general rules have been made to represent this increase in lift coefficient. In [61], different correction methods were analyzed in order to include the rotational effects on aerodynamic coefficients. Although similarity was found, some methods needed insight in the amount of rotational augmentation or depended strongly on the maximum lift coefficient. Therefore, the correction model of Snel, Houwink and Bosschers was used [11]. In their model, the correction is proportional to $(\frac{c}{r})^2$:

$$C_{l,rot} = C_{l,2D} + 3(\frac{c}{r})^2(C_{l,pot} - C_{l,2D}) \tag{4.1}$$

To put this improvement to the test, the correction model was implemented into the data of some earlier reports. Figure 4.4 shows how this model alters the lift polar for a specific airfoil-type, i.e. the Clark Y airfoil, used in many of our propeller tests. The correction was applied up to 60% of the radius since the improvement is very small for larger radii, as can be seen in Figure 4.4. The same conclusion was made in [61]. The results that include the implementation of this correction are shown in Figure 4.5 to Figure 4.8.

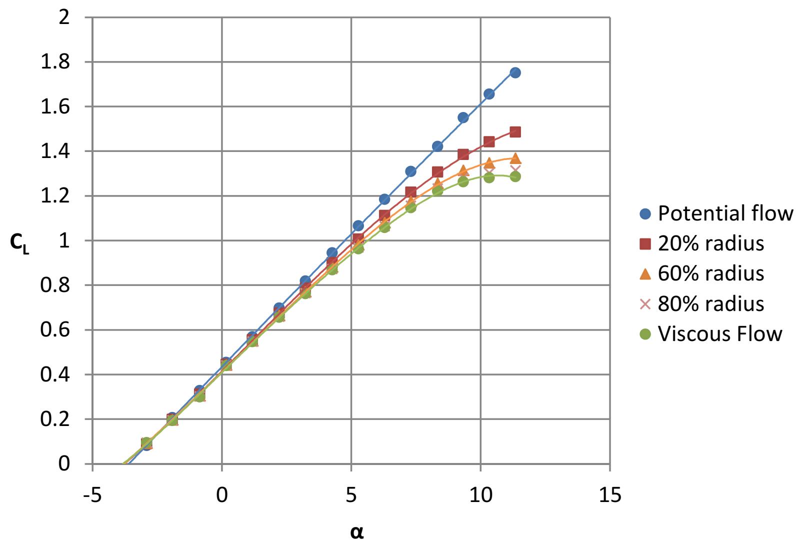

Figure 4.4.: Application of the correction model according to Equation 4.1 for the lift polar of the Clark Y airfoil (viscous flow).

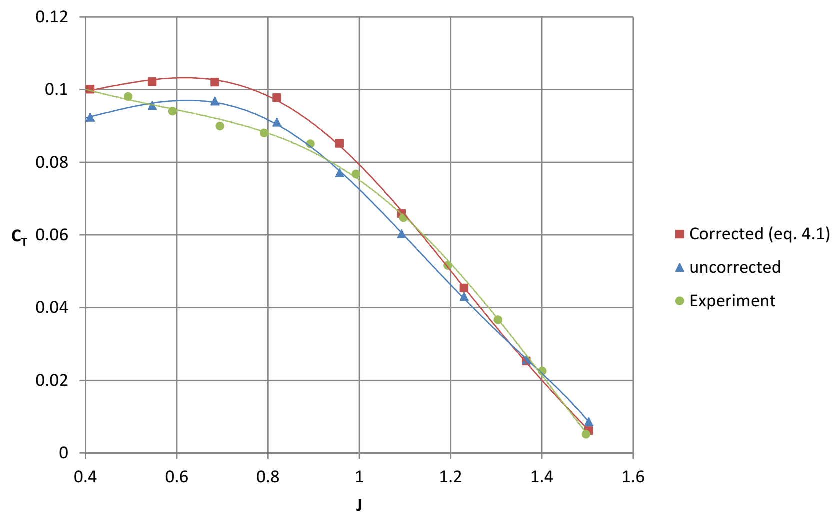

Figure 4.5.: Comparison of the Himmelskamp correction in Qprop with experimental values attained from [6].

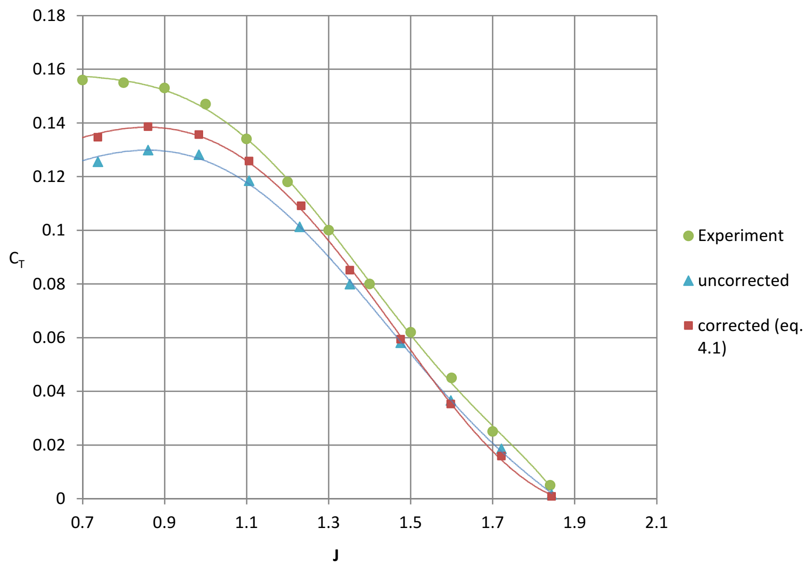

Figure 4.6.: Comparison of the Himmelskamp correction in Qprop with experimental values attained from [3].

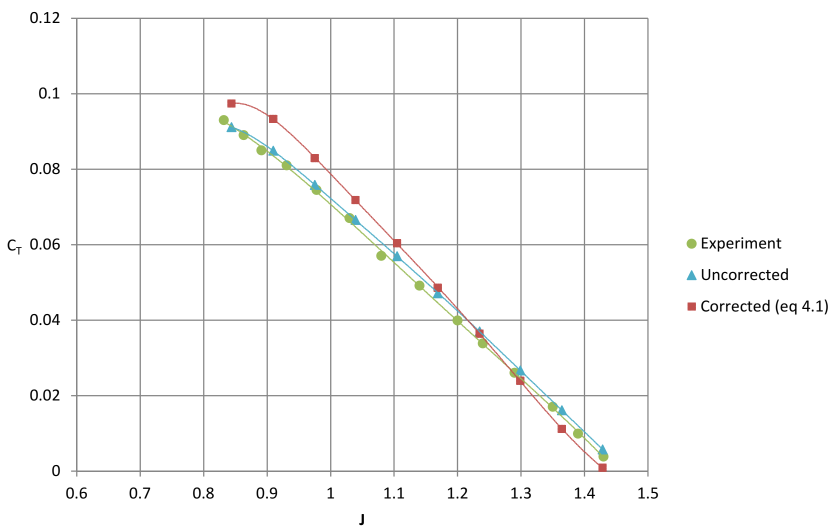

Figure 4.7.: Comparison of the Himmelskamp correction in Qprop with experimental values attained from [5].

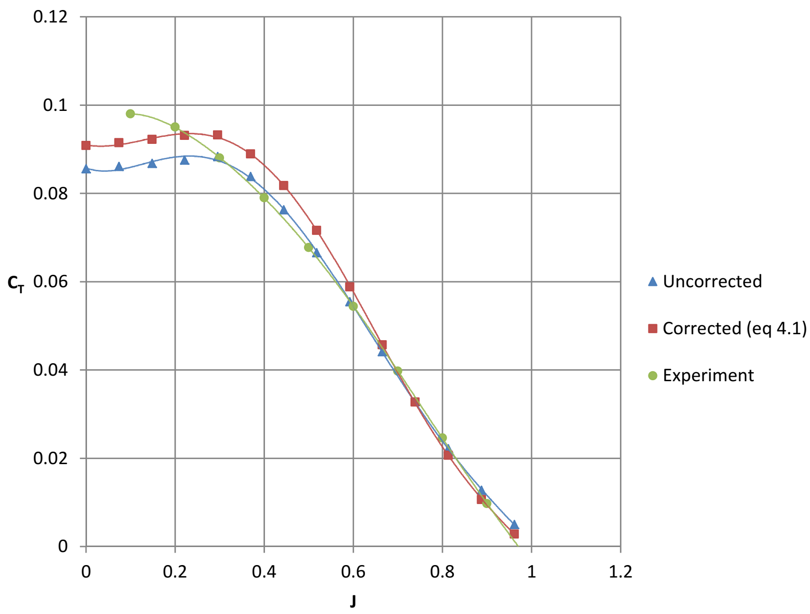

Figure 4.8.: Comparison of the Himmelskamp correction in Qprop with experimental values attained from [5].

It appears that the correction gives an improvement for two propellers. In the other two cases, the representation in Qprop was almost perfect, meaning that the use of the correction would only decrease the resemblance with experiment. When investigating other literature in the next section, it is wise to analyze every propeller case separately before we decide to incorporate the correction model. Looking to Figure 4.4 and the elaboration below, a possible explanation can be given as to why the correction for lower J is possibly larger as the one for higher J. It states that for lower J, larger values of α are found. This implies that the correction of the Himmelskamp effect will have more influence at lower J.

$$\varphi = arctan(\varphi' + \alpha_i) = arctan(\frac{V_\infty + V_a}{\omega_p r_p - V_t}) = arctan[\frac{J}{\pi}(\frac{1+a}{1-a'})] \tag{4.2}$$

$$(\varphi = \beta - \alpha), \;\; J \downarrow \Rightarrow \alpha \uparrow \tag{4.3}$$

Where a is the axial inflow factor and a' is the angular inflow factor. The elaboration is made with the aid of Figure 2.2.

4.1.3. Point of observation

A small observation is made when looking at the analysis of the different reports. In Figure 3.5, a comparison is made between Qprop and references of Dimchev's thesis [8]. We can see an over- or under scaling between the data depending on the fact that the β angle at 0.75 radius was larger or smaller than a certain value. As a crude rule for this observation, $\beta = 27°$ can be taken. Looking back at the data of Qprop and our reports, we see a similar trend: the Qprop thrust values are over predicted with respect to the reported test data when $\beta \leq 27°$ and vice versa. A possible explanation for this phenomena could be the Himmelskamp effect. The cross flow component over the blade will increase when β is increased. This leads to a larger effect of the Himmelskamp effect on the flow. The difference between experiment and Qprop for larger β could therefore be caused by the lack of the incorporation of the Himmelskamp effect.

4.2. Validation and investigation with Qprop

In the earlier sections a useful propeller program was put forward in order to have a reliable basis for the investigation. Some improvements and influences in the program have been explained. The program will now be used to validate the difference between the scaled wind tunnel models and the full scale cases. As a next step, we will investigate the differences in the performance characteristic that are caused by this offset in data from the different test cases. More specifically, the focus is put on the axial and swirl velocities of the rotor disk and how the results change as a consequence of the shift between model and full case.

4.2.1. Validation of the propeller performance (WT-FS)

4.2.1.1. Consistent difference between data

In order to do the validation, literature [12] is used where the focus was put on the comparison of propeller tests between in-flight and wind tunnel models. The data will be put in graphs first, followed by a representation in Qprop. The full scale equipment included five propellers in combination with a VE-7 airplane and the coefficients of interest were derived according to section 2.3. The model part was carried out at the aerodynamic laboratory of Standford University and the corresponding coefficients and elements of performance were directly measured. In Figure 1.7, the geometry was already presented for one propeller.

The representation in Qprop will be done for all five propellers. It can be seen in [12], that the thrust coefficient (but also the power coefficient) for the full scale is about 6 to 10 percent larger than the one derived from model tests with a mean around 8 percent. This difference appears to be too large and consistent to be attributed to experimental or accidental error [12]. In the paper it is noted that three different causes appear for the consistent difference between full scale and model tests.

A. The scale effect. It could be stated that this actually represents the Reynolds influence in the tests as an increase in Re tends to increase/shift the lift polar in a beneficial way. This was already mentioned in subsection 4.1.1. The scale ratio of the full-size propellers and the models is 2.72 and the freestream velocity for full flight is about three times the one for the models. This means that $V_\infty l$ for the sections of the full flight is about eight times the one for the model. If the formula

$$C_{l_{FS}} = C_{l_{WT}} + 0.057 * log\frac{V_{\infty_2} l_2}{V_{\infty_1} l_1} \tag{4.4}$$

is applicable, the increase in life coefficient for the full scale sections is such as to increase the thrust and power about the 8 percent experienced. This formula is the result of an investigation by Diehl [13] into the effect of changes in size and speed upon the airfoil lift and drag coefficient and it was used in [12] to represent the difference between WT and FS.

Using this adaptation in our formula, good resemblance can be seen in the graphs of the next section.

In Qprop we saw that it was merely the lift polar that influenced the change in data when small changes were made, for example under the influence of Reynolds number variation. And again in this paper, only an adaptation in the lift coefficient is prescribed to deal with the scale effect. Yet another indication that this makes up for the bigger part of the deviation between the different data.

B. Difference in geometry between model and full scale. In the case of the model tests, the propeller shaft is parallel and constant to the flight path whereas for the in flight tests the propeller is generally in yaw due to the angle of the propeller shaft. It appeared that the effect of this yaw is to increase both power and thrust absorbed.

C. Lack of complete similarity between model and full scale. For the model tests, the tail surfaces and rear portion of the fuselage are omitted. It is observed that at distances one to one-half diameters of the propeller an effect is produced on the propeller which stays within the error of observation. On the other side it is found unlikely that the interference of the slipstream with the tail surfaces would have any influence on the shaft thrust.

Knowing that we do not use the data for the combination of propeller and airplane but only the data for the propeller-alone case, and the geometry is perfectly scaled between model and full scale, we do not need to incorporate the effects of B and C as a possible cause. Before doing so, it is wise to investigate the contribution of

Himmelskamp and see what effect it has on the match between the data from Qprop and the paper [12]. On the other hand, the Himmelskamp effect doesn't guarantee that better data will be found for comparison with this paper.

4.2.1.2. Contribution of Himmelskamp to the validation process

It is evident that a good match for the literature is sought in Qprop. One would therefore assume that the incorporation of the Himmelskamp effect in the data is necessary. However caution should be paid when making this decision.

In the next figures, i.e. Figure 4.9 and Figure 4.10 ,two sets of five different performance data are given for a specific propeller, i.e. propeller B.

Figure 4.9 gives the first performance data set:

- full scale and model case of the NACA paper (Experiment FS & Experiment WT)
- the data for the model case without Himmelskamp effect which is put in Qprop (Uncorrected WT)
- the data that represent the full scale case in Qprop in theory (Uncorrected FS Theory)
- data for the full scale case in Qprop, which is obtained by using Equation 4.4 (Uncorrected FS)

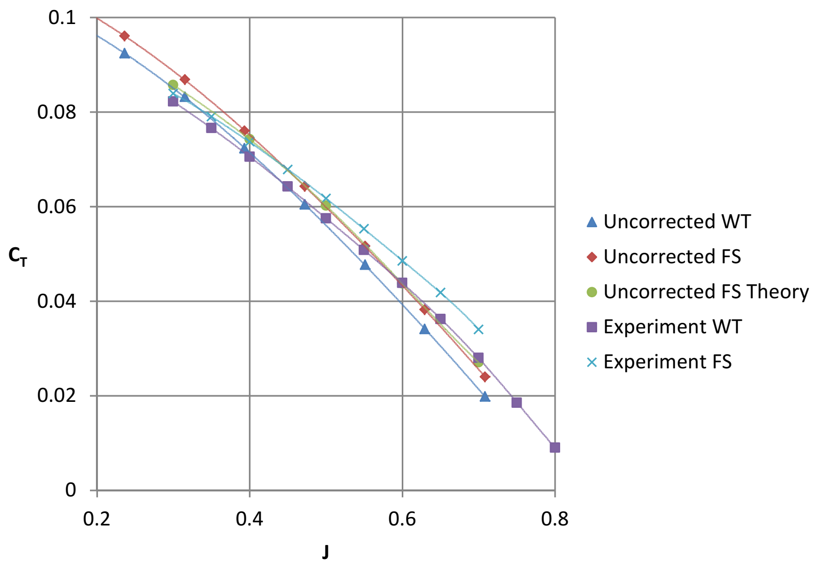

Figure 4.9.: Comparison of WT and FS case in Qprop with experimental values attained from propeller B in [12].

Figure 4.10 gives the second performance data set:

- full scale and model case of the NACA paper (Experiment FS & Experiment WT)
- the data for the model case with Himmelskamp effect which is put in Qprop (Corrected WT)
- the data that represent the full scale case in Qprop in theory (Corrected FS theory)
- data for the full scale case in Qprop, which is obtained by using Equation 4.4 (Corrected FS)

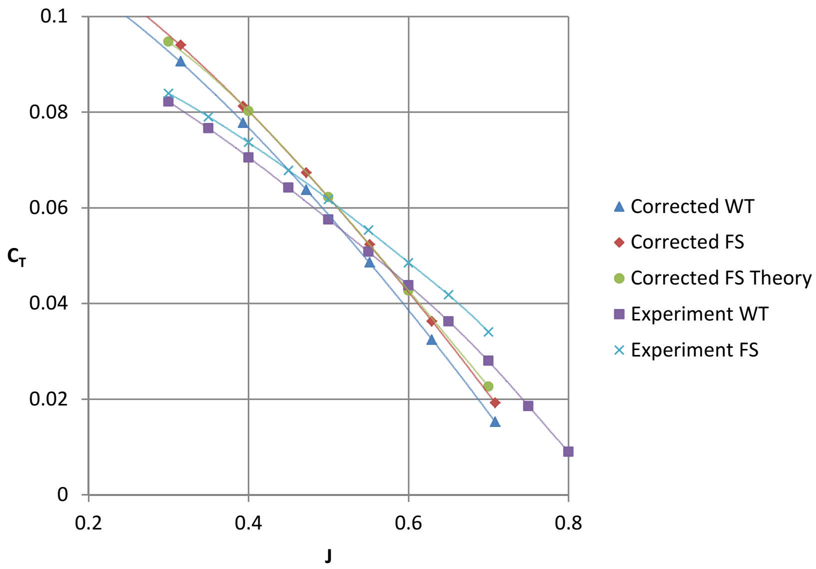

Figure 4.10.: Comparison of WT and FS case in Qprop when the Himmelskamp effect is included with experimental values attained from propeller B in [12].

Although Himmelskamp appeared to have a positive effect in some cases of our previous investigation, it gives a few unwanted deviations in this case. On one hand, an overshoot is seen for the higher values of the thrust coefficient. On the other hand, for larger values of advance ratio, the differences almost remain the same as it is merely seen in a change of the slope. Because of the important fact that we focus on larger values of J and knowing the negative effects such as overshoot and a small deviation in the slope, we state with certainty that the evaluation of the data can be done without the incorporation of the Himmelskamp effect. Important to note here, is that this decision can be different for other investigations, as the focus of interest may differ.

Deviation between experiments and Qprop

In the investigation of the five propellers, there is a small difference in the performance characteristic between the actual values of the paper and Qprop. As the correction for the Himmelskamp effect didn't give the expected improvement, other reasons should be sought for this lack in resemblance. In what is next to come, a possible explanation is brought forward, based on the only uncertainty in our data input: inconsistent data for the same type of airfoil. One of the more obvious reasons could be the use of incorrect data of the airfoil. More specifically, we focus on the parameters that characterize the polars in Qprop. When looking at different papers as [14],[15] and [59], we come across small differences in the parameters that are used to characterize the lift polar in Qprop. It is actually the extraction of the aerodynamic characteristics like polars that is not straightforward in Qprop when comparing it to others. It was noticed in chapter 3, that for other programs the large edibility of the data could be very useful. Unfortunately in Qprop a careful interpretation of the lift and drag polars is needed since small changes in the values can result in unexpected deviations of the propeller coefficients. The main reason, as already mentioned in subsection 3.4.2, is that it uses specified fitting techniques to determine the aerodynamic characteristics, assuming a parabolic fit for the drag polar and a linear fit for the lift polar.

The difference in lift polar between literature is certainly seen in the lift coefficient at the zero angle of attack. Looking at paper [59], values of 0.45 and higher are noticed. It is important to keep in mind that our test data is situated around values of chord Reynolds number of ~3.4×10^5. In Appendix C, an exact overview of the *Re* range for WT and FS is given. By implementing the increase at zero angle of attack in our data set from Figure 4.9, a better match can be found for the larger values of J. This was already concluded in chapter 3, when doing the comparison of different programs and can be seen in Figure 4.11.

This aspect could be an improvement to our data in this specific case, but it might not be necessary to take this into account for the following reasons. On the one hand we are not sure about the exact cause of the difference, although we have enough reason to assume that an augmentation of this lift parameter is justified. On the other hand we are trying to get an insight in the quantity of error in thrust coefficient between full scale and model tests w.r.t. the total thrust coefficient. This means that the exact value is of secondary importance in our investigation. With this in mind, a further evaluation can be made with our Qprop data.

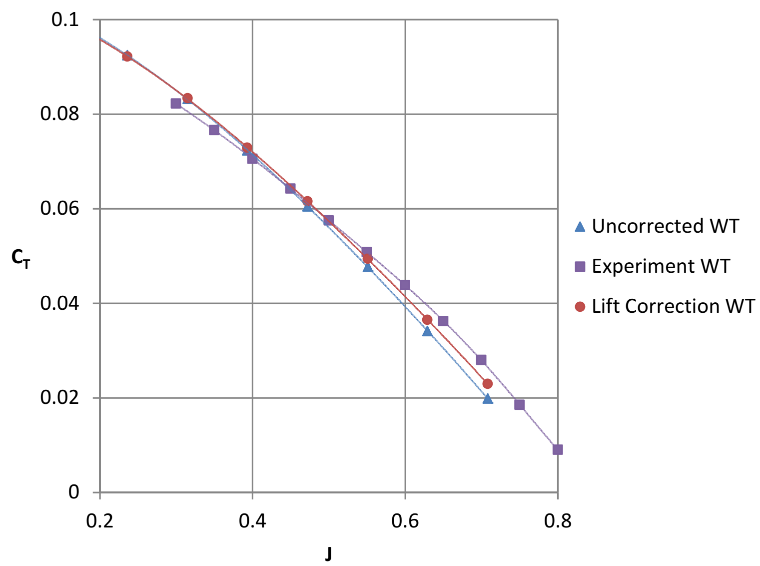

Figure 4.11.: Incorporation of a lift augmentation at zero angle of attack for propeller B [12].

4.2.1.3. Evaluation of the first performance data set

All the data without Himmelskamp effect will now be compared in order to understand the general differences. This is needed for our next purpose, i.e. translating the differences found in these data to differences in velocity. These velocities, as already mentioned, are the axial and swirl (tangential) velocity. It can already be said that because there is still a difference between the paper and Qprop, the quantity of the difference with respect to the total value is of first importance, rather than the actual values that are obtained.

In Figure 4.12, it can be seen that by using Equation 4.4, almost a perfect match is found in Qprop with the theoretical data for FS. If there is still a 'gap', it is most likely caused by other aspects as mentioned earlier. Again it remains important to note that we focus on a narrow band of higher advance ratios for two reasons. On the one hand the paper only gives values of higher advance ratios, where on the other hand it was already stated by Dimchev [8] that for higher J, Qprop is more likely to give a good resemblance with the reference data.

The entire procedure, here shown for propeller B in section 4.2, is repeated for the other four propellers (D, I, K and L) in Appendix C.

For one propeller, i.e. propeller D, this procedure doesn't give the expected result. The reason is that the results in [12] are already different from the rest. The general conclusion in the paper was an increase in thrust coefficient for the full scale case. Unfortunately for propeller D this is not case and the data for the full scale case is for the greater part found below the values of the model tests. This means that

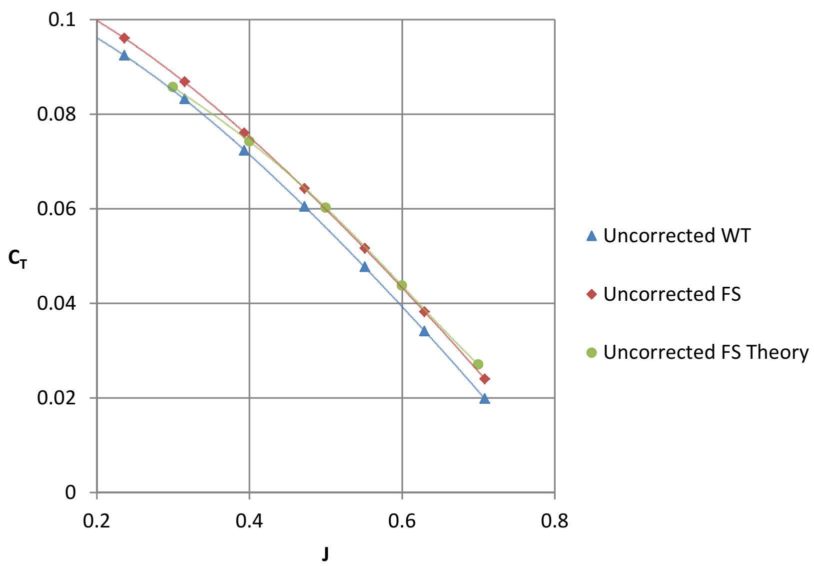

Figure 4.12.: Qprop data of propeller B for WT and FS case with formula Equation 4.4, used to represent the FS case.

the use Equation 4.4 has an opposite effect as it would only increase the thrust coefficient. Despite this exception, good results are obtained for the other propellers in Appendix C.

4.2.1.4. Transition position

Last but not least we did speak about the topic of free and fixed transition. The question was brought up if fixing the transition position in wind tunnel tests would alter the results in such a way as to improve the resemblance with the full scale case. As the position of transition alters the flow over the blade, it is interesting to take a quick look at the effect it would have on our performance data of the previous section. The interest in altering the transition position originated from the fact that fixed transition was used on wing airfoils at low *Re* in order to get a better representation of the flow behavior that corresponds to the full scale case. Lowering the chord Reynolds number gives rise to unwanted flow phenomena and it moves the position of transition backward. It was therefore argued that by fixing the transition position in the chordwise direction, good agreement could be found with the free flight condition. But caution should be paid when extending this argument to propellers. An investigation of the transition effect for propellers was done by Giguere and Selig [14] for different airfoils that can be used on horizontal axis wind turbines. In order to simulate the leading-edge roughness, they fixed the airfoils with zigzag trip tape at 2% chord and 5% chord on the upper and lower surface respectively. The trips would promote early transition over a considerable distance along the airfoil. The data with fixed transition position simulates the roughness effects, as opposed to the results for free transition. The focus was put on the percentage difference in performance parameters between fixed and free transition, i.e. $(C_l/C_d)_{max}$ and $C_{l_{max}}$. For our specific airfoil, Clark Y, the decrease in these parameters is 49.4 % and 16.5 % respectively. For different airfoils in general, the average decrease is found to be around 47 % for $(C_l/C_d)_{max}$ and a small but positive decrease for $C_{l_{max}}$. A new input file was made where the drag and lift polar are altered according to the data in [14], illustrated in Figure 4.13 and Figure 4.14.

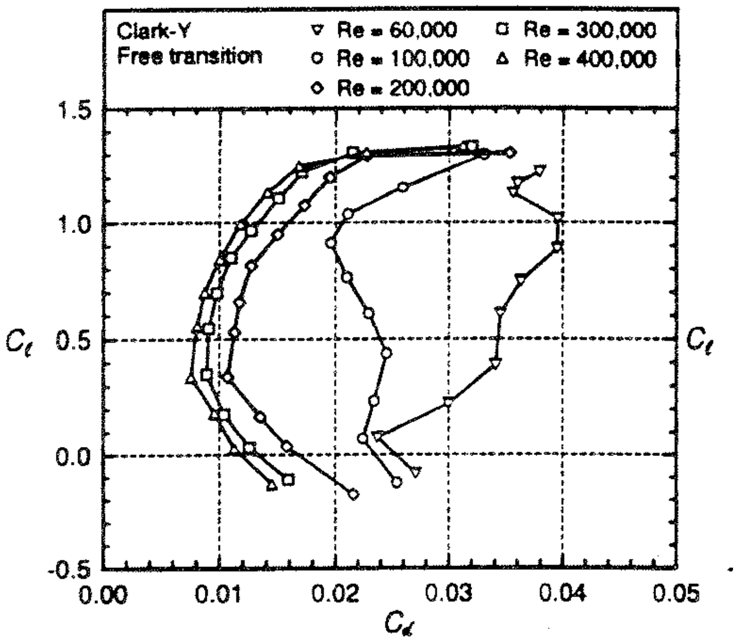

Figure 4.13.: Drag polars for the Clark Y airfoil for different values of *Re* (free transition). Figure from [14]

Another paper [15] confirms this trend from Selig [14]. Here it is also noticed that a downward shift of the entire lift curve together with an upward shift in the lower part of the drag bucket is noticed when fixing the transition to a forward position.

Even without the investigation in Qprop it can be seen that as the performance parameters decrease, it is especially the thrust coefficient that will decrease for a given advance ratio. This is a general consequence in the investigation when the transition position is fixed to a forward position.

If we then take a look at Figure 4.15, it can be seen that the graph shifts in a downward direction. This is completely the opposite of the results obtained for full scale tests. For this reason, fixed transition is not a good option in order to get better resemblance with the full scale case.

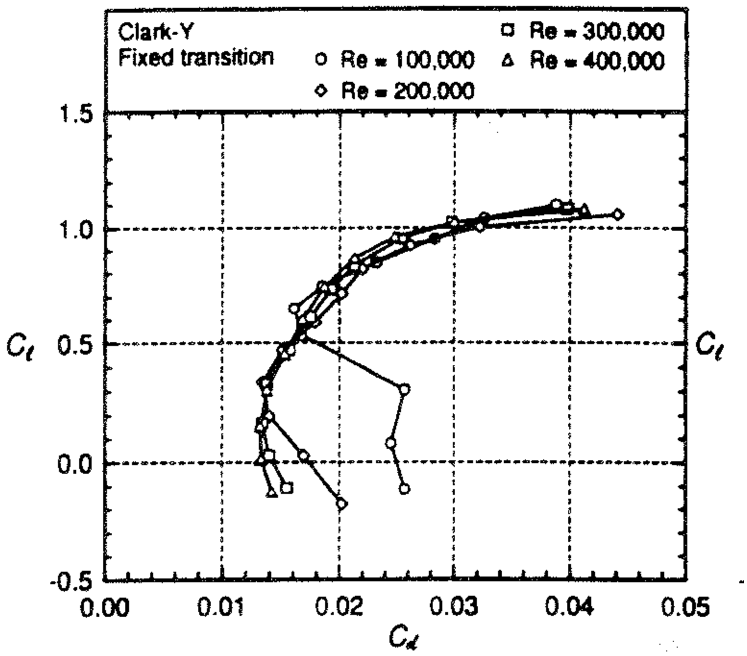

Figure 4.14.: Drag polars for the Clark Y airfoil for different values of *Re* (fixed transition). [14]

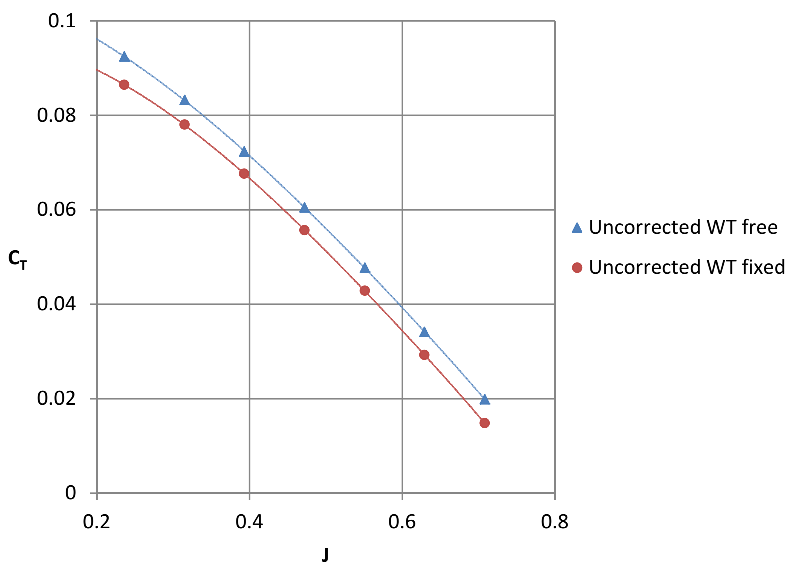

Figure 4.15.: Effect of fixed transition on performance data in Qprop for propeller B using data from [14].

4.2.2. Investigation with the propeller performance (WT-FS)

4.2.2.1. Change in induced velocities of the propeller

As the differences in performance data between the full scale and model tests are understood, our point of focus shifts to the consequences for the specific velocities of the propeller. To do this, a good understanding of the relations between certain parameters is needed. From Figure 4.16, one can conclude that it is impossible to keep all the parameters of an experiment equal to the ones in full flight. For example, if the advance ratio is kept constant (red line), a shift in thrust coefficient is seen between the two cases. Or in other words, if in our program a certain performance curve is given for a propeller, another curve can be set up by using the average known shift in C_T. This other curve then represents the full scale case.

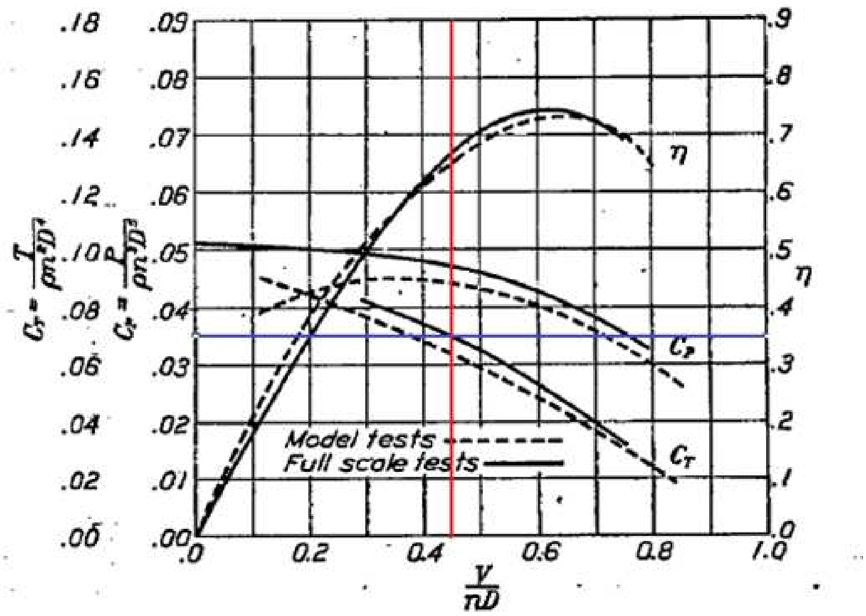

Figure 4.16.: Illustration of different options to attain resemblance between full scale and experiment [12].

From basic theory, two quantities of interest for propellers are the thrust and torque. It was already explained that they both depend on the same parameters (i.e. lift, drag etc.). This means that as the thrust coefficient changes, the torque coefficient will change as well. A direct result of these changes is a difference in both tangential and axial velocity. In [17], it was depicted that the wing will experience swirl velocities that initiate from the propeller and result in a deformation of the lift distribution. Through the use of a vorticity tube model the induced velocities can be calculated and were illustrated in Figure 2.4. In this paper the effect of the slipstream on the wing was investigated by changing the thrust coefficient. Because the thrust coefficient is changed, both the dynamic pressure and the swirl angle, i.e. the local angle of attack, will change. In our study similar investigations are made; different thrust coefficients, corresponding to experiment and full scale, are used to examine the differences in slipstream parameters like the swirl velocities for example. These differences, as already mentioned, will be used to investigate the changes noticed by the wing, i.e. the local angle of attack between full scale and experiment. In doing so, use is made of a program that takes the interference between propeller and wing into account (chapter 5).

Test case propeller B

To start the investigation, we take a certain case for which J is constant in order to analyze the shift in C_T. At a value of $J = 0.45$, we examine the data for the induced velocities, both for Uncorrected WT and Uncorrected FS. Figure 4.17 shows the shift in axial velocities, while Figure 4.18 shows the shift in tangential velocities. The corresponding values are given in appendix B. Note that at the boundary, i.e. at the tip and root, the values tend to go to zero. In [17], a tendency towards a smaller axial velocity than the free stream can be seen towards the root. It is probably a direct consequence of the presence of the hub, which gives smaller velocities than the free stream since it blocks the passage.

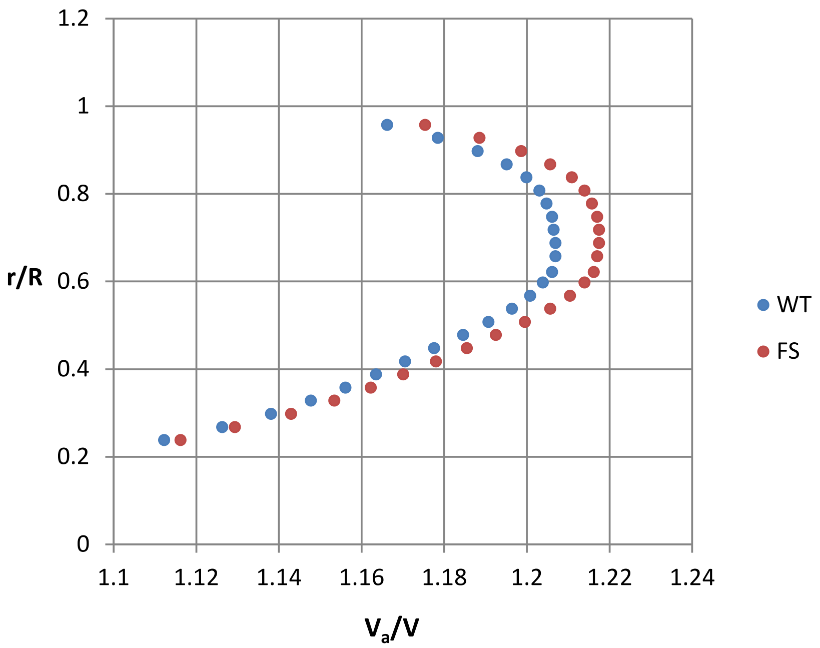

Figure 4.17.: Axial velocities in function of the radial position for WT and FS case for propeller B.

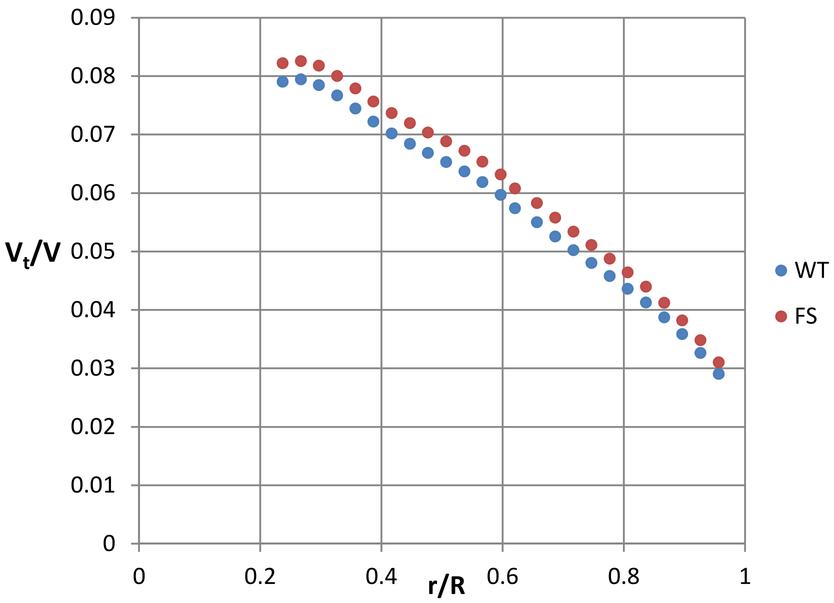

Figure 4.18.: Tangential velocities in function of the radial position for WT and FS case for propeller B.

When we look back at Figure 4.12, we notice that for our particular value of J, the correction formula [13] makes up for almost the entire difference. In this case, going to lower values of J, we lose the good resemblance and for values of $J \leq 0.45$ we get an overshoot of our Qprop values. This means that the data we receive will be aggravated w.r.t. the real data. With the aid of the figure, a fair estimate of the over- or undershoot can still be made.

As the induced velocities change, we notice a difference in the local inflow angle. This can be seen with the aid of Figure 2.2, where the angle $\varphi = (\varphi' + \alpha_i)$ will change as both V_t and V_a increase. Figure 4.19 shows the difference between WT and FS for propeller B. A similar shape and difference between the data can be found for the other propellers in Appendix D.

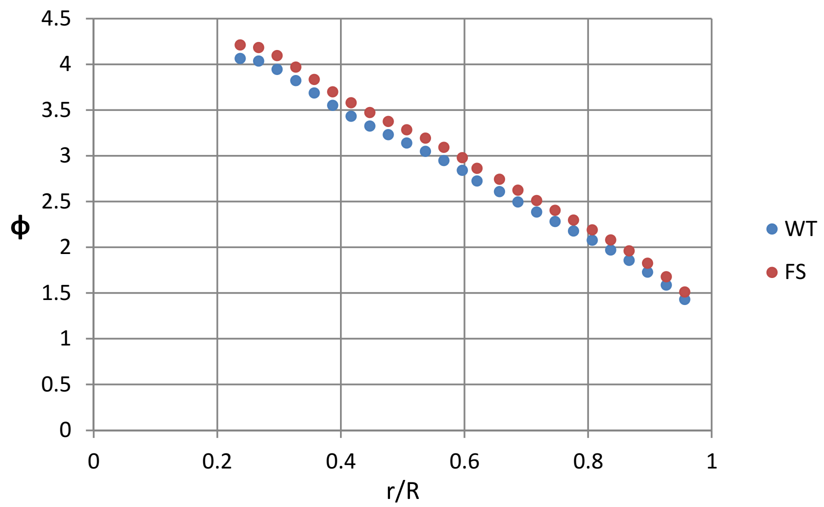

Figure 4.19.: Inflow angle in function of the radial position for WT and FS case for propeller B.

4.2.2.2. Choice of constant parameter

It was shown in Figure 4.16, that for a certain constant advance ratio (red line) the thrust coefficient has to be altered in order to get a match between full scale and experiment. Until now the focus was put on a constant J, whereas we could also ask ourselves whether a constant thrust coefficient (blue line) would be better.

In order to do this we will again use propeller B from the NACA report as an example [12]. The induced velocities for both constant advance ratio and for thrust coefficients will then be compared in Qprop. This sequence will hereafter be repeated for the other propellers in order to come up with a general recommendation. In the following figures, the induced velocities in the slipstream are compared for the two choices of constant parameters. Some interesting outcomes can be noticed. Looking to Figure 4.23, it seems that by keeping the thrust coefficient constant and altering the advance ratio, a smaller difference is found for the outer values of the tangential velocities. By keeping C_T constant, an overshoot is found for the wind tunnel data w.r.t. the full scale case, instead of the lower value found at constant J. Aside from these observations, it can be concluded that in general a larger deviation is found between FS and WT when C_T is kept constant. The choice of taking a constant J seems to be justified, as there are less fluctuations between the velocities of FS and WT over the radius position.

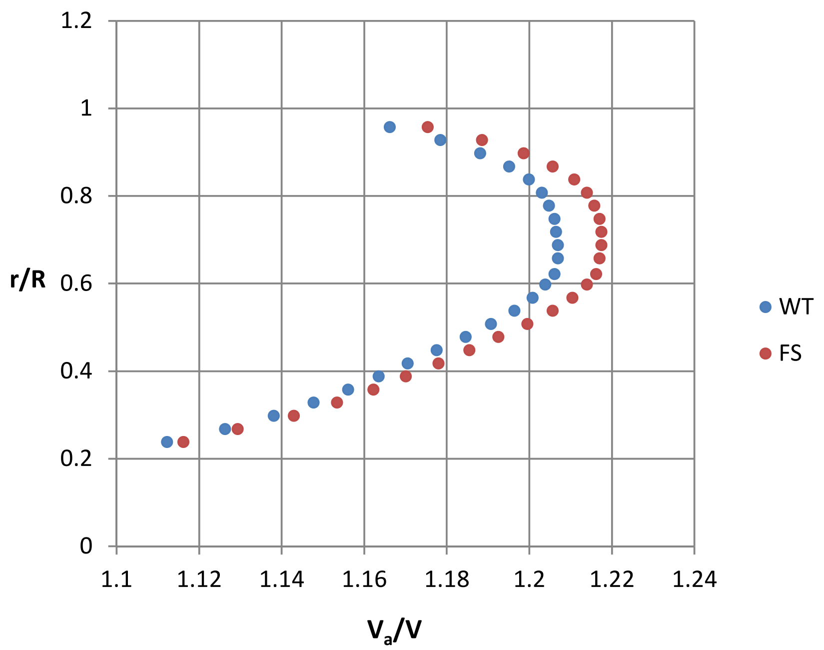

Figure 4.20.: Local axial velocities versus the radial position for full scale and wind tunnel of propeller B with constant advance ratio.

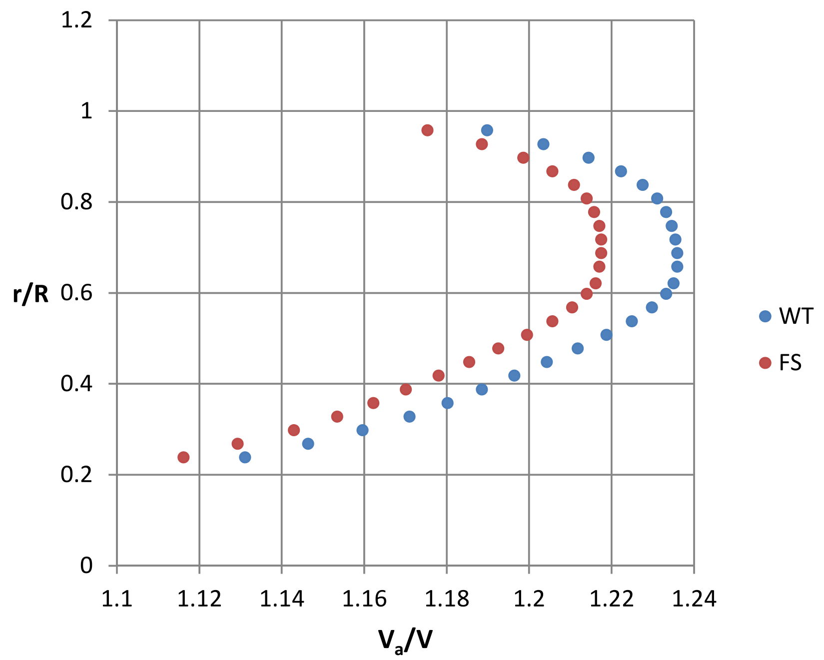

Figure 4.21.: Local axial velocities versus the radial position for full scale and wind tunnel of propeller B with constant thrust coefficient.

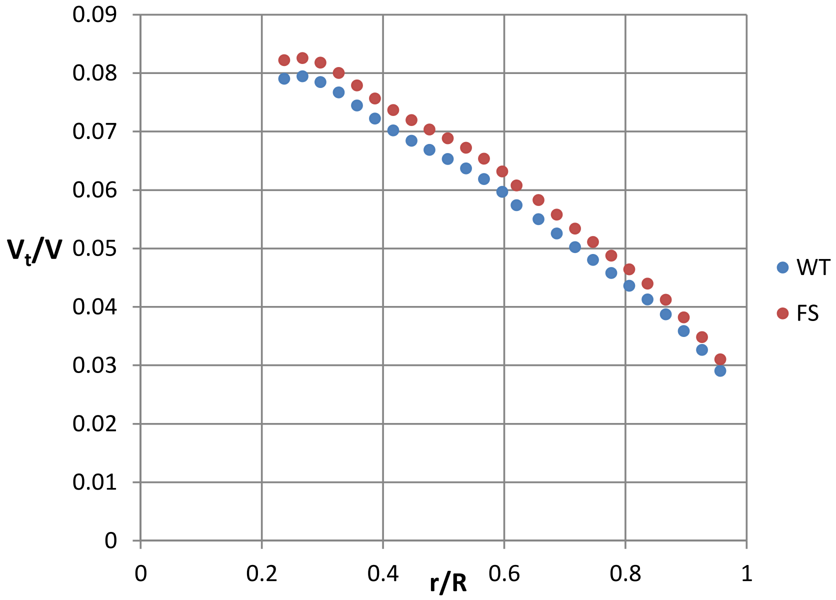

Figure 4.22.: Local tangential velocities versus the radial position for full scale and wind tunnel of propeller B with constant advance ratio.

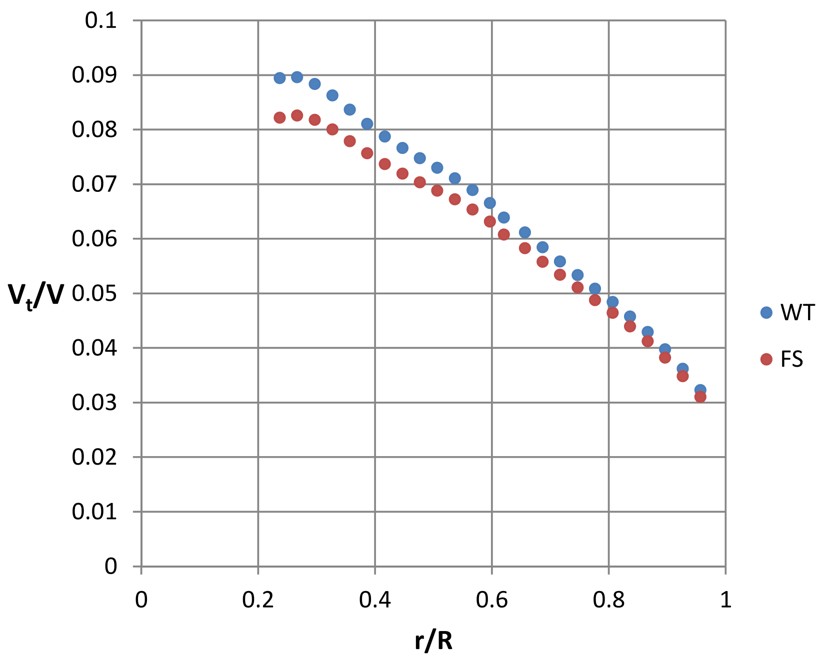

Figure 4.23.: Local tangential velocities versus the radial position for full scale and wind tunnel of propeller B with and constant thrust coefficient.

If we then take a look into the other propellers for which the data is shown in Appendix A , a similar but less profound result can be observed. For the axial velocity, a larger deviation is found when keeping C_T constant. The only exception is propeller D where the resemblance does not improve, but doesn't get worse by this choice. For the tangential velocity, an good match is found between the wind tunnel and full scale data for radial positions between 70% and 100%. The deviation of WT w.r.t. FS increases towards the inward position of the radius.

4.3. Intermediate conclusion uninstalled propeller

In the beginning of this part, different sets of data were used in Qprop in order to investigate the influence of the Reynolds number. Since a shift in the maximum value and slope of the lift coefficient are the more common phenomena when changing Re, it was seen that the change of these parameters result in visible differences of the propeller characteristics.

Afterward, an analysis is made that incorporated the Himmelskamp effect and the question was brought up whether it could be used to improve our program data. Unfortunately, this resulted in some unwanted deviations like for example the high overshoot for higher thrust coefficients. It was therefore concluded that the investigation could be done without the incorporation of the Himmelskamp effect. This was confirmed since the effect merely increases the slope of the curve, which resulted in a worse match between Qprop and the reference data. It is of course important to keep in mind that if the point of focus changes, these assumptions should be reconsidered. Another possible improvement was found in the input data. Looking at different papers, we come across a small difference in the parameters that are used to characterize the lift polar in Qprop. By adapting the lift polar accordingly, a better match was found between Qprop and experiment. Despite this improvement, the research was conducted without the implementation of the difference for the following two reasons. In the first place, we are primarily interested in the quantity of the errors and secondly, Qprop already gave a good match with the reference data.

A general idea about the behavior of the induced velocities of the propeller w.r.t. the radius position was already given in [17]. With the understanding of the difference in performance characteristics between full scale and wind tunnel, an insight was found on how this affects the induced velocities. From the investigation with constant advance ratio, the values of axial velocities between FS and WT w.r.t the freestream velocity, show an increase of 0.3 % towards to root and 0.8 % at the tip, with a maximum of 1% at $\frac{r}{R} = 0.75$. For the tangential velocities, an increase of 0.2% is seen towards the tip which increases to a value >0.3% in the direction of the root. The changes in induced velocities have a direct implication on the local inflow angle. This means that an increase is seen of 3% at $\frac{r}{R} = 0.2$ and 5% towards the tip. The change at each radius is taken w.r.t the local inflow angle. The representation of all these differences can be seen in Appendix D for the different propellers.

Thereafter the question was raised how the resemblance between full scale and wind tunnel would be altered if we preferred a constant thrust coefficient for comparison instead of the constant value of advance ratio. The induced velocities of WT w.r.t FS were examined at both constant C_T and J. It was seen that the differences between WT and FS were smaller and more consistent in the case of constant J. More specifically, the differences in both axial and swirl velocities were smaller compared to the differences found when keeping C_T constant. An exception was found for the outer part ($\frac{r}{R} > 0.7$) of the radius at constant C_T where the difference in swirl velocity became smaller than for a constant J.

5. Interference effects of installed propeller

5.1. Analysis

5.1.1. Converting uninstalled propeller data

In the previous part a general idea was attained about the average error between the performance data of full scale and experiment. It also became clear what this meant for the induced velocities over the propeller. A statement will now be made about our second point of interest in this work. More specifically, we are interested in the differences between full scale and experiment in the slipstream and what this means for the trailing devices, i.e. the wing. This will be done by using the FS and WT data and with the aid of a dedicated vortex lattice based program (VLM4D). This program investigates the effect of the interference between the wing and the propeller. A detailed description is given in section 5.2.

5.1.2. Point of interest w.r.t wing interference

Focusing on the immersed part of the wing in the slipstream, we see that through a variation of the induced velocities in the slipstream, the characteristics of the wing will change. Restricted to a 2D analysis, the 2 components of the induced velocity, i.e. axial and tangential component, will have a direct influence on the wing. Early observations came up with general concepts as a lift increase due to the slipstream [36] or an increase of lift coefficient with increasing Re_c (increasing rotational speed) [30]. In [37], a general consensus was made which stated that the slipstream reduces the laminar flow by forcing the transition to occur earlier. From several investigations it was concluded that the slipstream caused the point of transition to move forward to a location in the direction of the leading edge, although no consistent conclusions resulted from these early observations [37]. Even more, it was shown that the boundary layer cycles between laminar state and turbulent transitional state at a rate of the propeller blade passage [21]. Because of adequate research on the propeller wing interaction, it is well known that for the tractor configuration, the performance improvement is mainly manifested in wing drag reduction [24].

In [22], it is mentioned that the largest contribution to the local angle of attack of the wing is the one from the propeller slipstream rotation. In our case, it is not of great importance what its exact value is, but more how the variation in local angle of attack of the wing is altered in accordance to the error between full scale and experiment, i.e. the change in the angle of attack variation($\triangle(\triangle\alpha)$). An interesting way in using this information is by looking at the loading (lift) distribution over the wingspan and investigate how the difference in WT and FS will alter the distribution. To do so, a good understanding is needed on how the propeller influences the loading of a wing. This was already elaborated in the introduction. Finally, with the aid of the interference program, the differences in the spanwise loading distribution, as a result of the errors between full scale and experiment, will be investigated.

5.2. Program

5.2.1. Introduction

For the investigation, a program (VLM4D) is used which was made by L.L.M. Veldhuis [27]. It is based on a vortex lattice method (VLM), using a panel distribution. In the formulation, visualized in Figure 5.1, a division of the wing is made into equidistant panels with a horseshoe vortex placed on each panel. In our case, each horseshoe vortex is bound at the quarter chord line of each panel and extends to infinity. The flow boundary condition is applied at the control points which are located at the center of the 3/4 chord line of each panel [24]. The effect of the propeller on the wing loading characteristics is based on the fact that at the control point position an additional velocity vector induced by the propeller slipstream is introduced. It is shown to be very easy to use while providing insight into wing aerodynamics and component interaction, which in our case features the full interaction between the propeller and wing. A thorough description of the vortex lattice method is given by Bertin and Smith [25].

5.2.2. Set up and theory of the program

The evaluation of the program goes as follows. First a large amount of input data is needed to specify the begin conditions. In our case, the most important data is the one that specifies the geometry of the propeller and the different polars of the propeller. The polars characterize the difference between experiment and full scale. We saw in [12] that most of the difference was caused by the influence of variation in Reynolds number so that it can crudely be stated that the different propeller airfoils represent the influence of Reynolds number variation. Important to note is that the focus is put on unswept wings since the effect of sweep is not a point of interest. With the aid of the input data, intermediate calculations are made in order

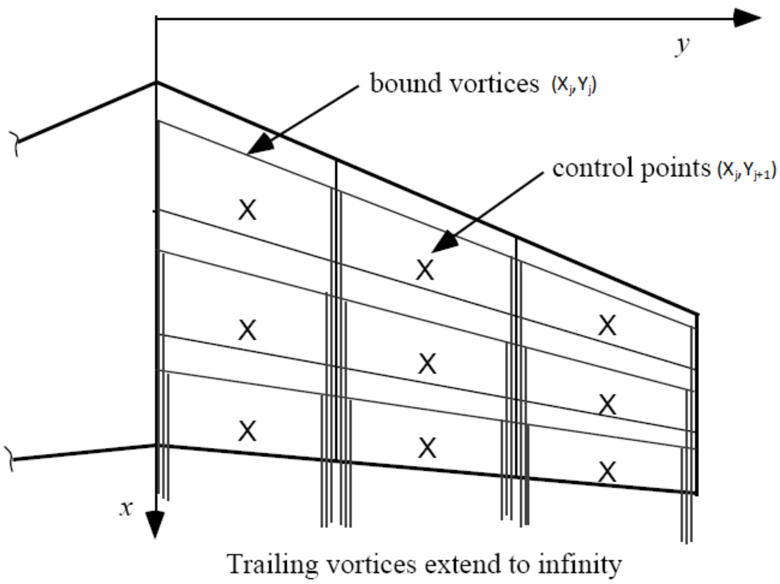

Figure 5.1.: Layout for the classical vortex lattice method[38].

to specify the aspect ratio, disk/wing area, etc. In using the VLM method, various panels are generated and the location of their bound vortex and control points are specified. Starting with the BEM initialization, a representation is made of the local blade and chord distribution of the propeller together with initial calculations for the radius, dynamic pressure, rounds per minute, etc. The induced velocities also receive an initial value, after which the first BEM iteration loop is initiated. In such a loop, the local parameters (blade angle of attack, Reynolds number, etc.) and velocity at each blade section are calculated after which a determination of the loading and induced velocities is made with the aid of Equation 2.7, Equation 2.8 and Figure 2.2. The inflow factors and induced velocities are defined in each loop as follows:

$$V_a = \frac{V_{a,prev} + V_{a,new}}{2}, V_t = \frac{V_{t,prev} + V_{t,new}}{2}, a = \frac{V_a}{V_\infty}, b = \frac{V_t}{\omega r} \tag{5.1}$$

After this step, a first summary is given of the final values of the BEM iteration together with the propeller coefficients (post processing). Next, the propeller reference system is transferred onto the wing's system and the slipstream velocities are calculated, followed by a final calculation of the thrust coefficient. The unknown circulation strength is then calculated according to:

$$\Gamma(y).C = rhs \tag{5.2}$$

where rhs is the right hand side, which contains the velocity components over the wing as affected by the propeller slipstream and matrix C holds the influence of the horse shoe vortex on the velocity in each control point.

A representation is made of the lift and loading distribution together with a short summary that includes the wing's lift, drag, rolling moment and propeller coefficients. The lift distribution is given with the aid of the following formula:

$$C_l(y) = \frac{2\Gamma(y)}{V_\infty c(y)} \tag{5.3}$$

Important to note is that until now only the influence of the propeller on the wing is taken into account and not yet the secondary influence, i.e. the wing influence on the propeller. Based on the calculated Γ - distribution, the incoming flow field for the propeller is redefined. With the final induced velocities for the propeller, the BEM calculations are repeated. This is done for both propellers separately as the induced velocities for the left and right side can be different due to the asymmetry in the loading distribution. Afterward, the same sequence is followed as before, i.e. the transfer of the propeller onto the wing's system and the calculation of the circulation distribution. At the end, a final summary with full interaction is given. A full overview and understanding can be found in [27] and a flow diagram is given in Figure 5.2.

5.3. Investigation

Point of focus

The part of the wing that is immersed in the slipstream will notice a variation in α. By changing the Reynolds number or taking the cases of experiment and full scale, the fluctuations in the angle of attack in the immersed part of the wing will alter again. As already mentioned, it is not of great importance in our case what these exact values are, but more how the variation in local angle of attack of the wing is altered in accordance to the error between full scale and experiment, i.e. the change in the angle of attack variation($\triangle(\triangle\alpha)$). A direct effect due to this change and as a consequence of the Reynolds variation is the change in loading distribution over the wingspan. By using the different polars, characterizing the difference between full scale and experiment, an analysis can be made with different loading distributions as result. As is it is very difficult to map $\triangle(\triangle\alpha)$, it is more convenient to put the focus on the final loading (lift) distribution that results at the end of the VLM4D program.

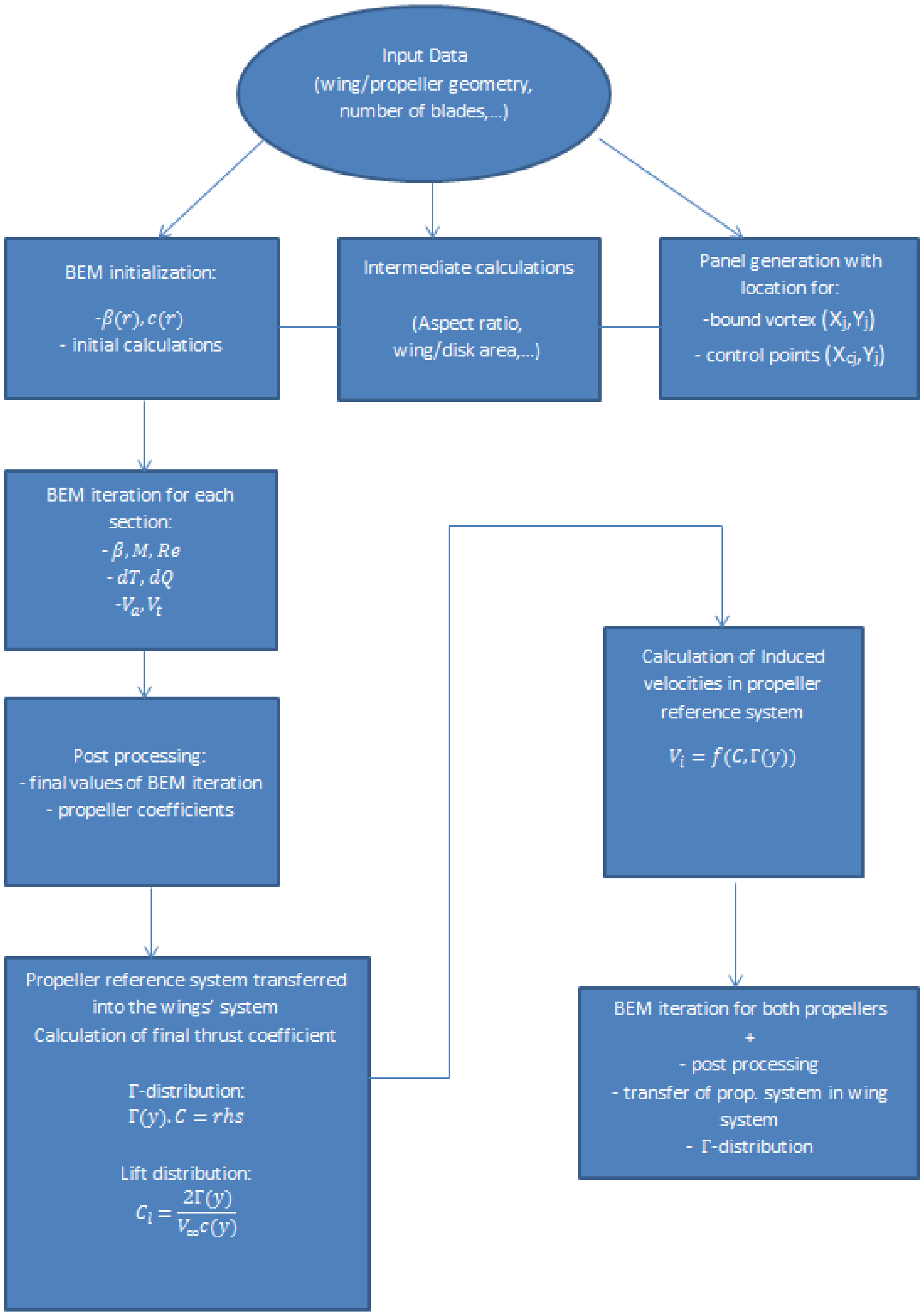

Figure 5.2.: Flow diagram for the analysis part of VLM4D.

5.3.1. Implementation of the propellers

For this investigation, we use the propellers from [12], since they were also used in our previous analysis. For most of the parameters in the input box of the VLM4D program, it is argued that general values will be used. For example we do not use any sweep and the effect of the fuselage and nacelle is left out. Several adaptations to this general lay out will be made further on in the report. Also the propeller angle and nacelle angle w.r.t. their reference axis are zero. The most important input that will influence our investigation is the airfoil data of the propeller that, as already mentioned, characterizes the full scale and experiment. In doing so, we can see how the difference in performance of the propeller is translated into the slipstream and onto the wing loading distribution. So in practice, the propeller geometry together with the different propeller polar data is of primary importance and the polars of the wing only of secondary importance. It is important to note that by using the different propeller polar data, defined as in section 4.2.1., a representation is made for the WT and FS case. Again, the main interest is to see the overall effect into the loading distribution and not necessarily the specific values.

As expected, it can be seen in Figure 5.3 that the lift coefficient takes more extreme values at local points of minimum and maximum in the rotor disk area. An overview of the differences between WT and FS is given in Figure 5.4. The lift distributions for WT and FS for the other propellers are given in Appendix E.

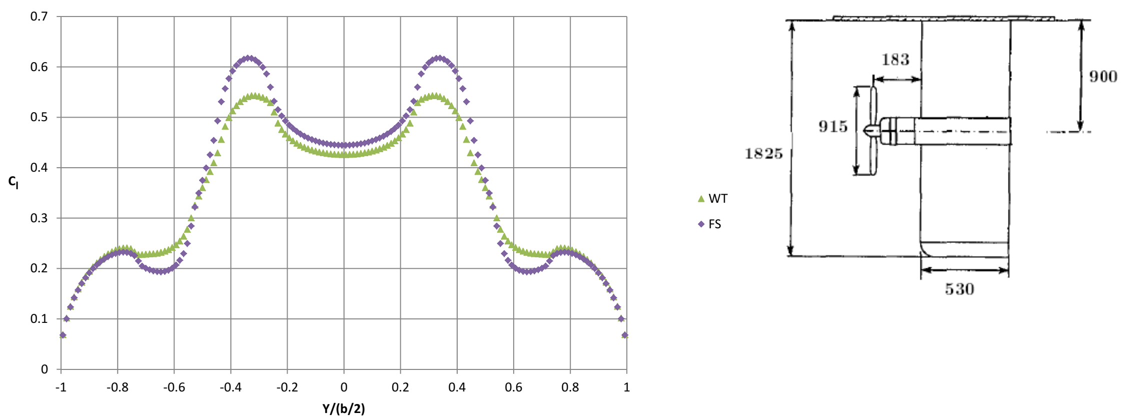

Figure 5.3.: Local lift coefficient in spanwise direction for WT and FS case of propeller L, $J = 0.511$ and the general wing lay out (in mm). [12]

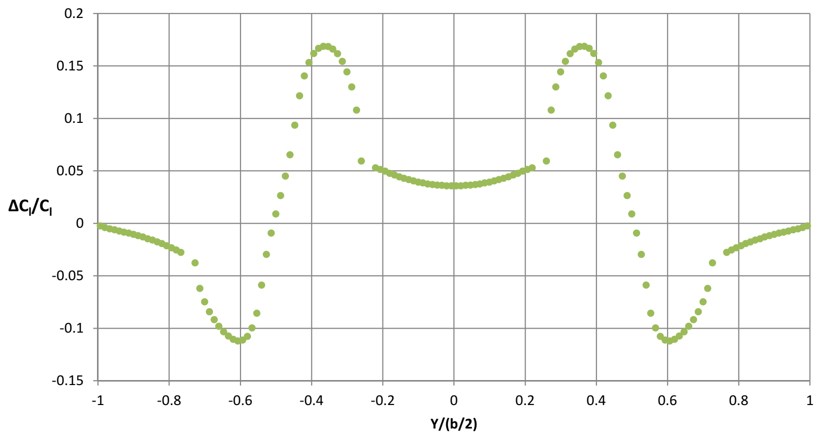

Propeller	$\frac{\Delta C_L}{C_{L_{WT}}}$
B	0.0658
I	0.0707
D	0.0853
K	0.082
L	0.0705

Figure 5.4.: The local difference in C_L between WT and FS w.r.t. the wing's lift coefficient for propeller L (left), together with an overview for all propellers (right). [12]

5.3.1.1. Influence of Reynolds number augmentation on the lift (distribution)

For the propellers of [12], a clear difference is noticed between WT and FS. It should be noted that the difference between experiment and full scale due to Re is consistent. To see the effect of a wide range of Reynolds numbers on the lift distribution, another analysis can be made with data from [9]. Here, typical polars for different Reynolds numbers are given for both wings and propellers. As a simple example, the polars from Figure 1.5 can be used. The exact values of the lift distribution are of secondary importance, as we are merely interested in the change of the distribution with the Reynolds number. The results are shown in Figure 5.5, and a close-up is made in Figure 5.6.

It can be seen that the improvement becomes smaller when we reach Re values for full scale. The difference between case 1 and 2 is responsible for the larger part of the entire difference. This is in agreement with the theory, where it was stated that above values of $Re_c > 7{\times}10^5$, the corrections become small for models [44]. In Table 5.1, some interesting parameters are given for Figure 5.5.

An important value in this table is the differences between Case 3 and Case 1, as ΔRe is similar to the one from our previous investigation. It appears that the value for $\frac{\Delta C_L}{C_{L_{case1}}}$ in Table 5.1 is in agreement with the one found in Figure 5.3, where $\frac{\Delta C_L}{C_{L_{case1}}} = 0.0705$.

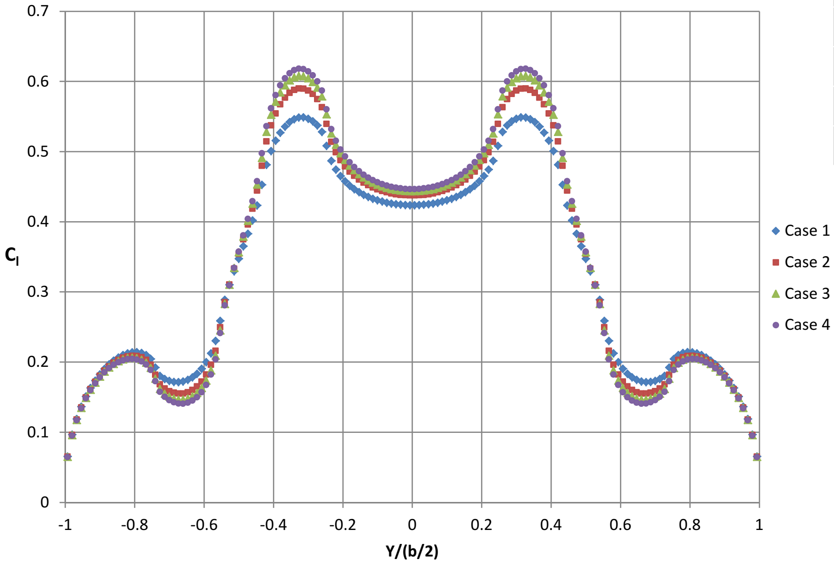

	Re_c
Case 1	3.3×10^5
Case 2	6.7×10^5
Case 3	1.3×10^6
Case 4	3.1×10^6

Figure 5.5.: Influence of *Re* on the lift distribution with propeller section from Figure 1.5, $J = 0.45$, on the same wing as in Figure 5.3.

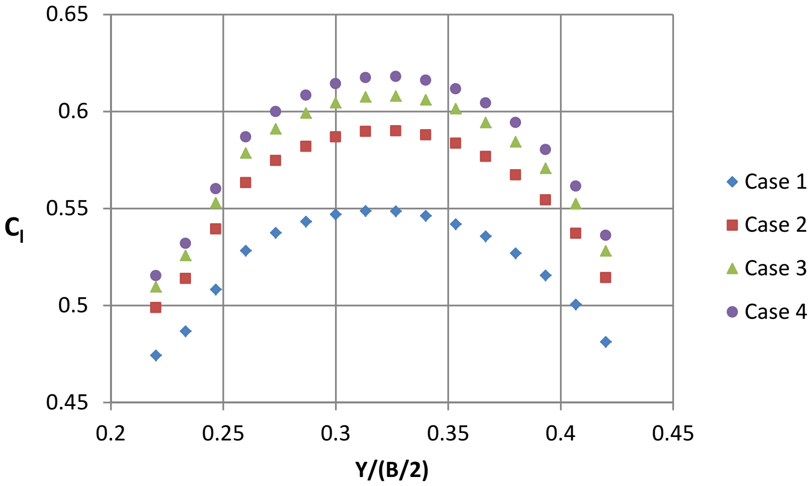

Figure 5.6.: Influence of *Re* on the lift distribution with propeller section from Figure 1.4, zoomed in for values of $0.2 < \frac{y}{b/2} < 0.45$.

	Case 1	Case 2	Case 3	Case 4
$\frac{\Delta C_L}{C_{L_{case1}}}$	/	0.053	0.072	0.083
$\frac{(\Delta C_l)_{max,1}}{C_{L_{case1}}}$	/	-0.051	-0.077	-0.094
$\frac{(\Delta C_l)_{max,1}}{C_{L_{case1}}}$	/	0.116	0.166	0.194

Table 5.1.: Overview of differences in lift distribution affected by *Re*, w.r.t case 1.

5.3.1.2. Influence of other parameters on Re-effect in the lift distribution

Propeller position

In [17], it was proven that by moving the propeller towards the tip, an increase in wing efficiency is noticed. Here, an investigation is done in order to see how the lift distribution will change with a shift in the propeller's position. The propellers from [12] are analyzed, where the propeller is shifted from $\mid \frac{y}{b/2} \mid = 0.5$ to the position $\mid \frac{y}{b/2} \mid = 0.6$. Figure 5.7 shows the results before and after the shift.

An outward shift of the lift distribution was expected, but it can also be seen that the local lift coefficients are lower at the outboard side of the propeller. On the other hand, a larger part of the wing is now characterized by a higher lift coefficient. This means that the wing's lift coefficient is also higher. It appears that the increase for WT remains smaller than the one for FS. This would imply that the difference between WT and FS is aggravated as the propeller is shifted towards the tip. In other words, the difference in lift coefficient due to Re, i.e. $((\triangle C_L)_{Re})$, will increase when the propeller is shifted outboard, as seen Figure 5.7.

$\frac{y}{b/2}$	$(\triangle C_L)_{Re}$
0.5	0.07
0.6	0.088

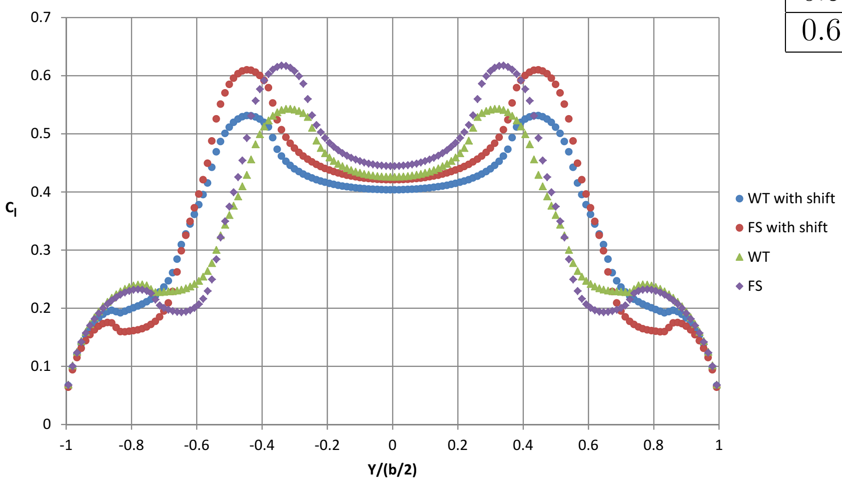

Figure 5.7.: Comparison of the lift distribution for WT and FS, with and without a shift towards the tip for propeller L, $J = 0.511$. [12]

If we do the same analysis for Figure 5.5, we see the same trend as for our previous propellers. A good way of comparing the data, is to look at Table 5.2. It appears that, although the same trend is visible, the differences become larger in case of a propeller that is positioned more outboard.

Before shift	Case 1	Case 2	Case 3	Case 4
$\frac{\Delta C_L}{C_{L_{case1}}}$	/	0.053	0.072	0.083
After shift				
$\frac{\Delta C_L}{C_{L_{case1}}}$	/	0.056	0.077	0.089

Table 5.2.: Changes in lift distribution as affected by Re, w.r.t case 1.

Wing planform

In the previous part, the effect of λ was left out. Here, an adaptation is made to the wing planform by altering λ. In Figure 5.8 some visible changes can be noticed when the taper is decreased from a value of 1.0 to 0.7. Equation 5.3 states that the lift coefficient is proportional to $\frac{1}{c}$, which means that higher values of the lift coefficient are seen towards the outboard part of the wing.

λ	$(\triangle C_L)_{Re}$
1	0.0705
0.7	0.0749

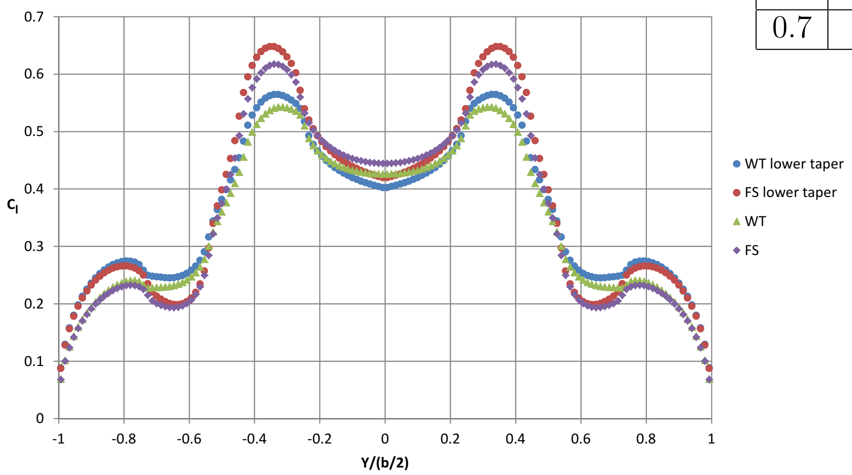

Figure 5.8.: Comparison of the lift distribution for WT and FS, with different λ for propeller L, $J = 0.511$.

Propeller diameter

In this last section, we will try to investigate to what extent $(\triangle C_L)_{Re}$ is affected by the propeller diameter. As an example, the propeller of the previous section will be taken and the radius is decreased with 30 %. It can be seen in Figure 5.9 that by decreasing the radius of the propeller, the overall lift becomes smaller but that also $(\triangle C_L)_{Re}$ decreases.

If we now evaluate the adaptations of all the previous parameters, a general trend can be seen. When and adaptation is made that leads to an augmentation of the

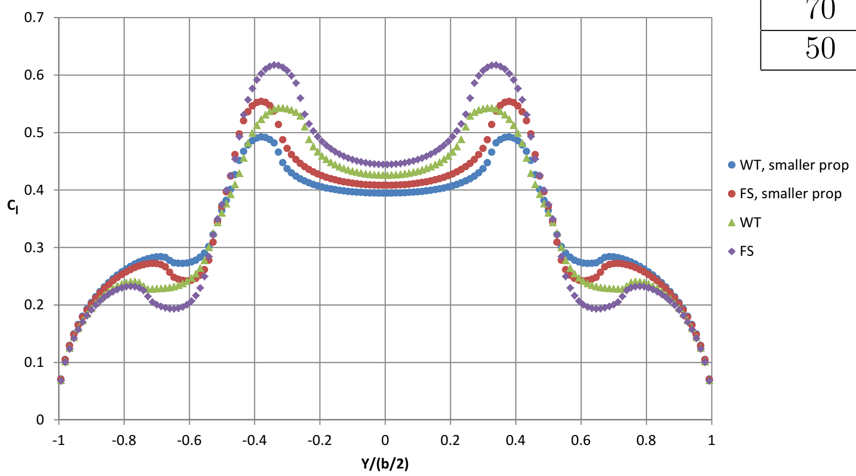

D (%)	$(\triangle C_L)_{Re}$
100	0.0705
70	0.067
50	0.045

Figure 5.9.: Comparison of the lift distribution for WT and FS, with a decrease in radius for propeller L, $J = 0.511$.

wing's lift distribution, an increase of $(\triangle C_L)_{Re}$ is noticed. This also implies that the effect of Re diminishes when the adaptation leads to a decrease in lift distribution.

5.4. Intermediate conclusion installed propeller

The intention in this chapter was to visualize how the difference in propeller data would influence other points of interest like the wing. A straightforward and clear way to do this was by looking at the lift distribution of the wing and see how this distribution would be affected by the propeller. At first, a description was given of the general effects that induced velocities of propellers have on a wing. The interference program was used in order to see if the adaptation, characterizing the effect of the Reynolds number, would also reveal the same general image as mentioned previously. By looking at the different propellers of [12], a similar trend was noticed: more extreme values were noticed for higher Re. It appeared that the increase in local lift coefficient on the upgoing blade was larger than the decrease of the downgoing blade. The final result of this observation was an increase in the wing's lift coefficient for higher Re. In a second stage, an analysis was made to see the effect of a certain Re increase on the lift distribution. The improvement on the lift distribution became smaller as we reached higher Re values. In the previous chapter, a difference of around 8 %, was seen in the propeller performance data as concluded. This chapter showed that this difference resulted in an error of over 7% on average at the wing when we focused on the loading distribution.

Hereafter, another investigation was made to see how the lift distribution changes with a certain Re. In order to do this, different polars were used that are characterized by certain Re. It was seen that the biggest part of the improvement of the lift distribution was situated in the lower region of Re ($< 7\times10^5$). We also noticed that the lift increase for the propellers from [12] was similar to the increase of the corresponding $\triangle Re$ in Figure 5.5. As a final analysis, we looked at the effect of parameter changes on the Re-effect in the lift distribution (propeller position, diameter, wing taper). For an outboard shift of the propeller, we did not only find an outward shift of the lift distribution, but also lower values of the lift coefficient on the side of the downgoing blade. This eventually resulted in an increase of the Re-effect. For an increase in propeller diameter or a decrease in wing taper, an increase in Re-effect could also be noticed. This led to the conclusion that for any previously mentioned adaptation, $(\triangle C_L)_{Re}$ became larger in case that the specific adaptation resulted in a lift augmentation over the wing.

6. Conclusions and recommendations

In preparation of this project and also during the research it was very important to keep track of the objective and research questions. By concentrating on the scaling effects and more in particular the *Re* number effects, we needed a thorough understanding on how this parameter could influence the major characteristics like lift, drag, etc. It was noticed that in general for an increase of *Re*, an augmentation of the maximum lift coefficient and its linear slope was observed together with a decrease of the drag coefficient. With this knowledge, it was clear how the effect of the Reynolds number could be implemented into the calculations that were done with different programs.

Before the investigation was started, it was necessary to investigate which program was most compatible for a representation of our point of interest. In order to do this, several papers were used and presented in different programs. As a result, Qprop earned our preference in this case.

Another important aspect was the limitation of the Reynolds number. In earlier studies it was well argued that above values of 3×10^5, representable data could be found for the full scale and that for this reason investigations were performed with the crude rule of using $Re > 5\times10^5$. It was also mentioned that under values of 2×10^5 no reliable data could be gathered in general as below this value unwanted and unexpected deviations appeared. In this work papers were used of values $> 3\times10^5$. By taking this lower limit, it is clear that the resemblance between full scale and wind tunnel only gets better with increasing Reynolds number and that the effect of scaling is at its highest value here. This statement holds as for lower values no reliable representation can be made. As a result no conclusions can be drawn under this region. From different papers that laid their focus on scaling effects, different formula were stated that mainly focused on the improvement of the lift polar. In this project, the focus is then merely centralized around this improvement. Although enough reasons are present to neglect the adaptation of the drag, it could be recommended to incorporate the influence of *Re* on drag when using the different programs. This recommendation can be implemented in two ways: one could analyze which input data in the program is available for adaptation in order to include the influences or one could adapt the program in case the deviations in the area of interest are not yet incorporated.

As the limitations and effects were clear, the investigation was started in the next part by analyzing the different propellers. This was done by using the data that characterizes the deviation between wind tunnel and full scale tests. In a first instance the focus was put on the uninstalled propeller, i.e. the performance characteristics. With the aid of known performance data, we were able to make an analysis in Qprop and see how well the reference data could be represented. As a result, good agreement was found for the slope of the performance data between tests and program. This resemblance was mainly manifested in larger values of the advance ratio. Despite this resemblance, there was still room for improvement between the used data. The reason for this deviation could be found in the lack of consistency between the data. Despite this observation, it was seen that the general conclusions from the paper [12] hold, as the difference due to the scaling effect in the program was in agreement with the one found in tests.

The question about consistency of some used data needs further clarification. This was done in section 4.2, where it was pointed out that the unwanted deviation of data in the program is most certainly emanating from an incorrect use of available data points since in our case it was noticed that different values for one particular case were found. For this reason, it is recommended that the investigation should be supported by taking other data from airfoils in order to get a perfect match between the results from the program and paper.

Other important results that were investigated are the differences in induced velocities, which followed directly from the differences in the performance data. Also in this stage the scaling effect could be seen.

An interesting question that came up while doing the investigation was whether or not the choice of constant advance ratio for the propeller performance was the best one. In order to give a good answer, the different variables (thrust coefficient and advance ratio in our case) were held constant separately. As a good match was sought, we focused on how the induced velocities would behave for propellers in WT and FS tests.

Focusing on the different induced velocities, it appeared rather quick that the use of constant thrust coefficient gave an overshoot in comparison with FS. For constant J, the differences in both axial and swirl velocities were smaller compared to the differences found when C_T was kept constant. An exception was found for the outer part ($\frac{r}{R} > 0.7$) of the radius at constant C_T, where the difference in swirl velocity became smaller than for a constant J. As a conclusion, the specific values for constant J are given:

- In case of constant J, an increase of 0.3 % towards the root and 0.8 % at the tip was found on average, with a maximum of 1% at $\frac{r}{R} = 0.75$. For the tangential velocities, an increase of 0.2% is seen towards the tip which increases to a value >0.3% in the direction of the root. This difference remained rather constant along the radial position, unlike the difference in case of the axial velocities. These differences have a direct implication on the local inflow angle: an increase was seen of 3% at $\frac{r}{R} = 0.2$ and 5% towards the tip.

  It can also be seen that the Reynolds effect in the propeller performance results in a 'chain reaction', i.e. $\triangle C_T = \triangle V_a, \triangle C_Q = \triangle V_t$ and $\triangle(\triangle\alpha)$ in the slipstream. By using an interaction program in the last chapter, we saw that the scaling effect on the propeller also affects the wing. The '$\triangle(\triangle\alpha)$', or in full words the fluctuation caused by scaling effect on the fluctuation of the angle of attack as a consequence of the slipstream, could be an interesting parameter to keep track of. A method of looking into the effect of $\triangle(\triangle\alpha)$, was by investigating how the wing's lift distribution is altered, as a consequence of the data of the uninstalled propeller.

In investigating the different propellers, the same trends as from theory where noticed in the program. More in particular, these trends contain the differences between quasi elliptical loading distributions and loading distributions in the presence of a propeller. The difference between the full scale and wind tunnel data could especially be seen at positions where the blade tip crossed the wing. The final result of this analysis resulted in a deviation of over 7% on average for the wing's lift coefficient between WT and FS when a general wing lay out was used.

In order to see how the lift distribution changes with a certain *Re* increase, another investigation was conducted where different polars were used that characterize certain *Re*. It was seen that the biggest part of the improvement of the lift distribution was situated in the lower region of *Re* ($< 7\times10^5$). Finally, we focused on the effect of parameter changes on the *Re*-effect in the lift distribution (propeller position, diameter, wing taper). This led to the conclusion that for any previously mentioned adaptation, $(\triangle C_L)_{Re}$ became larger in case that the specific adaptation resulted in lift augmentation over the wing.

Acknowledgments

As I am almost at the point of receiving the degree in Master of Science, it is time to show my gratitude to the following people as this was not possible without their support and advice.

First of all I would like to thank Mr. Veldhuis for his guidance and feedback throughout the entire project. In addition I would like to express my appreciation to Mr. Eitelberg and Mr. Timmer for taking part in my Graduation committee.

I am also thankful to my fellow graduates for making my working place a pleasant and productive environment. My friends outside the faculty also earn my gratitude as they kept my mind and spirit fresh by taking breaks outside the university from time to time.

An Claes, Herman Ghekiere and Jens Vande Cavey also deserve my gratitude, reading my report in order to find flaws and imperfections.

And most important I would like to thank my family, especially my mother, for her persistent support and constant pushing, together with the support they gave me during difficult times.

Bibliography

[1] http://www.mh-aerotools.de/airfoils/javaprop.htm

[1b] Adkins, C. N.: Design of Optimum Propellers, AIAA-83-0190. Also published in the Journal of Propulsion and Power, Vol. 10, No. 5, September-October 1994.

[2] http://www.drivecalc.de/PropCalc/PCHelp/Help.html

[3] Edwin P. Hartman and David Biermann, “The aerodynamic characteristics of full-scale propellers having 2,3 and 4 blades of Clark Y and R.A.F.-6 airfoil sections”, NACA report 640.

[4] Hugh B. Freeman, “Comparison of full-scale propellers having R.A.F.-6 and Clark Y airfoil sections”, NACA report 378.

[5] Blake W. Corson and Julian D. Maynard, “Investigation of the effect of tip modification and thermal de-icing airflow on propeller performance”, NACA TN 1111.

[6] George W. Stickle and John L. Crigler, “Propeller analysis from experimental data”, NACA report 712

[7] http://web.mit.edu/drela/Public/web/qprop/qprop_doc.txt

[8] M. Dimchev, “Experimental and numerical study on wingtip mounted propellers for low aspect ratio UAV design”, Msc thesis report, Delft University of Technology, 2012.

[9] Eastman N. Jacobs and Albert Sherman, “Airfoil sections characteristics as effected by variations of the Reynolds Number”, NACA-1937.

[10] S. Breton, “Study of the stall delay phenomenon and of wind turbine blade aerodynamics using numerical approaches and NREL’s wind tunnel tests”, Doctoral thesis, Norwegian University of Science and Technology, Trondheim, 2008.

[11] H.snel, R. Houwink, J. Bosschers, “Sectional prediction of lift coefficients on rotating wind turbine blades in stall”, ECN, ECN-C–93-052, May 1993

[12] W. F. Durand and E. P. Lesley, “Comparison of tests on air propellers in flight with wind tunnel model tests on similar forms.” NACA TN220

[13] W. S. Diehl, “The variation of aerofoil lift and drag coefficients with changes in size and speed.” NACA TN 111, 1921

[14] P. Giguere and M. S. Selig, “Low Reynolds number airfoils for small horizontal wind turbines.” University of Illinois.

[15] Christopher A. Lyon, Andy P. Broeren etc.,”Summary of low-speed airfoil data.” Vol. 1, SoarTech Publications, Virginia Beach, VA, 1995, 292 pages.

[16] Abe Silverstein, “Scale effect on Clark Y airfoil characteristics from NACA full-scale wind-tunnel tests.”, NACA report 502.

[17] R. Miranda and E. Brennan, “Aerodynamic effects of wingtip-mounted propellers and turbines.” AIAA-1986-1802.

[18] P. B. S. Lissaman, “Low-Reynolds-number airfoils”, Ann. Rev. Fluid Mech. 1983, 15: 223-39, California.

[19] D. F. Volkers, “Preliminary results of wind tunnel measurements on some airfoil sections at Reynolds numbers between 0.6 x 105 and 5.0 x 105”,Delft University of Technology, 1977.

[20] Richard Eppler and M. Somers, “Airfoil design for Reynolds numbers between 50000 and 500000”, Conference on low Reynolds number airfoil aerodynamics, page nr. 1, June 1985.

[21] J. Miley, M. Howard and J. Holmes,”Wing laminar boundary layer in the presence of a propeller slipstream.” Journal of Aircraft, Vol. 25, No. 7 (1988).

[22] M. George and E. Kisielowski, “Investigation of propeller slipstream effects on the wing performance”, (Book) 1st edition published in 1967.

[23] L. Veldhuis, “Propeller Wing Aerodynamic Interference.” Phd thesis, Delft University of Technology, 2005.

[24] Dave P. Witkowksi, Alex K. H. Lee and John P. Sullivan, “Aerodynamic interaction between propellers and wings”, Purdue University, VS, AIAA-1988-0665.

[25] Bertin, J.J., and Smith, M.L., Aerodynamics for Engineers, Prentice-Hall, Inc., Englewood Cliffs, 2nd Ed., 1989, pp: 261-282, 3rd Ed. 1998, pp: 291-311.

[26] W.H.Mason, “Applied Computational Aerodynamics Text/Notes.” (Vol 1,Chapter 6; http://www.dept.aoe.vt.edu/~mason/Mason_f/CAtxtTop.html)

[27] L. Veldhuis, “Vortex Lattice Analysis of a Twin-engine Tractor Propeller-Wing Model.” Mathcad program: -VLM4D-

[28] B. W. McCormick. Aerodynamics, aeronautics and flight mechanics. John Wiley and Sons, Inc., second edition edition, 1995. ISBN 0-471-57506-2.

[29] L. Veldhuis and S. Nebiolo, “A propeller-integration study comparing experimental data with numerical flow solutions based on the navier-stokes equations”, Harrogate, UK, ICAS congress 2000, paper 264.

[30] M. A. Takallu and G. L. Gentry Jr., “ Aerodynamic characteristics of a propeller powered high lift semi-span wing”, Virginia, US, AIAA-1992-388.

[31] P. C. M. van den Borne and J. van Hengst, “Investigation of propeller slipstream effects on the Fokker 50 through in-flight pressure measurements”, the Netherlands, AIAA-1990-3084.

[32] M. Lino, ”Numerical investigation of propeller-wing interaction effects for a large military transport aircraft.”, Thesis report, Delft University of Technology, 2010.

[33] F. M. Catalano, “On the effects of an installed propeller slipstream on wing aerodynamic characteristics”, Acta Polytechnica Vol. 44 No. 3/2004.

[34] M Drela QPROP user guide, 2005.

[35] M. K. Rwigema, “Propeller blade element momentum theory with vortex wake deflection”, Proceedings of the 27th Congress of the International Council of the Aeronautical Sciences, Nice, France, September 19–24, 2010.

[36] M. Brenckmann, “Experimental investigation of the aerodynamics of a wing in a slipstream”, Toronto University, Journal of Aeronautics, 1957.

[37] S. J. Miley, R.M. Howard and B.J. Holmes, “Propeller Slipstream/Wing boundary layer effects at low Reynolds numbers”, Conference on low Reynolds number airfoil aerodynamics, page nr. 335, June 1985.(page 342 for figure Figure 4.3)

[38] R. Enoiu, “Application of vortex lattice method to analyze the performance of a glider”, Fascicle of Management and Technological Engineering, Volume VI (XVI), 2007.

[39] Hermann Schlichting, “Boundary Layer Theory”,page 695. ISBN 0-07-055334-3.

[40] T. De Leeuw, “Investigation of scaling effects in propeller testing”, Delft, 2012

[41] M. Lino,”Numerical investigation of propeller-wing interaction effects for a large military transport aircraft”,Delft, 2010

[42] Fred E. Weick, “Propeller scale effect and body interference”, Bureau of Aeronautics, NACA-TC-225.

[43] C. Rohrbach and F. B. Metzger, “The prop-fan, a new look in propulsors”, Windsor Lock Connecticut, AIAA-1975-1208.

[44] SAE-AIR-4065, page nr. 75.

[45] L. Troost, “Reynolds number for model propeller experiments”, Report of International Committee and Introductory, London conference, 1948.

[46] H. E. Saunders, “The choice of suitable Reynolds number for model propeller experiments”, Berlin conference 1937.

[47] Antonio Filippone, “Data and performances of selected aircraft and rotorcraft”, Progress in Aerospace Sciences 36 629-654, Denmark 2000.

[48] Richard Eppler and Martin Hepperle, “A procedure for propeller design by inverse methods”, Stuttgart, Germany.(http://www.mh-aerotools.de/company/paper_1/epplerhepperle.htm last visited on 26 dec. 2011)

[49] John Stack, Eugene C. Draley James B. Delano and Lewis Feldman, “Investigation of the NACA 4-(3)(08)-03 and NACA 4-(3)(08)-45 two-blade propellers at forward mach numbers of 0.725 to determine the effects of compressibility and solidity on performance”, NACA-Report 999.

[50] “Experiments on airfoil at low Reynolds numbers”, 34th Aerospace Sciences Meeting and Exhibit, AIAA-1996-62.

[51] V. Ustinov and P. Ostroukhov, “Experimental investigation of propellers at low Reynolds numbers”, Competition, Workshop and Conference”, Toulouse, France, September 2007.

[52] R. M. Bass and D. G. M., “A review of some recent U.K. propeller developments”, Gloucester, England, AIAA-1985-1261.

[53] McGraw-Hill series in mechanical engineering, Boundary Layer theory p. 694.

[54] R. A. Wahls, L. R. Owens and S. M. B. Rivers,” Reynolds number effects on a supersonic transport at transonic conditions”, Nevada, US, AIAA-2001-912.

[55] Ehab A. Elsaadawy and Colin P. Britcher, “Experimental investigation of the effect of propeller slipstream on boundary layer behavior at low Reynolds number”, Old Dominion University, VS, AIAA-2000-4123.

[56] R.M. Howard, “An investigation of the effects of the propeller slipstream on a wing boundary layer”, Texas, 1987. (http://adsabs.harvard.edu/abs/1987PhDT........47H : last visited on 22-12-2011)

[57] S. Goldstein, “On the vortex theory of screw propellers.”, Proceedings of the Royal Society, 123, 1929.

[58] M. Arschwanden, “Wind tunnel simulation of propeller effects in the A400M FLA-4 model”, AIAA-2005-3706.

[59] W. Shyy,Y. Lian, “Aerodynamics for low Reynolds number flyers”, Cambridge, 2008, ISBN 9780521882781.

[60] L. Veldhuis, “Review of propeller-wing aerodynamic interference”, ICAS 2004-6.3.1., 24th International Congress of the Aeronautical Sciences,Yokohama, Japan .

[61] C.Lindenburg, ”Investigation into rotor blade aerodynamics”, ECN-C–03-025, 2003.

[62] http://web.mit.edu/drela/Public/web/qprop/qprop_theory.pdf

A. Validation of Mach and Reynolds regimes

In section 1.3, we pointed out the general tip Mach en Reynolds regimes. A verification for these regimes was made at the end of that section for 2 different cases; the A400M and the F-50. The tables and calculations to validate the regimes are listed below.

case 1: A400M

Table A.1

		Full scale (0 ft)	Full scale (24000 ft)	WT (1:15)
Re_c	$\frac{C_{3/4}V_{Re}}{\nu}$	5×10^6	$9.2{\times}10^6$	4.8×10^5
M_t	$\frac{V_M}{a}$	0.68	0.78	0.61
J	$\frac{V}{nD}$	2.1 (low speed)	2.7 (high speed)	1

with:

$V_M(km/h) = RPM \times Diameter \times \pi \times \frac{60}{1000}$

$V_{Re} = \frac{2\times\pi\times r\times RPM}{60}$

values for full scale:

$C_{3/4}$= 0.45 m at 75% of chord

$Diameter$= 5.3 m

RPM= 864 (max)

ν = 14.81.10-6 m^2/s (at 293K and 0ft)

ν = 9.01.10-6 m^2/s (at 235K and 24000ft)

true airspeed = 160 m/s (low)

true airspeed = 210 m/s (high)

a = 1255 km/h (0ft)

a = 1093 km/h (24000ft)

values for WT (1:15):

$C_{3/4}$= 0.03 m

$Diameter$= 0.355 m

RPM= 12000 m

WT speed = 70 m/s

case 2: F-50

Table A.2

		Full scale (0 ft)	WT (1:15)
Re_c	$\frac{C_{3/4}V_{Re}}{\nu}$	$3.5x \times 10^6$	4.8×10^5
M_t	$\frac{V_M}{a}$	0.68	0.45
J	$\frac{V}{nD}$	2.4	2.4

values for full scale:

$C_{3/4}$= 0.3 m

$Diameter$= 3.66 m

RPM= 1200 (max)

ν = 14.81.10-6 m^2/s (at 293K and 0ft)

true airspeed = 147 m/s

values for WT (1:15):

$C_{3/4}$= 0.06 m

$Diameter$= 0.7 m

RPM= 4300

WT speed = 100 m/s

B. Data preliminary survey

Different reports were used in section 3.3 to validate the accuracy of the theoretical programs. The data points, characterizing the performance of the propellers, are listed below. Their corresponding graphs were already given in chapter 3.

Report 640

Report 640		Qprop		PropCalc	
J	C_T	J	C_T	J	C_T
0.4	0.164	0	0.12	0.05	0.132
0.5	0.162	0.1226	0.123	0.18	0.133
0.6	0.159	0.2459	0.126	0.31	0.135
0.7	0.156	0.368	0.13	0.44	0.1381
0.8	0.155	0.4919	0.134	0.57	0.1422
0.9	0.153	0.614	0.1398	0.63	0.1446
1.0	0.147	0.737	0.145	0.7	0.1472
1.1	0.134	0.86	0.15	0.83	0.1525
1.2	0.118	0.983	0.148	0.96	0.1538
1.3	0.1	1.1	0.139	1.02	0.1515
1.4	0.08	1.22	0.122	1.15	0.1399
1.5	0.062	1.35	0.099	1.28	0.121
1.6	0.045	1.47	0.074	1.41	0.099
1.7	0.025	1.59	0.05	1.54	0.0757
1.84	0.005	1.72	0.029	1.67	0.0522
		1.84	0.004	1.8	0.0312
				1.93	0.0123

Report 378

Report 378		Qprop		PropCalc	
J	C_T	J	C_T	J	C_T
0.15	0.0949	0	0.0855	0.05	0.0849
0.2	0.0861	0.0741	0.0860	0.12	0.0851
0.25	0.0826	0.148	0.0867	0.18	0.0855
0.3	0.0793	0.2212	0.0875	0.25	0.0857
0.35	0.0763	0.2954	0.0883	0.31	0.0848
0.4	0.0739	0.3695	0.0838	0.38	0.0809
0.45	0.07	0.4437	0.0762	0.44	0.0747
0.5	0.0655	0.5178	0.0665	0.51	0.0673
0.55	0.0586	0.5920	0.0554	0.557	0.0594
0.6	0.0518	0.6649	0.0441	0.64	0.051
0.65	0.045	0.7319	0.0328	0.7	0.0422
0.7	0.038	0.8132	0.0221	0.77	0.0336
0.75	0.0309	0.8874	0.0127	0.83	0.0251
0.8	0.0238	0.9616	0.0049	0.9	0.0169
0.85	0.0165	1.0357	0	0.96	0.01
0.9	0.0091			1.03	0.0039
0.95	0.00018			1.06	0.0015

TN 1111

TN 1111		Qprop		PropCalc	
J	C_T	J	C_T	J	C_T
0.832	0.093	0	0.0749	0.73	0.1027
0.863	0.089	0.065	0.0754	0.78	0.1018
0.891	0.085	0.129	0.0761	0.84	0.0991
0.931	0.081	0.195	0.769	0.89	0.0945
0.978	0.0745	0.259	0.0779	0.94	0.0887
1.03	0.067	0.325	0.0790	0.99	0.0824
1.08	0.057	0.389	0.080	1.05	0.076
1.14	0.0491	0.454	0.0817	1.1	0.0691
1.2	0.0399	0.520	0.0832	1.2	0.0549
1.24	0.0338	0.650	0.0865	1.26	0.0475
1.29	0.026	0.779	0.0898	1.31	0.0398
1.35	0.017	0.975	0.0758	1.36	0.0314
1.39	0.0099	1.104	0.0569	1.41	0.0232
1.43	0.0038	1.234	0.0369	1.47	0.016
1.455	0	1.364	0.016	1.52	0.0089
		1.428	0.005	1.57	0.0033

report 712

report 712		Qprop		PropCalc	
J	C_T	J	C_T	J	C_T
0.094	0.1046	0	0.110	0.05	0.1185
0.1987	0.1045	0.137	0.112	0.16	0.1187
0.2926	0.1035	0.273	0.115	0.27	0.1185
0.3933	0.1014	0.410	0.120	0.38	0.1127
0.494	0.098	0.546	0.116	0.49	0.1056
0.591	0.094	0.683	0.102	0.6	0.0963
0.695	0.0899	0.819	0.088	0.71	0.0867
0.792	0.088	0.956	0.073	0.82	0.0766
0.893	0.085	1.09	0.057	0.93	0.0662
0.993	0.0767	1.22	0.041	1.03	0.0553
1.097	0.0647	1.36	0.025	1.14	0.044
1.194	0.0516	1.50	0.009	1.25	0.0327
1.304	0.0366			1.36	0.0214
1.401	0.0225			1.42	0.0158
1.497	0.0051			1.47	0.0102
				1.53	0.0047

C. Validation and evaluation of propellers

Propeller B was already used as an example in the report and in this appendix the data for the other 4 propellers are listed below, i.e. D,I,K and L. The data focuses on the analysis with Qprop, which is done in Chapter 4.

Reynolds number range for reference propellers

$Re_c(\frac{C_{3/4}V_{Re}}{\nu})$	WT	FS
Propeller B	3.3×10^5	1.7×10^6
Propeller D	3.7×10^5	1.5×10^6
Propeller I	4.1×10^5	1.6×10^6
Propeller K	3.2×10^5	1.3×10^6
Propeller L	4.8×10^5	1.5×10^6

propeller D

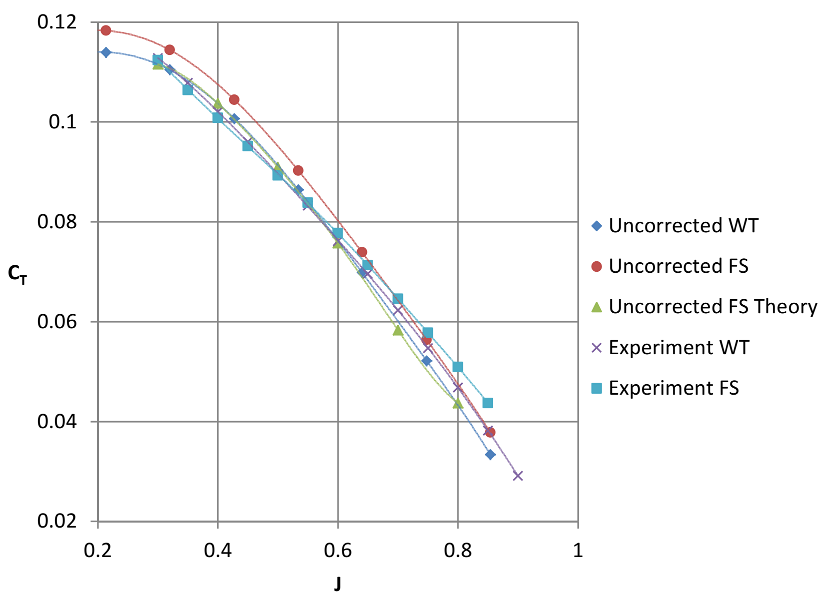

Figure C.1.: First data set without the Himmelskamp effect for propeller D.

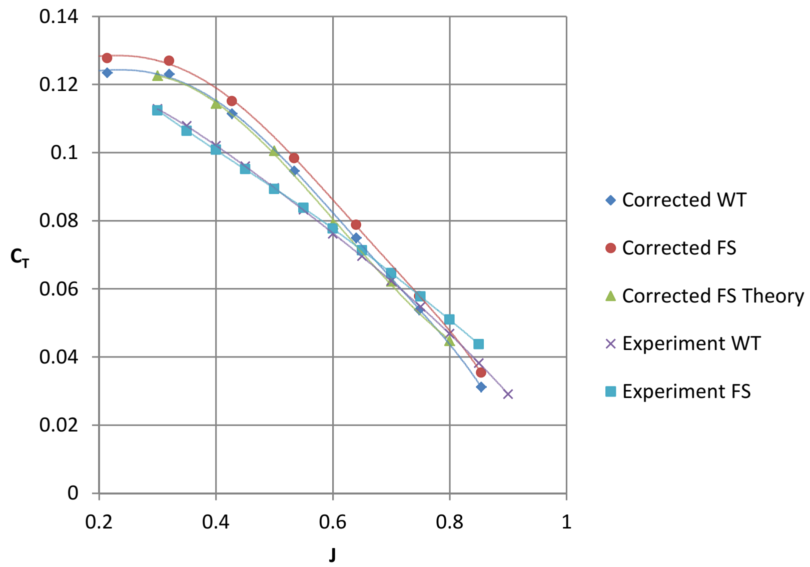

Figure C.2.: Second data set with the Himmelskamp effect for propeller D.

propeller I

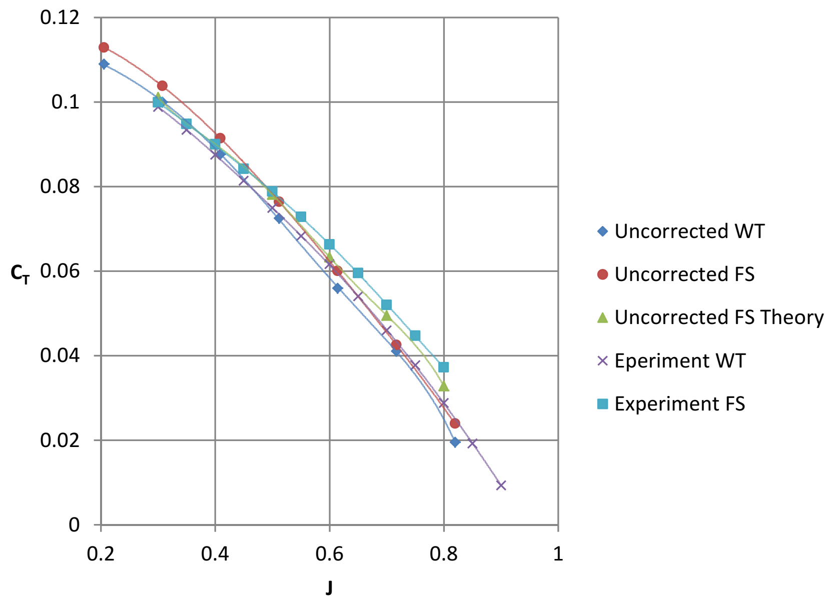

Figure C.3.: First data set without the Himmelskamp effect for propeller I.

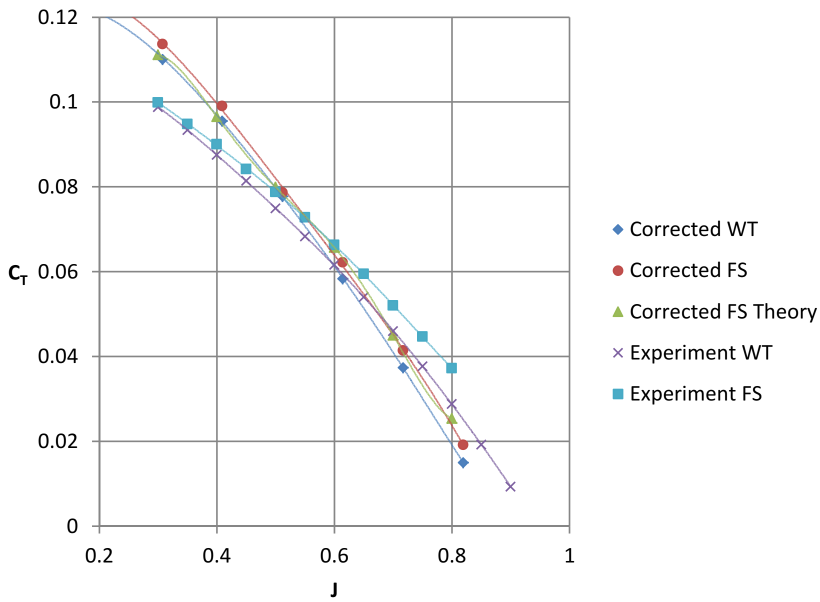

Figure C.4.: Second data set with the Himmelskamp effect for propeller I.

propeller K

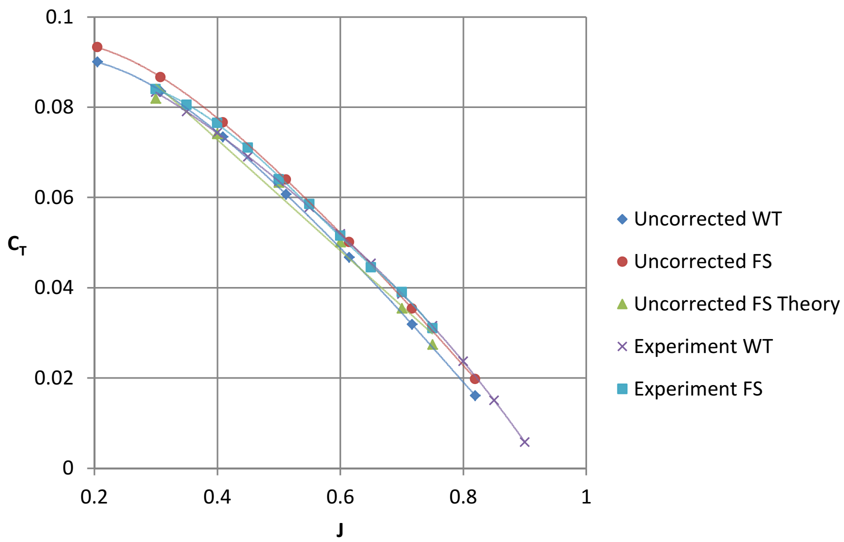

Figure C.5.: First data set without the Himmelskamp effect for propeller K.

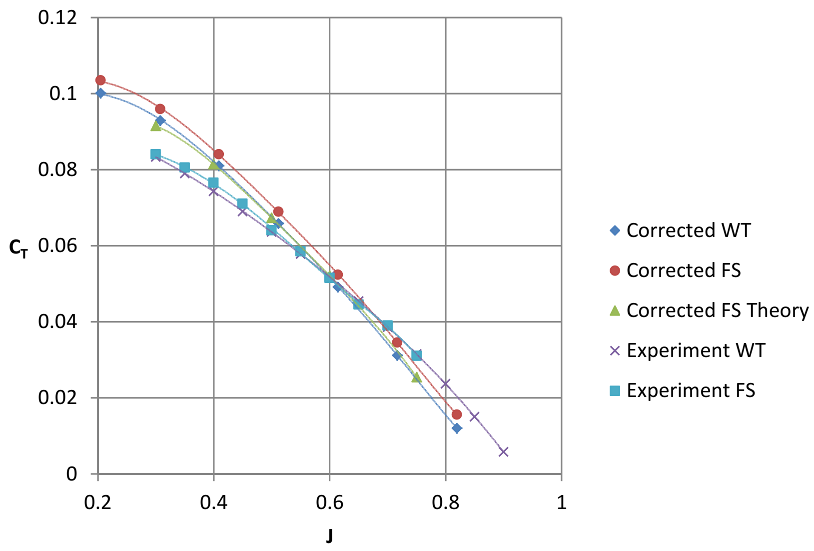

Figure C.6.: Second data set with the Himmelskamp effect for propeller K.

propeller L

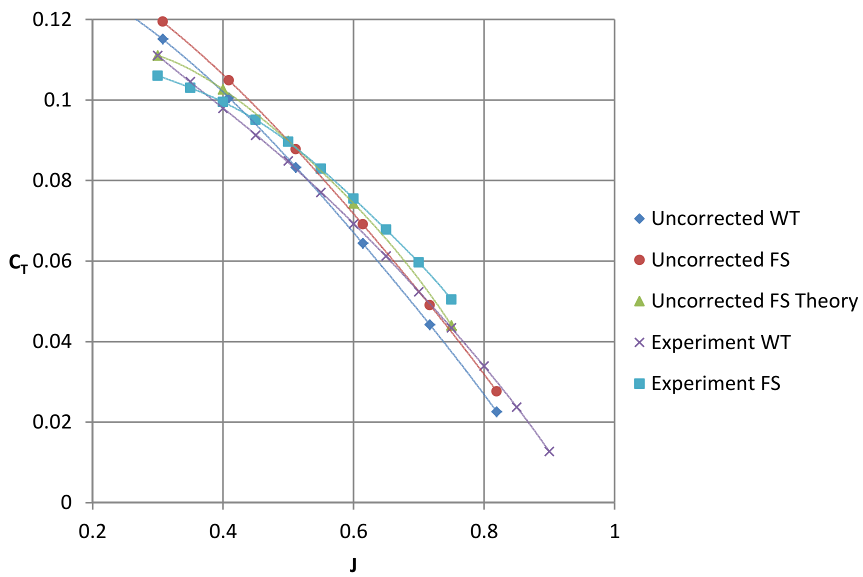

Figure C.7.: First data set without the Himmelskamp effect for propeller L.

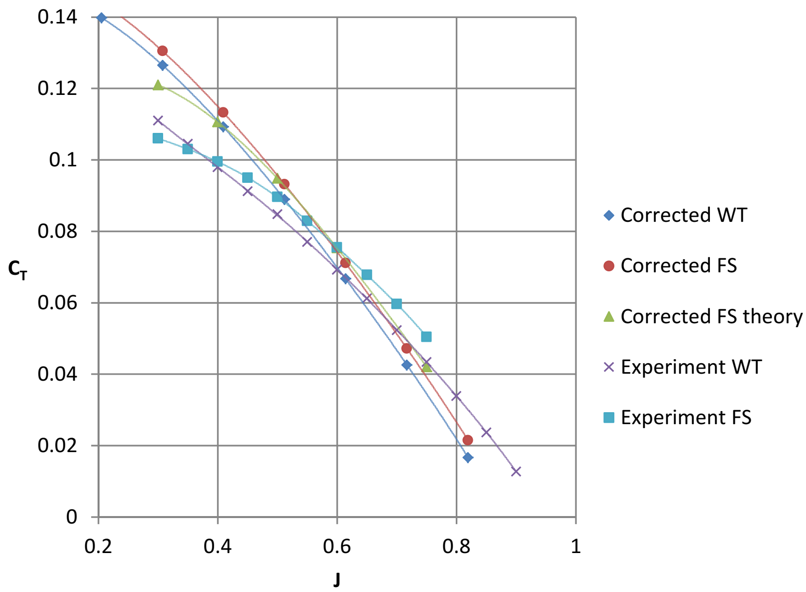

Figure C.8.: Second data set with the Himmelskamp effect for propeller L.

D. Comparison with constant performance parameters

Propeller B was already used as an example in the report and in this appendix the data for the other 4 propellers are listed below, i.e. D,I,K and L. The data focuses on the resulting induced velocities of the two analysis done with Qprop, where either J or C_T is kept constant.

propeller D

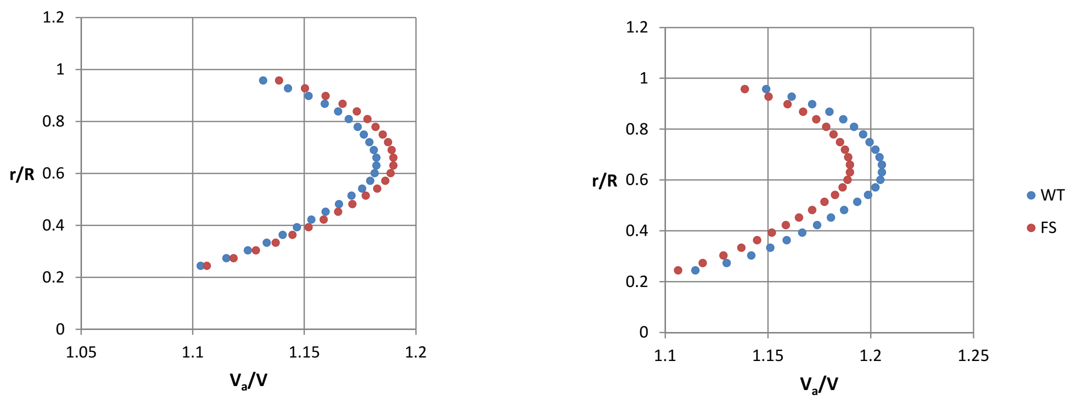

Figure D.1.: Local axial velocities versus the radial position for full scale and wind tunnel of propeller D with constant advance ratio (left) and constant thrust coefficient (right).

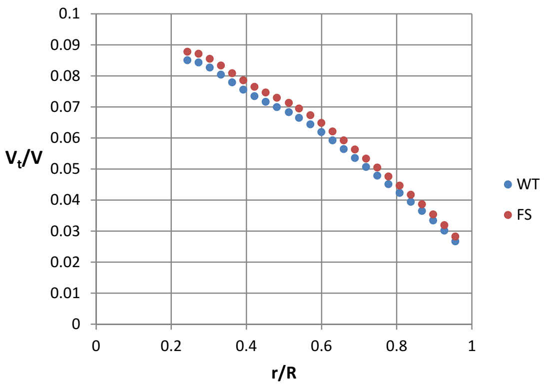

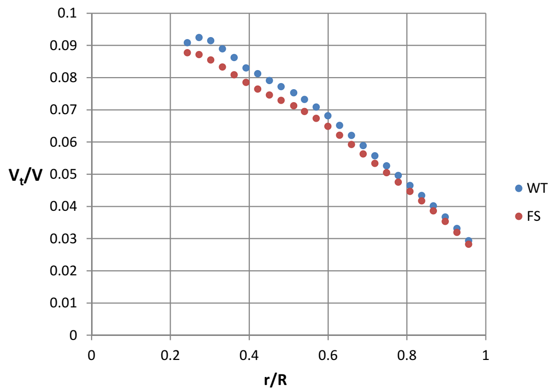

Figure D.2.: Local tangential velocities versus the radial position for full scale and wind tunnel of propeller D with constant advance ratio (left) and constant thrust coefficient (right).

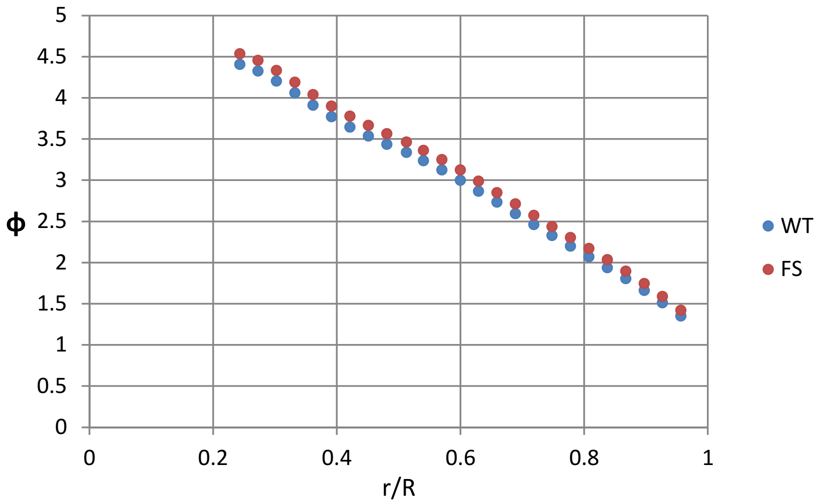

Figure D.3.: Inflow angle in function of the radial position for WT and FS case for propeller D.

propeller I

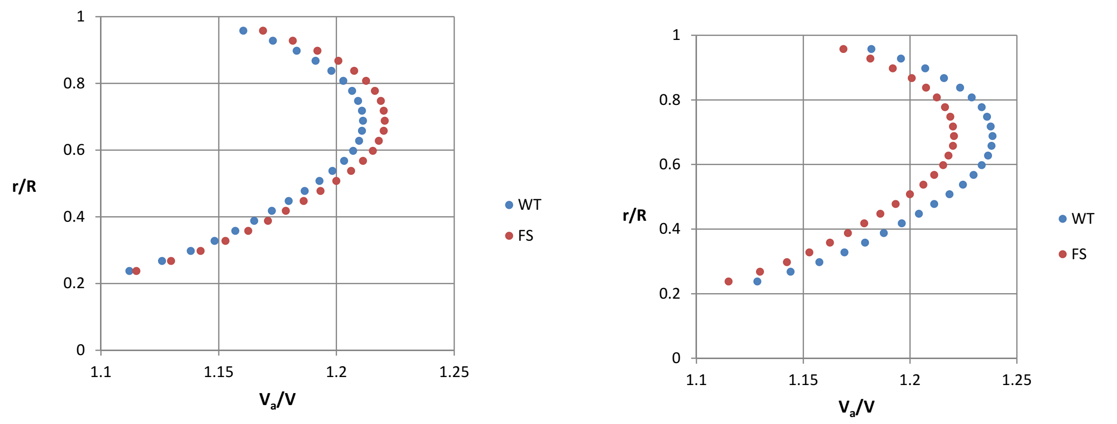

Figure D.4.: Local axial velocities versus the radial position for full scale and wind tunnel of propeller I with constant advance ratio (left) and constant thrust coefficient (right).

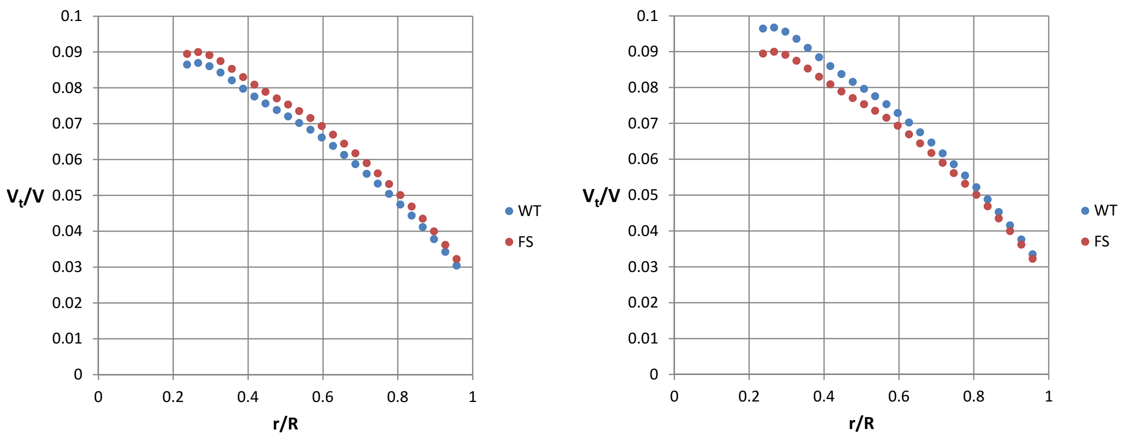

Figure D.5.: Local tangential velocities versus the radial position for full scale and wind tunnel of propeller I with constant advance ratio (left) and constant thrust coefficient (right).

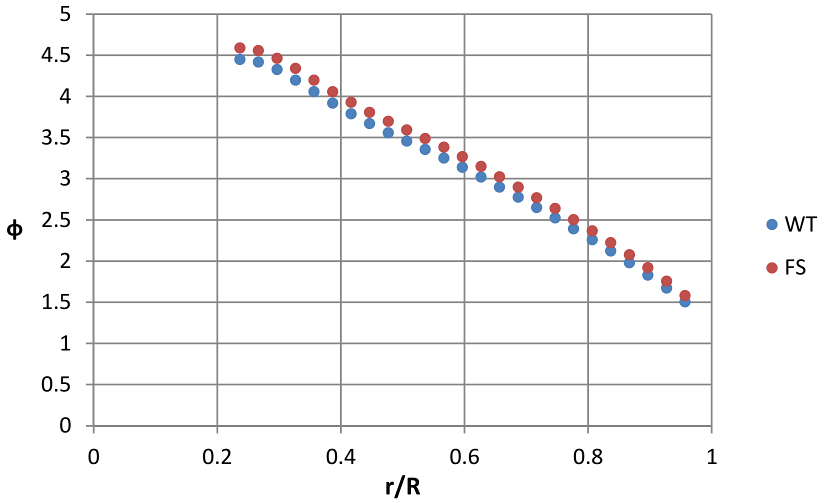

Figure D.6.: Inflow angle in function of the radial position for WT and FS case for propeller I.

propeller K

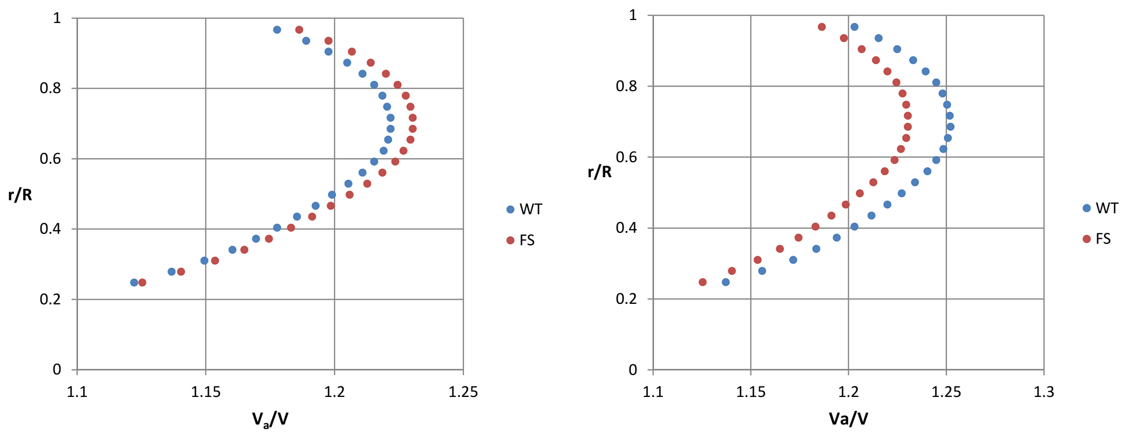

Figure D.7.: Local axial velocities versus the radial position for full scale and wind tunnel of propeller K with constant advance ratio (left) and constant thrust coefficient (right).

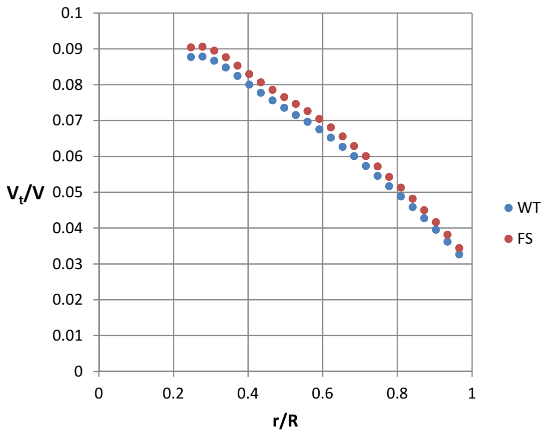

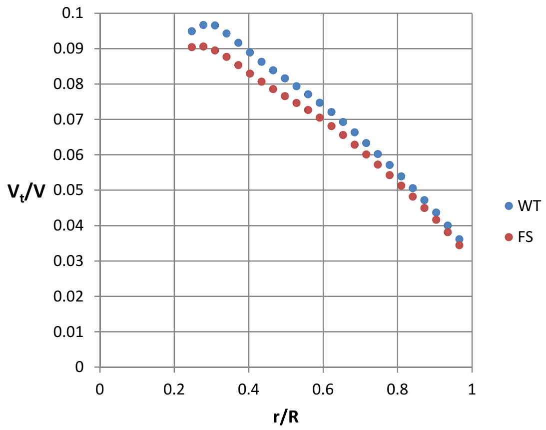

Figure D.8.: Local tangential velocities versus the radial position for full scale and wind tunnel of propeller K with constant advance ratio (left) and constant thrust coefficient (right).

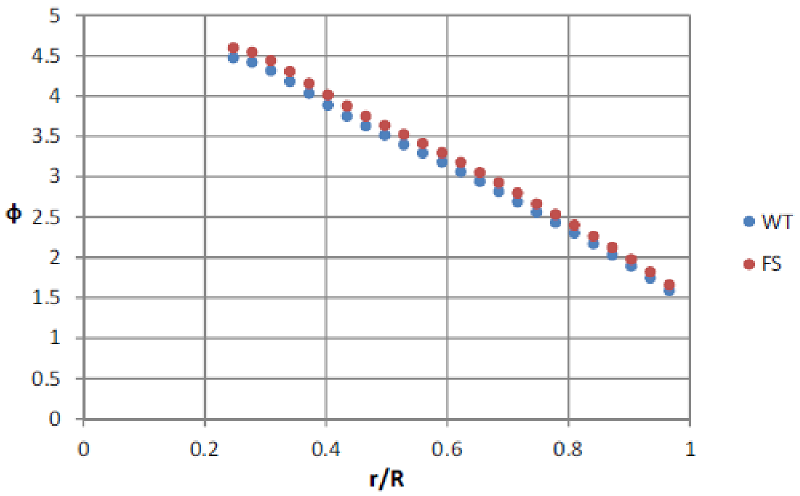

Figure D.9.: Inflow angle in function of the radial position for WT and FS case for propeller K.

propeller L

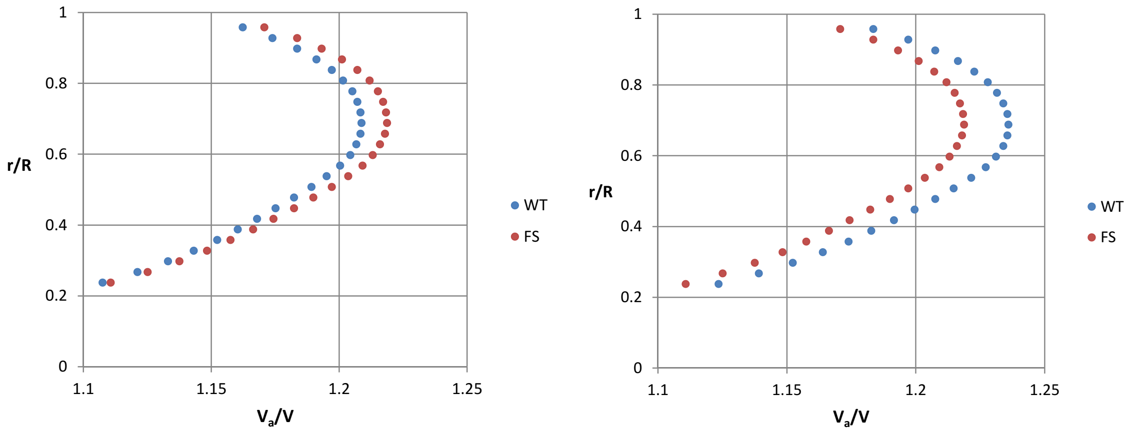

Figure D.10.: Local axial velocities versus the radial position for full scale and wind tunnel of propeller L with constant advance ratio (left) and constant thrust coefficient (right).

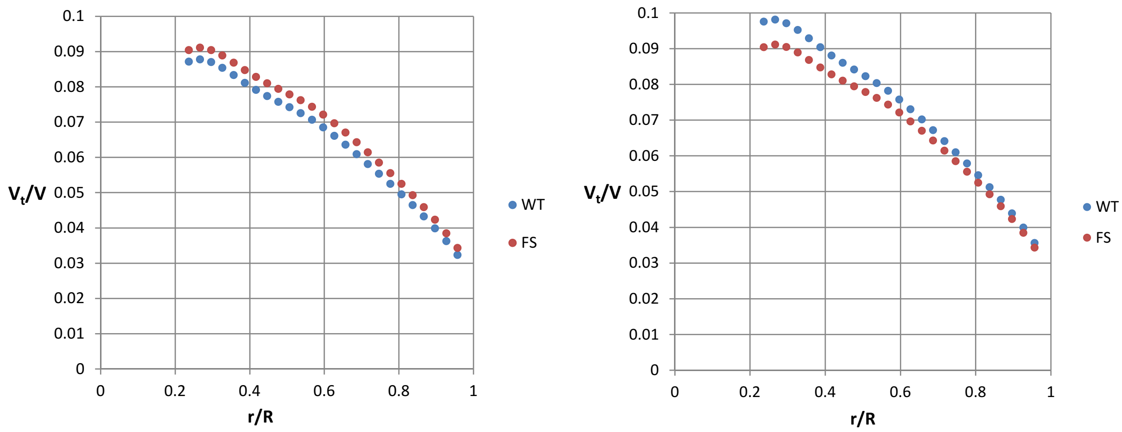

Figure D.11.: Local tangential velocities versus the radial position for full scale and wind tunnel of propeller L with constant advance ratio (left) and constant thrust coefficient (right).

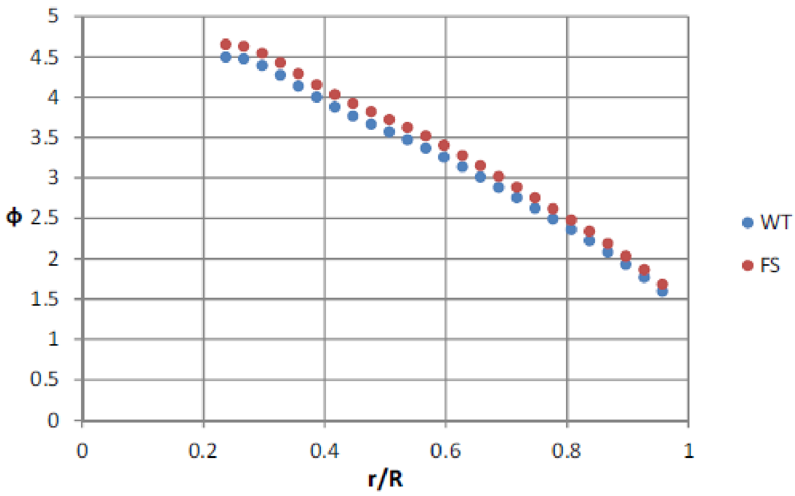

Figure D.12.: Inflow angle in function of the radial position for WT and FS case for propeller L.

Difference in induced velocities between WT and FS with constant J

	Propeller B			Propeller I			Propeller D		
$\frac{r}{R}$	$\frac{\Delta V_a}{V_\infty}$	$\frac{\Delta V_t}{V_\infty}$	$\frac{\Delta\varphi}{\varphi_{local}}$	$\frac{\Delta V_a}{V_\infty}$	$\frac{\Delta V_t}{V_\infty}$	$\frac{\Delta\varphi}{\varphi_{local}}$	$\frac{\Delta V_a}{V_\infty}$	$\frac{\Delta V_t}{V_\infty}$	$\frac{\Delta\varphi}{\varphi_{local}}$
0.23	0.0039	0.0031	0.036	0.0029	0.0029	0.031	0.0028	0.0027	0.029
0.35	0.0061	0.0034	0.040	0.0054	0.0032	0.034	0.0044	0.0029	0.033
0.45	0.0079	0.0035	0.044	0.0063	0.0032	0.037	0.0056	0.0030	0.036
0.59	0.0100	0.0035	0.049	0.0084	0.00323	0.041	0.0072	0.0029	0.041
0.71	0.0109	0.0031	0.052	0.0092	0.0030	0.044	0.0084	0.00269	0.045
0.80	0.0109	0.0028	0.054	0.0096	0.0026	0.047	0.0084	0.00236	0.048
0.92	0.0100	0.0021	0.056	0.0084	0.0019	0.050	0.0076	0.00179	0.0052
0.96	0.0092	0.0019	0.058	0.0084	0.0018	0.052	0.0072	0.0016	0.053

	Propeller K			Propeller L		
$\frac{r}{R}$	$\frac{\Delta V_a}{V_\infty}$	$\frac{\Delta V_t}{V_\infty}$	$\frac{\Delta\varphi}{\varphi_{local}}$	$\frac{\Delta V_a}{V_\infty}$	$\frac{\Delta V_t}{V_\infty}$	$\frac{\Delta\varphi}{\varphi_{local}}$
0.23	0.0031	0.0026	0.027	0.0032	0.0032	0.034
0.35	0.0045	0.0028	0.029	0.0052	0.0035	0.037
0.45	0.0059	0.0029	0.033	0.0072	0.0036	0.040
0.59	0.0081	0.0029	0.036	0.0088	0.0036	0.044
0.71	0.0086	0.0027	0.040	0.0100	0.0032	0.047
0.80	0.0090	0.0024	0.042	0.0104	0.0029	0.050
0.92	0.0086	0.0019	0.045	0.0096	0.0022	0.053
0.96	0.0086	0.0017	0.046	0.0084	0.0019	0.054

E. Comparison of lift distributions

In chapter 5, it was investigated how the difference between WT and FS of the propeller affects the wing in a tractor configuration. This effect can be seen for all propellers in the graphs below, implemented on the general wing lay out as seen in section 5.3.

propeller B

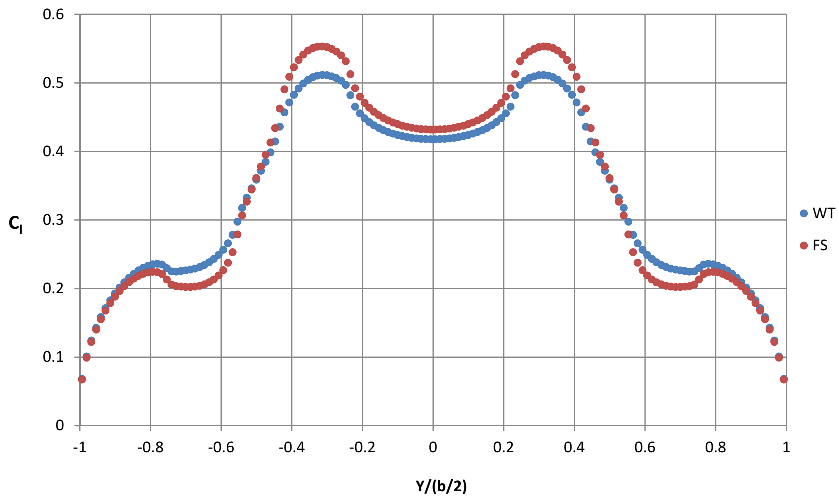

Figure E.1.: Effect of difference between wind tunnel and full scale case on lift distribution for propeller B.

propeller D

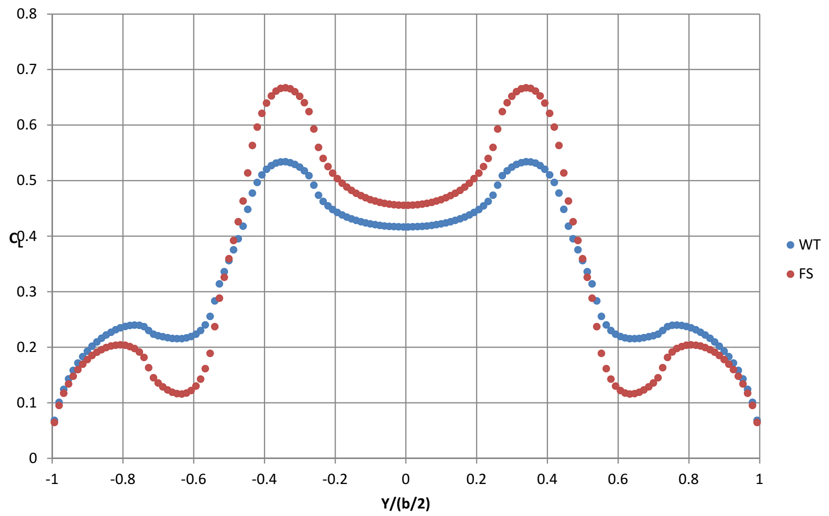

Figure E.2.: Effect of difference between wind tunnel and full scale case on lift distribution for propeller D.

propeller I

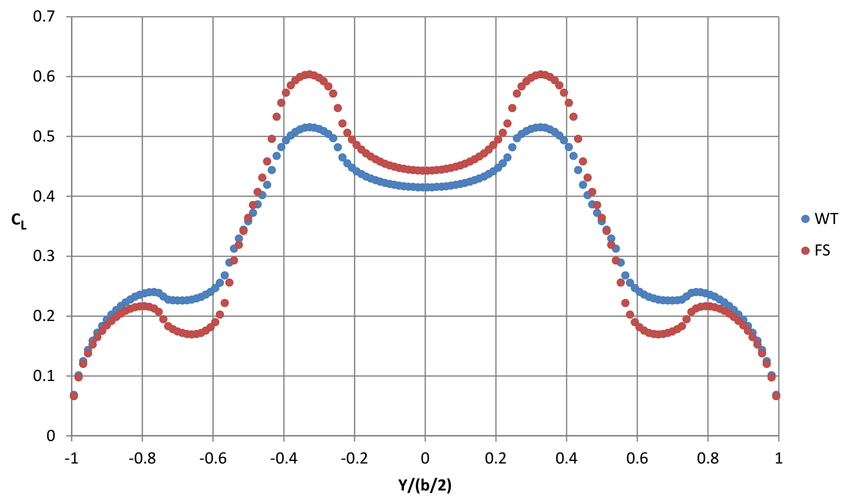

Figure E.3.: Effect of difference between wind tunnel and full scale case on lift distribution for propeller I.

Propeller K

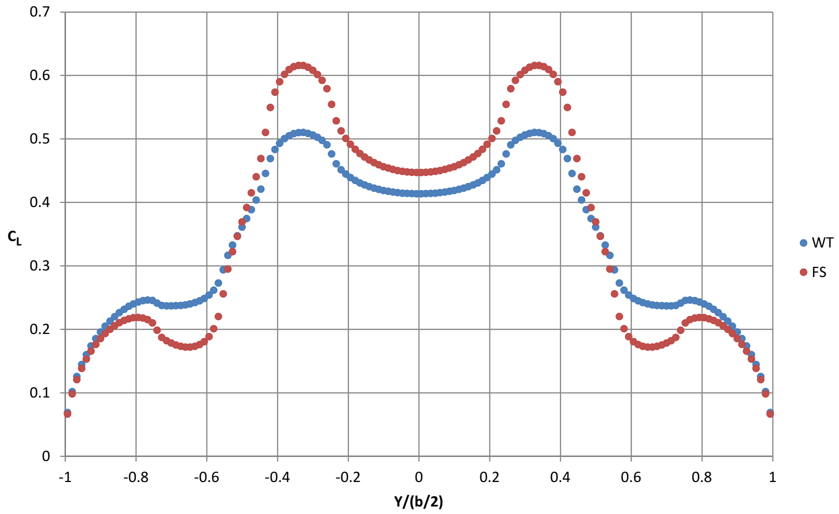

Figure E.4.: Effect of difference between wind tunnel and full scale case on lift distribution for propeller K.